Calibration and Implementation of a Functional Global Auto-ignition Model

Andrew Winstanly

WNSAND003

Thesis presented for the degree of
Master of Science in Engineering

Sasol Advanced Fuels Laboratory
Department of Mechanical Engineering
University of Cape Town

March 2014

Plagiarism Declaration

1. I know that plagiarism is wrong. Plagiarism is to use another's work and pretend that it is one's own.
2. Each contribution to, and quotation in, this thesis from the work(s) of other people has been referenced using the ISO 690 convention.
3. I have not allowed, and will not allow, anyone to copy my work with the intention of passing it off as his or her own work.
4. I acknowledge that copying someone else's work, or part of it, is wrong, and declare that this thesis is my own work.

Andrew Winstanly

Acknowledgements

I wish to acknowledge the following people for their contributions and support:

1. My supervisor, Mr Marlan Perumal, for his guidance and advice throughout the course of my project.
2. Dr Gareth Floweday, for always having time to chat about problems as I ran into them.
3. Santhosh Gundlapally, Jonathan Brown, Ryan Dudgeon and Cem Ersungur at Gamma Technologies for their help with the implementation of the model into GT-Suite software.
4. My parents for urging me to further my education.

This work was performed at the Sasol Advanced Fuels Laboratory, which is run and funded by Sasol Technology Fuels Technology.

Abstract

This research is based on a functional global reaction-rate-based auto-ignition model (FGAM) developed at the Sasol Advanced Fuels Laboratory (SAFL). During the development of the model, its performance had been validated against a detailed kinetic auto-ignition mechanism in regions of lean to stoichiometric air-fuel ratio for n-heptane, iso-octane, 1-hexene, toluene, methanol and a quaternary gasoline surrogate blend of iso-octane, toluene, n-heptane and n-hexane. Subsequent to the publication of the model, sets of reaction coefficients for PRF (Primary Reference Fuel) and TSF (Toluene Standardisation Fuel) blends had been developed and published. In its original form, however, the model could not be implemented in typical engine and chemical kinetic model simulation software.

In this work, an investigation was made into the form and stiffness limitations of the FGAM which prevented implementation into standard engine and chemical kinetic codes. Changes made to the form of the model that allowed implementation into these codes without significantly altering the behavioural functions of the model were investigated. Subsequent to the investigation, a modification was introduced to the FGAM in the form of a second pseudo-QSSA (quasi-steady-state assumption) which eliminated the need for calculation of the transient concentration of one of the model species. The resulting reduction in numerical stiffness allowed for the revised model to be implemented as a descriptor for combustions kinetics in engine simulations in GT-Suite.

A robust method of calibrating the model to reference data was also developed in this work. The range of conditions under which the calibration was performed included temperatures from 600 K to 1200 K, pressures between 20 and 60 bar, equivalence ratios from 0.8 to 1.5 and EGR (exhaust gas recirculation) rates from 0 to 45%. The calibration routine was able to reduce the average error across the ignition delay timing, cool flame ignition delay timing and cool flame temperature rise by 6% over existing coefficients for n-heptane and iso-octane. Additionally, a comparatively accurate set of coefficients was developed for PRF50.

However, through further investigation of the conditions where the model performed weakest subsequent to the calibration, it was found that the FGAM does not display correct sensitivity to equivalence ratio and EGR effects. The FGAM's lack of sensitivity to these effects was again displayed when the model was implemented in engine simulations. Major modification to the structure of the model is required in order to correct this behaviour and recommendations have been made in this regard.

Table of Contents

List of Figures

List of Tables

List of Abbreviations

CAD	Crank Angle Degrees
CF	Cool Flame
CI	Compression Ignition
CFdT	Cool Flame Temperature Rise
CFCT	Cool Flame Ceiling Temperature
CFD	Computational Fluid Dynamics
CFID	Cool Flame Ignition Delay
DKM	Detailed Kinetic Mechanism
EGR	Exhaust Gas Recirculation
FGAM	Functional Global Auto-ignition Model
GA	Genetic Algorithm
HCCI	Homogeneous Charge Compression Ignition
ID	Ignition Delay
LFL	Lower Flammability Limit
NTC	Negative Temperature Coefficient
NOx	Combination of NO and NO_2
PSO	Particle Swarm Optimisation
PRF	Primary Reference Fuel
QSSA	Quasi-Steady-State Assumption
RCM	Rapid Compression Machine
RKM	Reduced Kinetic Mechanism

SI Spark Ignition

T Temperature

TSF Toluene Standardisation Fuel

UFL Upper Flammability Limit

Chapter 1

Introduction

1.1 Background

The use of computational models in design has become increasingly popular in recent history due to their repeatability of results and their versatility with regard to application. Physical models or prototypes often require large capital expenditure to construct and can have a limited range of applicability due to their design. However, where physical models are able to recreate the required conditions for a specific experiment, a computational model is based on mathematical concepts. Consequently, the main challenge encountered in computational modelling is to align mathematical concepts to the physical ideas that they represent. Mathematical models of complex systems often make use of abstract ideas and assumptions in order to capture the event to be modelled. Validation is therefore necessary in order to determine whether or not the model is producing useful data.

Outright accuracy is not the only factor to consider when creating a model for a particular application. In order for a model to make a meaningful contribution to knowledge in a certain area, it first needs to be adopted for use in the research. Issues relating to the implementation and stability of the model can become barriers which discourage its adoption. A highly accurate model that is plagued by numerical instability issues is not as useful as a less accurate, but more robust model. In addition, due to the fact that most models are based on a set of assumptions, each model has a limited range of applicability which often correlates to the accuracy of the assumptions. Determination of these operating limits is required in order to ensure that the model is not used in areas in which it is not valid.

Auto-ignition modelling in essence tries to capture the heat release behaviour of a fuel-air

mixture as it ignites through auto-ignition. Accurate prediction of auto-ignition behaviour for a fuel in terms of ignition delay and heat release rates is essential for improving combustion efficiency through engine and fuel design. Auto-ignition modelling can aid in the formation of new fuel blends as well as new engine operating cycles.

1.2 Context

A global reaction-rate-based auto-ignition model, herein referred to as the FGAM (functional global auto-ignition model), has been developed at the Sasol Advanced Fuels Laboratory (SAFL) [1] [2]. The global nature of the model means that it should be less computationally expensive to solve compared to more detailed auto-ignition mechanisms. The model is of the form of a set of differential equations. Each equation contains parameters that can be modified to change the predicted auto-ignition behaviour of the model. In this way, the model can be calibrated to the auto-ignition characteristics of different fuels. The FGAM is a global auto-ignition mechanism which targets accuracy in prediction of cool flame heat release and NTC (negative temperature coefficient) behaviour in conjunction with accuracy in overall ignition delay. Other global auto-ignition models which existed during the development of the FGAM [21] [22] [20] [18] were identified as displaying incorrect or inaccurate behaviour with regard to the cool flame heat release and ignition delay timing in the NTC region.

GT-Suite is a virtual engine/power train platform, for integrated simulations of engines and vehicles. It is most widely used by vehicle manufacturers as well as other engine researchers in their design process. Demonstrating that the FGAM can be successfully integrated into GT-Suite software can increase the adoption rate of the model amongst its users. However, the system of differential equations that describe the model are very stiff, meaning that difficulty is encountered in both implementation and optimisation of the system. The stiffness, which is a common trait amongst reaction rate based auto-ignition models, is a consequence of the fact that certain reactions in the model take place quickly, whilst others take place comparatively slowly. The different speeds of the reactions rates is required in order for the model to exhibit the correct auto-ignition behaviour. However, the stiffness of the model still needs to be addressed if the model is to become widely adopted by researchers in the field of auto-ignition.

During the development of the model [1] [2], its performance was validated against the detailed kinetic mechanism (DKM) of Mehl et al. [3] in regions of lean to stoichiometric air-fuel ratio for n-heptane, iso-octane, 1-hexene, toluene, methanol and a quaternary gasoline surrogate of iso-octane, toluene, n-heptane and n-hexane in the ratio 44/30/18/8% by moles. The average ignition delay error achieved by the model ranged from 11% to 23%. Subsequent to the publication of the model, sets of coefficients were developed for

PRF (Primary Reference Fuel) and TSF (Toluene Standardisation Fuel) blends [4]. The average ignition delay error achieved for these blends ranged from 6% to 15%. The models performance for rich fuel air mixtures has not previously been documented.

1.3 Research Objectives

The main work encompassed in this project will be to improve upon this existing model by:

- Developing a calibration methodology which can be used to fit the model to the auto-ignition behaviour of fuels.
- Determining the operating limits of the model by investigating its performance in previously untested regions.
- Addressing the stiffness in the model, through possible minor modification to its structure, in order to facilitate easier and faster solving of the model.
- Integrating the model into engine simulations in GT-Suite software.

The calibration methodology will allow for improvement of the accuracy of the model, as well as simpler and faster characterisation of future fuels. The uncovering of the operating limits will indicate the useful range of the model. In order for the model to gain wider adoption, it is important that the operating limits of the model includes prominent regions being investigated in contemporary fuel and combustion research by vehicle manufacturers and research groups alike. Addressing the stiffness of the model will also increase the probability of widespread adoption of the model, and allow for easier implementation of the model with different numerical solvers and software packages. Integrating the model into GT-Suite will serve to demonstrate that the stiffness of the model has been successfully addressed, and that the model is capable of describing combustion kinetics in engine simulations.

1.4 Thesis Outline

The format of the thesis is as follows:

- A review of relevant literature, covering the following topics:

  - Auto-ignition and ignition delay principles
  - Detailed description of the FGAM
  - Numerical optimisation and validation techniques
- An investigation into the causes of the FGAM's stiffness and challenges with solving the FGAM using standard techniques
- Formulation of the calibration methodology for the FGAM
- Integration of the model into GT-Suite software
- Conclusions
- Recommendations
- Appendices containing:
  - Calibrated coefficients for the FGAM.
  - Additional mathematical derivations.
  - Additional graphs displaying the performance of the calibrated FGAM.
  - User manuals for the calibration code and implementation of FGAM into GT-Suite.

Chapter 2

Literature Review

This literature review begins by defining auto-ignition and ignition delay, two topics of relevance to this research. Following this, a detailed explanation regarding the structure of the FGAM is presented. Thereafter, the mathematical techniques that can be used to calibrate the reaction coefficients will be described, along with the methods of validation.

2.1 Auto-ignition of Fuels

Heywood [5] describes auto-ignition as an event whereby a fuel-air mixture ignites purely due to the temperature and pressure conditions to which it is exposed, without the aid of an ignition source. Auto-ignition is a multi-step process, comprised of several reactions between interdependent species, ultimately resulting in heat release. The following three reaction types are dominant during an auto-ignition event:

1. Initiating Reactions: highly reactive radicals are formed from stable molecules in the fuel and oxygen.

2. Propagation Reactions: the radicals formed in the initiating reactions react with the original stable reactants to form other products and radicals.

3. Terminating Reactions: these reactions serve to control the heat release rate and the overall speed of the auto-ignition event by removing the chain propagating radicals from circulation.

The need for accurate auto-ignition prediction is necessitated by the effect this phenomenon has on both spark and compression ignition engines.

2.1.1 Auto-ignition in Spark Ignition Engines

Knock is the auto-ignition of the unburnt mixture in the cylinder before it is consumed by the spark initiated flame front. It is an unwanted event in spark ignition (SI) engines where combustion is controlled by an ignition source, conventionally a spark plug. Gasoline, the traditional fuel of SI engines, is designed to be highly resistant to auto-ignition; the measure of this resistance is known as the octane number [6]. Knock disrupts the thermal boundary layer that exists in the vicinity of the cylinder wall, by creating shock waves which are reflected along in-cylinder surfaces [7]. This thermal boundary layer normally ensures that the engine components do not reach their respective melting points even though the temperatures experienced during combustion are considerably higher than the melting points of materials used. Without this protection, the heat released from combustion would raise the temperature of the engine components until such a point where catastrophic engine failure can occur. The shock waves also directly damage engine components through erosive wear [8].

2.1.2 Auto-ignition in Compression Ignition Engines

In contrast to SI engines, auto-ignition is the means used to facilitate combustion in compression ignition (CI) engines, which operate without the aid of an external ignition source. Improved understanding of auto-ignition for the fuels used in these engines allows for greater engine efficiency and reduced emissions to be obtained during the design process.

Diesel Cycle

As mentioned previously, engines operating on a CI cycle, such as the diesel cycle, are reliant on auto-ignition for proper operation. Whereas in a SI engine, the combustion timing can be controlled by the spark plug, there is no means of directly initiating combustion in a diesel engine. Diesel fuel is designed to readily auto-ignite; the measure of a fuels propensity to auto-ignite is known as the cetane number [9]. In addition, diesel engines have comparatively higher compression ratios compared to SI engines in order to create an environment more conducive to auto-ignition [10]. Auto-ignition produces a distinct audible noise which gives CI engines operating on the Diesel cycle their characteristic sound [11].

Homogeneous Charge Compression Ignition (HCCI) Cycle

HCCI engine technology is focused on reducing the regulated emissions of soot and NOx (nitrogen oxides) compared to the emissions output of contemporary internal combustion engines. Soot and NOx are regulated emissions according to the European and U.S. Emissions Standards [12] [13]. Figure 2.1, shows the two regions in which soot and NOx emissions are most prominent during engine operation. Soot forms at high temperatures and for equivalence ratios (denoted by ϕ) greater than 2, whilst NOx is formed at high temperatures and equivalence ratio ranging from 0 to 2. NOx formation is the result of the reaction between the nitrogen and oxygen in the air at high temperatures. Soot is formed

a
T
a
d

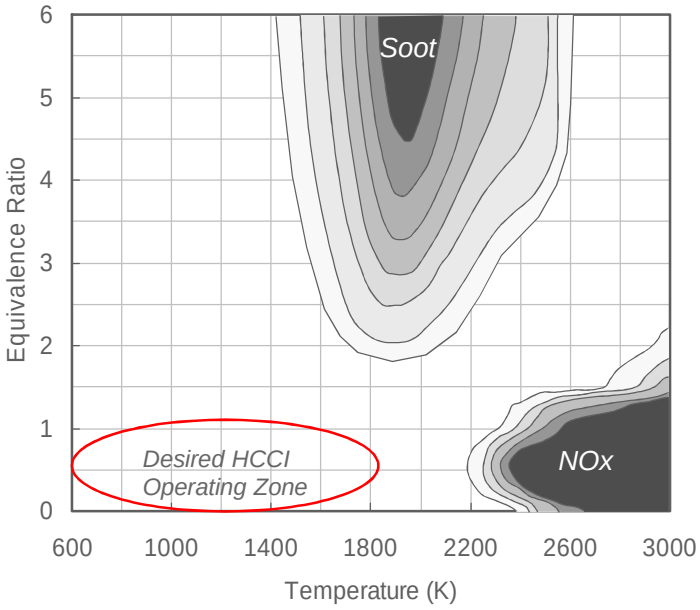

Figure 2.1: *The regions in which Soot and NOx emissions occur during operation of an internal combustion engine. Adapted from [14]*

In order to avoid the soot and NOx islands, the desired HCCI engine cycle operates with a homogeneous, lean and/or diluted (by way of exhaust gas) fuel-air charge [15]. The homogeneity of the charge will reduce soot emissions by ensuring no localised regions of high equivalence ratio occur. Exhaust products have higher specific heat capacity compared to the fuel-air charge, thus diluting the inlet charge with exhaust gas will serve to lower the peak combustion temperature. A leaner mixture, which has an equivalence ratio less than 1 (i.e. ϕ less than 1), will mean that the charge has less chemical potential energy, resulting in lower heat release during combustion, further reducing peak in-cylinder tem-

perature. Lower in-cylinder temperatures should serve to reduce NOx production. The main design challenge regarding this new engine technology is finding a fuel that mixes well in the limited time during the intake and compression stroke of the engine cycle, which also has the required ignition characteristics in order for the engine to operate, i.e. low temperature, lean combustion [16] [2]. Therefore, a means to accurately study the auto-ignition behaviour, especially the capturing of the heat release, of current and future fuels is needed.

2.2 Ignition Delay

Ignition delay is the time taken for the fuel to auto-ignite after it has been introduced into the high temperature and pressure conditions of the combustion chamber [17]. There are two different behaviours which can be exhibited by the fuel-air mixture during the ignition delay [2], namely single-stage and two-stage, both of which are dependent on the chemical composition of the fuel, temperature, pressure, dilution rate and equivalence (fuel-air) ratio. Higher temperatures and pressures are generally associated with shorter ignition delay periods, except in regions where two-stage fuels exhibit NTC (negative temperature co-efficient) behaviour. NTC behaviour is explained in more detail in section 2.2.2. In this section there are two types of graph that are used in the description of ignition delay. The first type is a temperature-time trace, as shown in Figure 2.2, which shows the temperature history of a single experiment throughout its ignition delay period.

The second type of graph, an example of which is given in Figure 2.3, is a plot of ignition delay versus the initial temperature of the experiment. For reasons that will become clearer later on, ignition delay is plotted on a logarithmic scale on the primary y-axis and the inverse of temperature is plotted on the x-axis. For this plotting scheme, low temperature experiments occur on the right, and high temperature experiments on the left. In order to simplify the reading of the graph, initial temperature is sometimes plotted on the secondary y-axis against its corresponding inverse on the x-axis. These ignition delay plots can be used to clearly display the effect of changing temperature and other variables on ignition delay when different experiments are plotted on the same set of axis.

2.2.1 Single-Stage Ignition Delay

This type of auto-ignition event is characterised by one main heat release event as shown in Figure 2.2. The main heat release can be defined as having occurred when the temperature of the mixture becomes sufficiently high or once the concentration of one of the combustion products has reached a critical value. The temperature of the mixture remains relatively

constant until auto-ignition occurs. Associated with single-stage ignition delays are single stage fuels. Single-stage fuels display straight line Arrhenius behaviour, meaning that as the initial temperature is increased, so the ignition delay shortens. Figure 2.3 , adapted from Floweday [1], displays the ignition behaviour of the single-stage fuel toluene. It should be noted that although two-stage fuels (section 2.2.2) may exhibit single-stage ignition behaviour in certain temperature zones, for example iso-octane in Figure 2.2, single-stage fuel

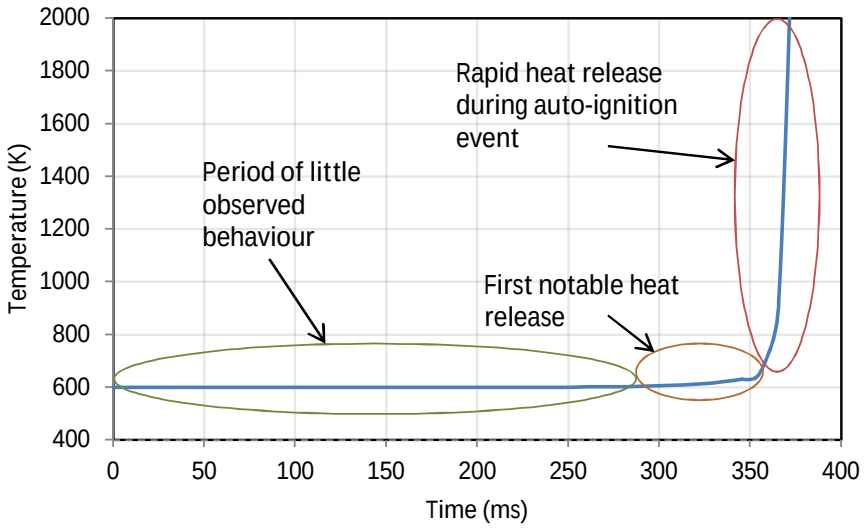

Figure 2.2: *Temperature-time trace for auto-ignition of iso-octane at 600 K, 20 bar, $\Phi = 1$. This is an example of single-stage auto-ignition behaviour. Data obtained using the Mehl DKM [3].*

2.2.2 Two-Stage Ignition Delay

Two-stage ignition delay describes an auto-ignition event whereby an initial smaller heat release occurs, followed by the main heat release. A temperature time trace of a two stage auto-ignition event is shown in Figure 2.4. The smaller heat release is known as the cool flame heat release [18]. The period of time which elapses between the initial conditions and the onset of the cool flame is known as the cool flame ignition delay.

The Cool Flame & NTC (Negative Temperature Coefficient) Behaviour

During the cool flame event, very little heat is released, rather, reactive molecules recombine to form a variety of stable compounds. After the cool flame has occurred, the mixture

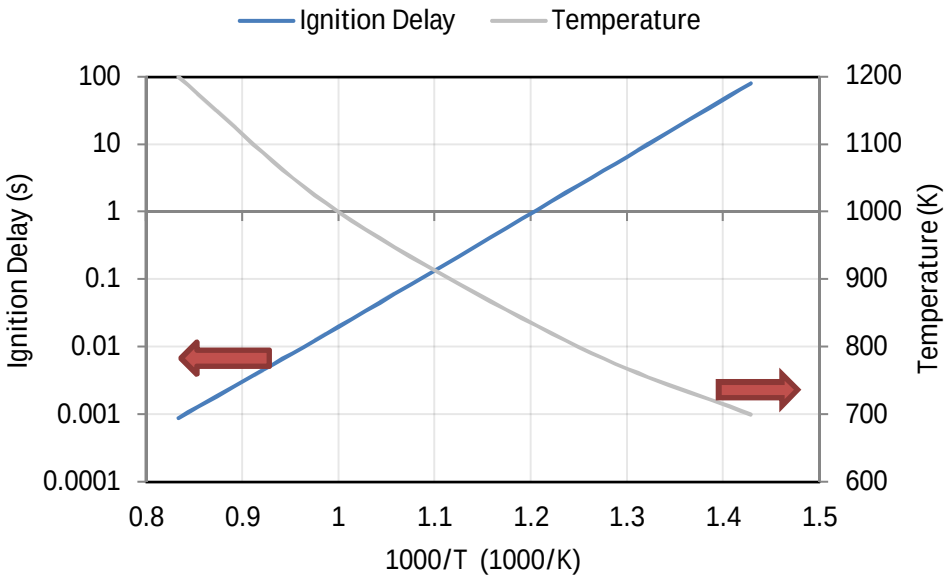

Figure 2.3: *Toluene, a single-stage fuel, displaying straight line Arrhenius behaviour at 20 bar, $\Phi = 1$, 0% EGR. The graph has been plotted using a logarithmic time scale for ignition delay against the inverse of temperature. This figure is adapted from Floweday [1]. The secondary y-axis correlates with the grey line for easier reading of the graph. Data obtained using the Mehl D.*

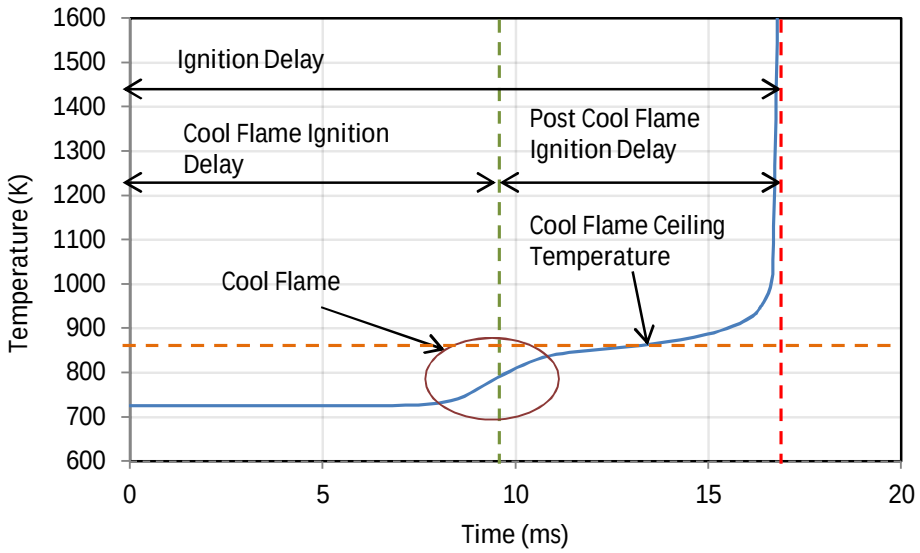

Figure 2.4: *Two-stage ignition delay behaviour of iso-octane at 748 K, 20 bar, $\Phi = 1$. The annotations show the cool flame ignition delay, the region of cool flame occurrence, the ceiling temperature, the post cool flame ignition delay as well as the overall ignition delay. Data obtained using the Mehl DKM [3].*

exists at a marginally elevated temperature known as the cool flame ceiling temperature. According to Halstead et al. [18], the temperature rise due to the cool flame cannot be greater than a maximum of 200 K. However, this is not always true as the cool flame heat release can be higher under certain conditions, as shown in Figure 2.5. The post cool-flame ignition delay is measured from the end of the cool flame event to the main heat release. Floweday [2] noticed that the post cool flame ignition delay starting at the elevated ceiling temperature is shorter compared to an ignition delay which begins at a temperature equal to that of the elevated ceiling temperature. It was therefore deduced that the cool flame also increases the reactivity of the chemical species present during the post cool flame ignition delay.

Associated with two-stage ignition delay are two-stage fuels [19]. Two-stage fuels initially follow the trend of decreasing ignition delay with increasing temperature in the low temperature region until the critical temperature associated with the commencement of the NTC behaviour for the fuel is reached. At this point the ignition delay increases for increasing temperature, as shown in Figure 2.6. Once the temperature has become sufficiently high, straight line Arrhenius behaviour is resumed (i.e. decreasing ignition delay with increasing temperature). From Figure 2.6, it can also be seen that the cool flame heat release decreases as the initial temperature increases, resulting in all of the two-stage auto-ignition traces shown in the figure having similar ceiling temperatures. This convergence of ceiling temperature is a common trait of two-stage fuels at a given condition [18] [2]. An ignition delay curve, shown in Figure 2.7, demonstrates the deviation from the straight line Arrhenius behaviour in the NTC region, producing an "S"-shaped ignition delay curve.

The cool flame ignition delay is also plotted alongside the overall ignition delay in Figure 2.7 . Starting from the low temperatures on the right, the two curves lie on top of each other as there is no discernible difference between cool flame ignition delay and overall ignition delay in this region. As the initial temperature increases, the two curves diverge as noticeable delay between the cool flame event and overall ignition delay is observed. As the initial temperature is increased further, the cool flame ignition delay also begins to increase slightly. Floweday refers to this as the cool flame hook. At this stage, the heat released from the cool flame is small, and further increase of the initial temperature results in the disappearance of the cool flame altogether.

Conventionally, NTC behaviour is defined as an increasing ignition delay for increasing initial temperature. However, NTC behaviour is also used to describe a slowing of the rate of increasing ignition delay with increasing temperature, which is recognised by a reduction in the steepness of the slope. An example of this displayed in Figure 2.8. In the high temperature region, straight line Arrhenius behaviour is resumed, offset by the effect of the NTC behaviour. Due to this NTC behaviour, a two-stage fuel which has the same high temperature behaviour as a single-stage fuel will not exhibit the same low temperature ignition behaviour as the single-stage fuel, as displayed in Figure 2.8. The maroon trace in this figure is a projection of the fuel's low temperature behaviour based

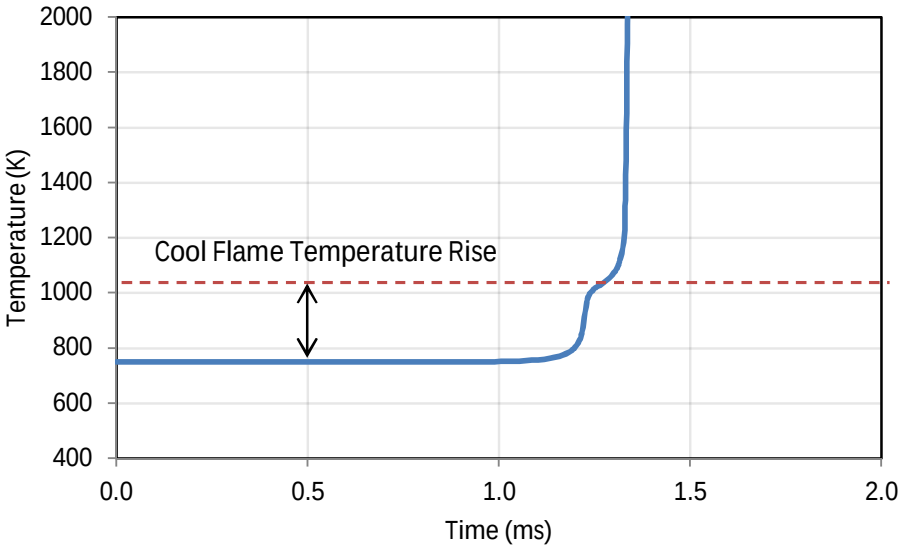

Figure 2.5: *Two-stage ignition delay behaviour of n-heptane at 750 K, 30 bar, $\Phi = 1$. Notice the cool flame ceiling temperature is over 1000 K, indicating that the cool flame temperature rise is greater than 250 K. This demonstrates that the assumption made by Halstead et al. [18] regarding maximum cool flame heat release does not hold true under all conditions. Data obtained using the Mehl DKM [3].*

2.2.3 Effect of Pressure, Equivalence Ratio and Exhaust Gas Dilution on Ignition Delay

In this section, observations made by Floweday prior to his development of the model [2] regarding the effect of pressure, EGR and equivalence ratio on various auto-ignition events were examined with reference to data produced by the Mehl DKM [3] for n-heptane. This is the same reference data used by Floweday for his auto-ignition behavioural study prior to development of the FGAM.

Pressure

As mentioned previously, increasing pressure results in a decreasing overall ignition delay period, evidence of which is displayed in Figure 2.9. However, pressure has little effect on auto-ignition behaviour in the low temperature region, as shown in Figure 2.10. Floweday noticed that the that the cool flame hook was delayed with increasing pressure (i.e. shorter cool flame ignition delays at high pressure), as well as increased cool flame ceiling temper-

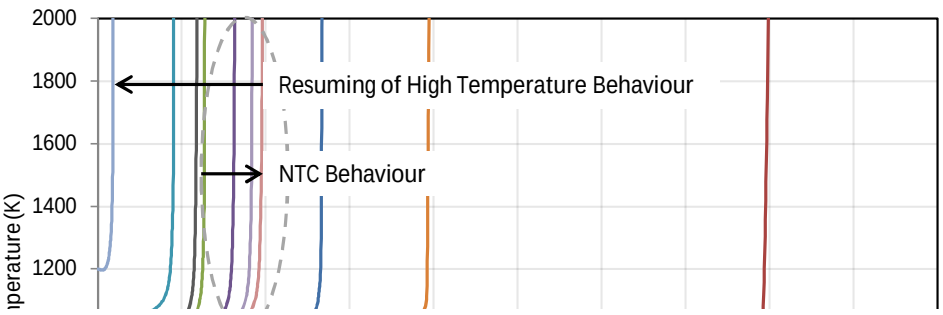

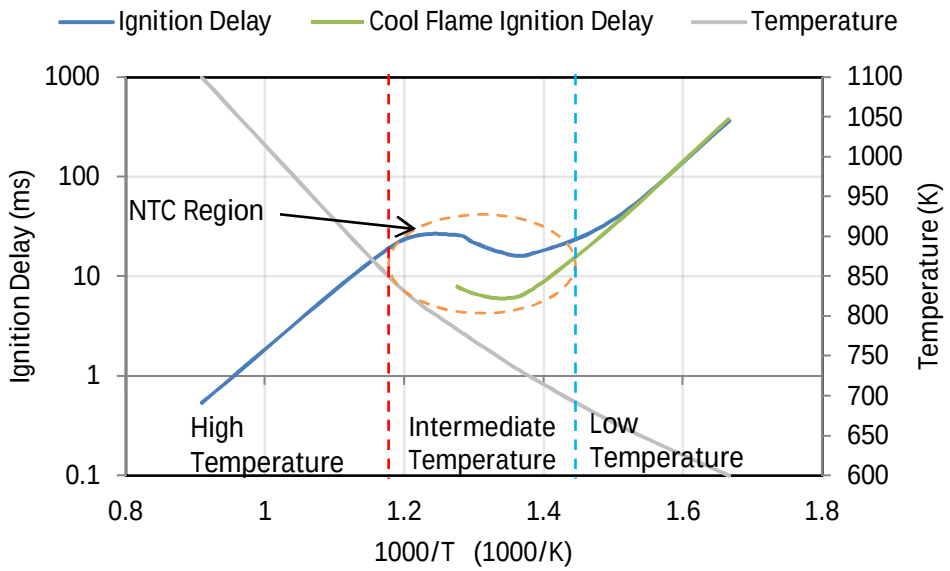

Figure 2.7: *An ignition delay curve of iso-octane at 20 bar displaying the ignition delay behaviour of the two-stage fuel. A plot of the cool flame ignition delay (green) for the region in which it is relevant has been included. The additional temperature axis correlates with the grey line for easier reading of the graph. Data obtained using the Mehl DKM [3].*

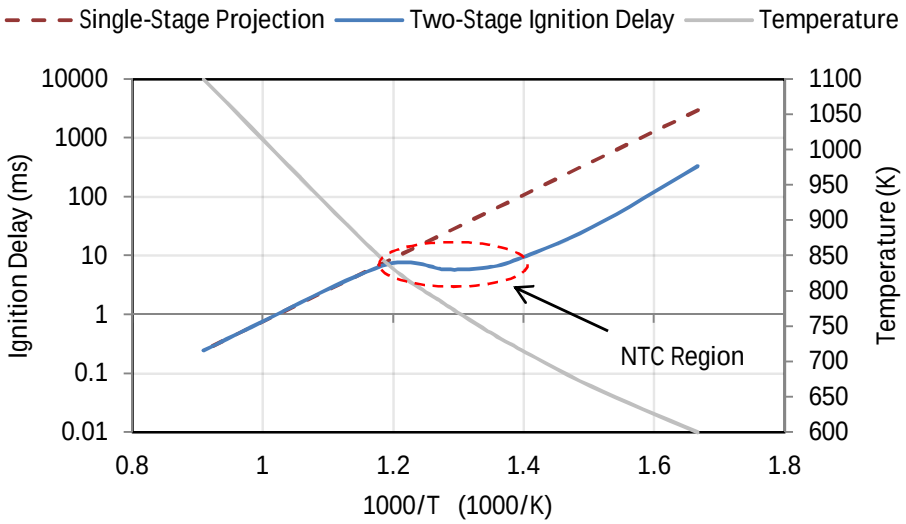

Figure 2.8: *An ignition delay curve of iso-octane at 40 bar which illustrates the difference between the two-stage auto-ignition behaviour and projected single stage ignition behaviour for the fuel. With regard to the NTC region of the two-stage curve, notice that although the slope does not change sign in this region, the magnitude of the slope is decreased. Data obtained using the Mehl DKM [3].*

atures at higher pressures, as seen in Figure 2.10. The higher heat release and shorter cool flame ignition delay are responsible for the shorter overall ignition delay periods at higher pressures for the affected temperature zones.

EGR

Decreasing EGR rates have the same effect on auto-ignition behaviour as increasing pressures, i.e. decreased ignition delay, decreased cool flame ignition delay and increased cool flame ceiling temperatures in the intermediate to high temperature region, as evidenced by Figures 2.11 and 2.12. As with pressure effects, EGR does not impact auto-ignition behaviour in the low temperature region.

Equivalence Ratio

Increasing equivalence ratio has the same effect on the auto-ignition behaviour as decreasing EGR or increasing pressure, as shown in Figures 2.13 and 2.14, i.e. decreased ignition delay, decreased cool flame ignition delay and increased cool flame ceiling temperature in the intermediate to high temperature region.

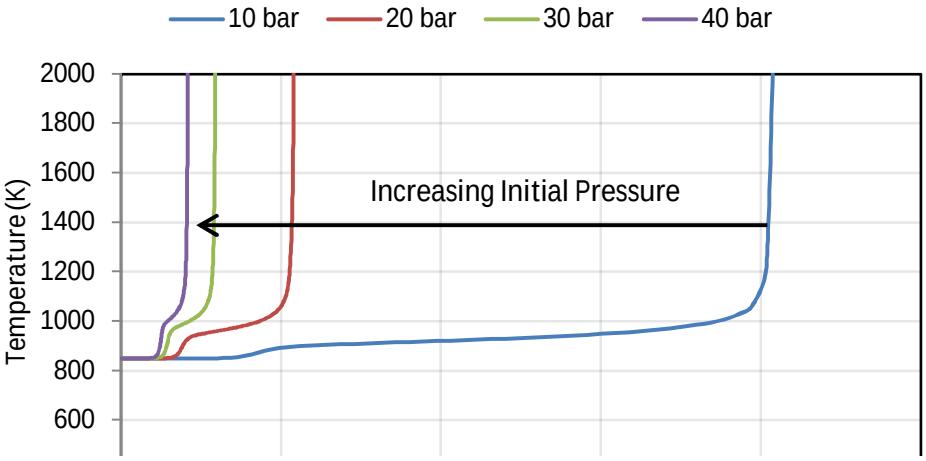

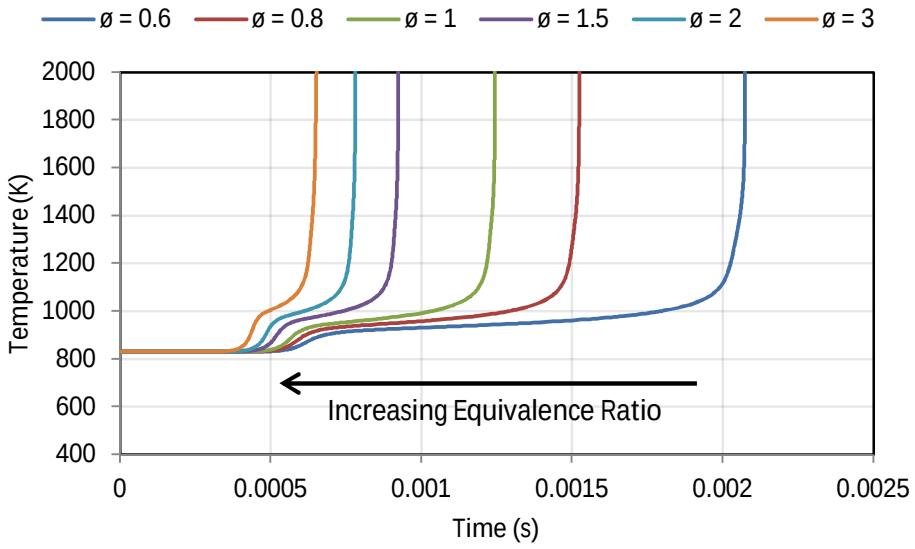

Figure 2.14: *Temperature-time traces of the auto-ignition of n-heptane at 830 K, 20 bar and 0% EGR with varying equivalence ratios. Notice that as the equivalence ratio increases, the ignition delay, cool flame ignition delay and post cool flame ignition delay decrease. Data obtained using the Mehl DKM [3].*

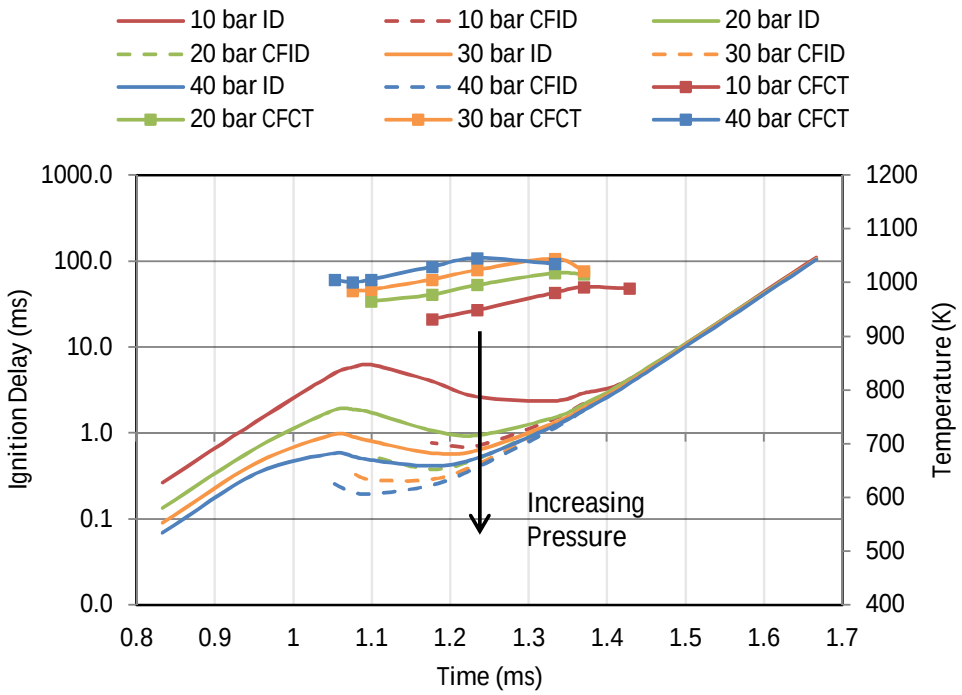

Figure 2.10: *The effect of pressure on the ignition delay, cool flame ignition delay and cool flame ceiling temperature of n-heptane at stoichiometric conditions with 0% EGR. Notice the delayed cool flame hook, greater cool flame ceiling temperatures and shorter overall ignition delay period for high pressures in the intermediate to high temperature regions. Pressure effects are not as pronounced in the low temperature region. Data obtained using the Mehl DKM [3].*

2.3 Functional Global Auto-ignition Model (FGAM)

This section details the structure of the FGAM, including the method used in solving for the kinetic rate parameters, as well as previous calibration and computational implementation of the model. A brief background to the development of the model has also been included.

2.3.1 Background

The FGAM, developed at Sasol Advanced Fuels Laboratory (SAFL), is a global reaction-rate-based model. The different classifications of reaction-rate-based auto-ignition mechanisms according to the conventions described by Zheng et al. [20] are presented in Table 2.1. A global reaction-rate-based model is described as having less than 10 species and less than 10 reactions. Of all the reaction-rate-based models, a global model has the potential to be the most computationally efficient as it has the least number of species and reactions. On the other end of the scale, a detailed model which includes 100s of species and 1000s of

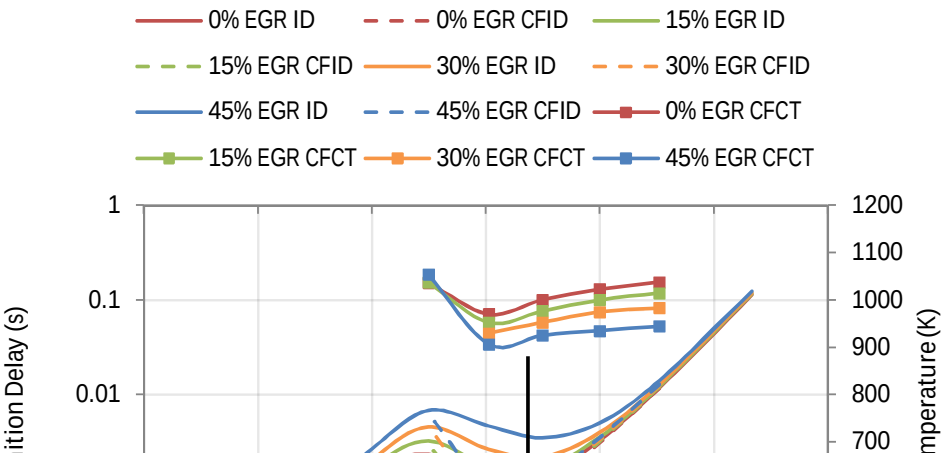

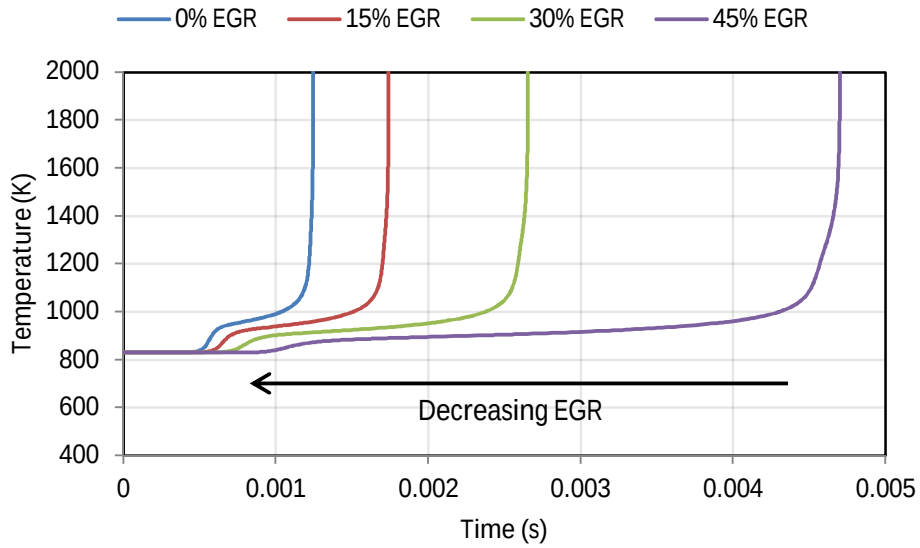

Figure 2.12: *Temperature-time traces of the auto-ignition of n-heptane at 830 K, 20 bar and stoichiometric conditions with varying EGR rates. Notice that as the percentage of EGR decreases, the ignition delay, cool flame ignition delay and post cool flame ignition delay decrease. Data obtained using the Mehl DKM [3].*

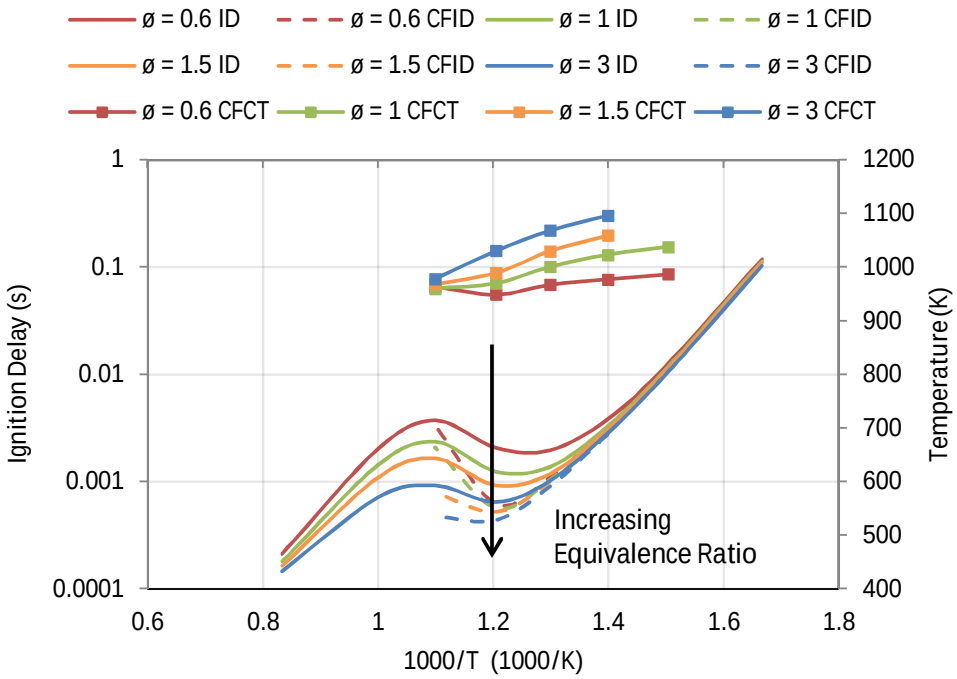

Figure 2.13: *The effect of equivalence ratio on ignition delay, cool flame ignition delay and cool flame ceiling temperature of n-heptane at 20 bar with 0% EGR. Data obtained using the Mehl DKM [3].*

reactions has the potential to be the most accurate. The reactions which take place during auto-ignition events are highly complex and equally numerous. A detailed mechanism is focused on achieving the greatest accuracy by accounting for as many of the reactions and species of a real auto-ignition events as possible. However, this added complexity makes detailed models computationally expensive and therefore slow to solve. The philosophy used in the development of reduced mechanisms is to condense the number of species and reactions by heaping similar side reaction pathways together, making the model faster to solve, whilst compromising on the accuracy achieved. The decreased computational expense makes reduced mechanisms more useful for a wider range of applications compared to detailed mechanisms. Nevertheless, if the desired outcome is to capture the highest possible accuracy with regard to the behavioural characteristics of auto-ignition events without conducting physical experiments, the use of detailed mechanisms are the most appropriate means by which this can be accomplished.

The FGAM was developed as part of an investigation into HCCI combustion. A major motivation for the FGAM was to have a model that could be fitted to experimental data of commercial boiling range fuels. Floweday [1] identified a lack of accuracy of the existing global reaction-rate-based auto-ignition models, specifically in the area of capturing both cool flame and the NTC behaviour, which is characteristic of two-stage fuels [2]. The models referred to by Floweday specifically are those formulated by Schreiber et al. [21],

Table 2.1: *Classification of Reaction-Rate-Based Auto-ignition Models according to Zheng*

Category	Species	Reactions
Detailed	100's	1000's
Lumped	100's	1000's
Reduced	10's	10's-100's
Skeletal	10's	10's
Global	< 10	< 10

Müller et al. [22], Zheng et al. [20], all of which were derived from the well-known Shell model by Halstead et al. [18]. In order to ensure that the FGAM performed better than existing reduced mechanisms in the aforementioned areas, Floweday identified the following nine key guidelines regarding auto-ignition prediction of reaction-rate-based models:

1. During the cool flame ignition delay period, the heat released is relatively small, especially when compared to the main heat release.

2. The formation of intermediate species which exist in the region of the cool flame needs to be diminished in the high temperature zone to create the hook-like behaviour seen in Figure 2.7.

3. The reaction which causes the cool flame heat release must be dependent on the concentration of the low intermediate temperature species as well as temperature in order to ensure that the cool flame heat release stops at high temperatures.

4. The point at which the cool flame heat release stops, namely the intermediate ceiling temperature, indicated the need for the inclusion of at least one reverse reaction in the model.

5. During a single ignition delay period, the lack of cool flame behaviour indicated at least one high temperature intermediate species was needed to control the ignition delay timing. Without this intermediate species, fuel and oxygen would immediately release heat at the beginning of the auto-ignition event, without a delay period.

6. The reaction which causes the high temperature heat release must be dependent on the concentration of the high temperature intermediate species as well as temperature to ensure that it is not triggered at low temperature.

7. Post cool flame, the reactivity of the species present is increased.

8. During combustion, the fuel is not completely consumed. Rather, the unburned fuel forms dissociated products to maintain chemical equilibrium. As such, the model should take this into account by limiting the fuel-air reaction in order to prevent an over prediction of the heat release.

9. In order to determine the constants appropriate for the reaction rates describing a two-stage auto-ignition fuel, the following five factors have priority:

   (a) The cool flame ignition delay at low temperature is not dependent on pressure, equivalence ratio or inert dilution.

   (b) The reverse reaction responsible for the cool flame hook is dependent on pressure, equivalence ratio and inert dilution.

   (c) The cool flame ceiling temperature is dependent on pressure, equivalence ratio and inert dilution.

   (d) The post cool flame ignition delay is not dependent on pressure, equivalence ratio or inert dilution.

   (e) The high temperature ignition delay, which occurs in the absence of cool flame activity, is dependent on pressure, equivalence ratio and inert dilution.

The structure of the FGAM, detailed in the next section, was based on the these guidelines.

2.3.2 Structure of FGAM

The reaction pathways present in the FGAM are displayed in Figure 2.15. In Floweday's development of the model, he attempted to have the mechanism represent the underlying chemistry of the reacting system as far as possible. Table 2.2 illustrates the chemical and radical species thought to be embodied by each of the intermediate species in the FGAM. However, of highest priority was that the model replicated the observed auto-ignition behaviour, specifically the temperature development. As such, the species and reactions in the FGAM should be considered to be purely mathematical constructs, whose form may differ from what might normally be expected in the chemistry.

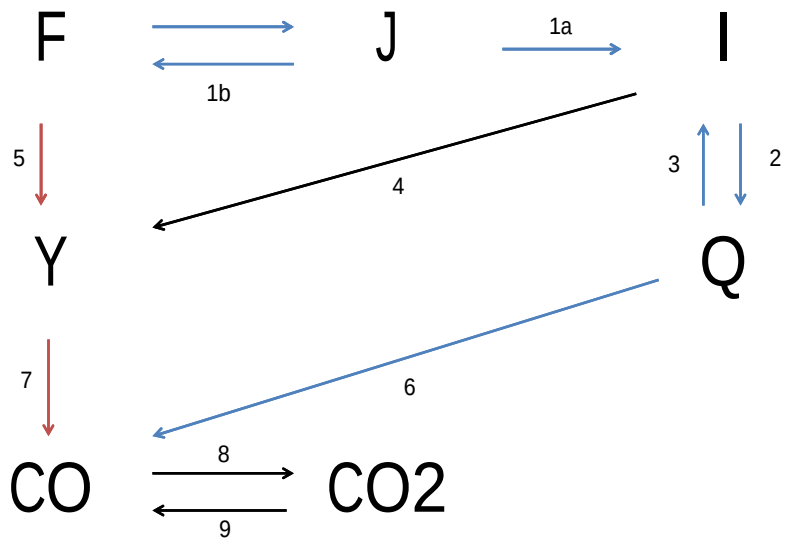

Figure 2.15: *FGAM reaction pathways, adapted from Floweday [2]. The low and high temperature pathways have been highlighted in blue and red respectively.*

Table 2.2: *FGAM Legend*

Species	Representation
F	fuel, oxygen and the alkyl radical pool
J	alkylperoxyl radical pool
I	hydroperoxyalkyl radical pool
Q	hydroperoxyalkylperoxyl and subsequent alkylhydroperoxide and/or ketohydroperoxide radical pools
Y	hydrogen peroxide, carbonyl radicals, lighter alkenes and ethers
CO	carbon monoxide and water
CO_2	carbon dioxide

An example of this is the pooling of species and reactions to achieve the very minimal number in the FGAM. This has resulted in the concentration terms in the reaction rate equation having non-integer exponents, which would not have been the case for elementary chemical reactions. Additionally, some reaction rate equations include species which are not involved in the chemistry purely because it was necessary in order for the reaction pathway to exhibit the correct response to changes in air-fuel ratio, EGR, etc.. These additional species may be thought of as catalyst for their respective reactions, though this may not strictly be the case.

Another case where the equation is not true to the underlying chemistry is the CO and CO_2

equilibrium of reactions 8 and 9. Usually this equilibrium is governed by constants derived from entropy considerations, however, in this case, the forward reaction may be thought of as including other reactants besides CO and O_2 to produce CO_2. This approach of using the CO—CO_2 equilibrium in a very loose way to replicate high temperature dissociation behaviour is based on the similar approach adopted by Zheng's 7—step model [20]. The resulting reaction rates would then not conform to the usual CO-CO_2 equilibrium reactions. Again, it must be noted that the purpose of these reactions is to match the auto-ignition behaviour of the system and not the specific species concentration.

This approach may be criticised from a rigorous chemical kinetic thermodynamics perspective, but global models typically use such simplifications in order to optimise their simplicity of structure. The previous success of the model in fitting auto-ignition data [1] and engine models [4] could have been thought to justify the model's structure. Indeed, some previous reduced mechanisms, such as the original Shell model [18], had not conserved mass and energy. For the purposes of this work, the model is accepted as is and no attempt will be made to change its underlying structure and dependencies. Any changes made will be aimed at making the model easier to solve and therefore, easier to implement.

For the purpose of the explanation of the working of a reaction-rate-based auto-ignition model, activation of a reaction is defined as the point at which the magnitude of the reaction rate becomes large enough to impact on the heat release predicted by the model.

The low temperature pathway is displayed in blue in Figure 2.15. This pathway is responsible for low temperature heat release, i.e. the cool flame timing and the cool flame heat release. The heat release for the low temperature pathway is achieved through the oxidation of species Q to CO via reaction 6. At low temperature, the conversion of CO to CO_2 will be negligible. This indicates a correlation between the concentration of Q and the low temperature/cool flame heat release, i.e. when species Q is at maximum concentration, the low temperature heat release will be at maximum [19]. This correlation is based on standard reaction rate kinetics where:

$$\text{Reaction Rate} \quad 6 \quad = \quad [Q]^{d6}[O_2]^{b6}K6$$

where,

$b6$ and $d6$ are constants with $d6 >> b6$,
$K6$ is an Arrhenius term of the form $Ae^{Ea/T}$.

Reaction 3 is responsible for controlling the cool flame ceiling temperature [19]. This is achieved through the redirection of Q back to I, which is subsequently moved to the high temperature pathway via reaction 4. The concentration of Q will reach a maximum

approaching the middle of the cool flame heat release event (based on the standard reaction rate kinetics described previously), before reaction 3 joins reaction 6 in depleting the concentration of Q in order to ensure that the correct ceiling temperature is attained.

During normal low temperature operation, species I acts in a bridging capacity, joining reaction 1 to 2, due to the fact that only reactions 1b and 6 control the low temperature fuel consumption [19]. Species I will only be able to reach significant concentration value once reaction rate 3 is activated. Therefore, it is observed that the peak concentration of I will occur after the cool flame heat release has ended.

Whilst reaction 3 controls the extent of the cool flame heat release, reaction 1b controls the occurrence of the cool flame through its impact on the low temperature pathway fuel consumption. Reaction 1b is also responsible for creating the hook behaviour of the cool flame ignition delay curve, observed in Figure 2.7 [1]. The high temperature pathway, shown in red in Figure 2.15, is governed by reactions 5 and 7. This pathway is responsible for the main heat release event. The bridge which controls the transfer species from the low and high temperature pathway in the case of a two-stage auto-ignition is reaction 4. The enhanced post cool flame reactivity is achieved by making the magnitude of reaction 4 significantly larger than all other reactions in the model once it is activated [1]. The increased speed of reaction rate 4 will boost the accumulation of intermediate species Y, which will in turn activate reaction rate 7 faster than if Y was only being fed by reaction 5. Finally, reactions 8 and 9 control adiabatic flame temperature. The forward reaction 8 is exothermic and will increase peak temperatures when activated, whilst the reverse reaction 9 will serve to reduce the final temperature. For these reactions, the CO and CO_2 terms are mathematical species and not representative of their namesake chemical species.

The reactions encompassed by the FGAM are:

$$F \rightarrow I \tag{2.1}$$
$$I \rightarrow Q \tag{2.2}$$
$$Q \rightarrow I \tag{2.3}$$
$$I \rightarrow Y \tag{2.4}$$
$$F \rightarrow Y \tag{2.5}$$
$$Q + ((x + y/2)/2)O_2 \rightarrow xCO + (y/2)H_2O \tag{2.6}$$
$$Y + ((x + y/2)/2)O_2 \rightarrow xCO + (y/2)H_2O \tag{2.7}$$
$$CO + 0.5O_2 \rightarrow CO_2 \tag{2.8}$$
$$CO_2 \rightarrow CO + 0.5O_2 \tag{2.9}$$

where **x** and **y** are the number of **C** and **H** atoms in the hydrocarbon fuel respectively.

The corresponding reaction rate equations for the FGAM are:

$$
\begin{aligned}
RR1 &= 1/(1/K1a + [F]^{a1}[O_2]^{b1}K1b) && (2.10)\\
RR2 &= [F]^{a2}[I]^{c2}K2 && (2.11)\\
RR3 &= [Q]^{d3}K3 && (2.12)\\
RR4 &= [I]^{c4}K4 && (2.13)\\
RR5 &= [F]^{a5}[O_2]^{b5}K5 && (2.14)\\
RR6 &= [Q]^{d6}[O_2]^{b6}K6 && (2.15)\\
RR7 &= [Y]^{e7}[O_2]^{b7}K7 && (2.16)\\
RR8 &= [CO]^{f8}[O_2]^{b8}K8 && (2.17)\\
RR9 &= [CO_2]^{g9}K9 && (2.18)
\end{aligned}
$$

Where the Arrhenius K terms are defined:

$$
\begin{aligned}
K1a &= A1_a e^{B1a/T} && (2.19)\\
K1b &= A1_b P^{n1b} e^{B1b/T} && (2.20)\\
K2 &= A2P^{n2}e^{B2/T} && (2.21)\\
K3 &= A3e^{B3/T} && (2.22)\\
K4 &= A4e^{B4/T} && (2.23)\\
K5 &= A5P^{n5}e^{B5/T} && (2.24)\\
K6 &= A6P^{n6}e^{B6/T} && (2.25)\\
K7 &= A7P^{n7}e^{B7/T} && (2.26)\\
K8 &= A8e^{B8/T} && (2.27)\\
K9 &= A9e^{B9/T} && (2.28)
\end{aligned}
$$

The species not directly involved in a specific reaction, but included in reaction rate equation (e.g. the F term in $RR2$), act as catalysts for their respective reactions. The units for temperature, pressure and concentration used in the reaction rates above are Kelvin, bar and moles per metre cubed respectively. The inclusion of a pressure dependency in the Arrhenius K terms was based on point number 9 from Floweday's guidelines used in the development of the FGAM, presented in section 2.3.1. From the equations presented above, it is noticed that all except for the first reaction rate expression have a standard

form. The first reaction rate was formed by combining reactions 1a, 1b and the fast reaction from F to J through a quasi steady-state assumption (QSSA) [23]. The need for the QSSA arose due to the fact that the equilibrium between F and J occurs at a much faster rate compared to reaction 1a between J and I. The difference in reaction speed allows for the faster reaction to dominate the slower one. In order to address this problem, the entire set of reactions between F, J and I were reduced under the QSSA such that the change in concentration of species J with respect to time is zero. This allows solvers to avoid having to deal with the complex issue of calculating the instantaneous concentration of species J, by simply accounting for the quantity of J consumed to the quantity of J produced. However, it should be noted that although the form of RR1 is stated to be based upon the QSSA [1], it is not strictly a QSSA reduction. This can be demonstrated through the following derivation of the QSSA form of the reaction set concerning F, J and I according to the method prescribed in [24]. Consider the following reactions:

$$\begin{aligned} RR1 &= [F][O_2]K_1 \\ RR2 &= [J]K_2 \\ RR3 &= [J]K_3 \end{aligned}$$

For QSSA, d[J]/dt = 0, therefore:

$$\begin{aligned} RR1 &= RR2 + RR3 \\ [F][O_2]K_1 &= [J]\,(K_2 + K_3) \\ [J] &= [F][O_2]K_1/(K_2 + K_3) \end{aligned}$$

Substituting for [J], RR3 becomes:

$$RR3 = [F][O_2]K_1K_3/(K_2 + K_3) \tag{2.29}$$

Which can be expressed as:

$$RR3 = [F][O_2]/(K_2/K_1K_3 + 1/K1)$$

Making the following substitutions:

$$\begin{aligned} K_{1a} &= K_1 \\ K_{1b} &= K_2/K_1K_3 \end{aligned} \tag{2.30}$$

The expression simplifies to:

$$\begin{aligned} RR3 &= [F][O_2]/(1/K1a + K1b) \\ RR3 &= 1/(1/K1a[F][O_2] + K1b/[F][O_2]) \end{aligned} \tag{2.31}$$

Compared to the FGAM's expression for RR1:

$$RR1 = 1/(1/K1a + [F]^{a1}[O_2]^{b1}K1b) \tag{2.32}$$

It is seen that the two forms of the QSSA are not equivalent. The FGAM's QSSA includes indices on the concentration terms whereas the correct QSSA does not. Additionally, the concentration terms in the denominator of the FGAM's QSSA should occur in both terms, yet they are only included in one. Due to these differences, the reduction used in the model can only be classified as a pseudo-QSSA.

The rates of change of the FGAM's species with respect to time are formed through the adding of the reaction rates where the species are products and subtracting the reaction rates where the species are reactants, whilst adhering to chemical balance relations. This results in the following equations for hydrocarbon fuels:

$$
\begin{aligned}
d[F]/dt &= -RR1 - RR5 && (2.33)\\
d[O_2]/dt &= -(x + y/2)RR6/2 - (x + y/2)RR7/2 \\
&\quad - 0.5RR8 + 0.5RR9 && (2.34)\\
d[N_2]/dt &= 0 && (2.35)\\
d[CO_2]/dt &= RR8 - RR9 && (2.36)\\
d[H_2O]/dt &= (y/2)RR6 + (y/2)RR7 && (2.37)\\
d[CO]/dt &= xRR6 + xRR7 - RR8 + RR9 && (2.38)\\
d[I]/dt &= RR1 - RR2 + RR3 - RR4 && (2.39)\\
d[Q]/dt &= RR2 - RR3 - RR6 && (2.40)\\
d[Y]/dt &= RR4 + RR5 - RR7 && (2.41)
\end{aligned}
$$

where **x** and **y** are the number of **C** and **H** atoms in the fuel respectively.

An important aspect of the implementation of a heat release model is the solving of the temperature. For the FGAM, the determination of the temperature at the next time-step based on the conservation of internal energy. In this system, the ideal gas law is assumed. For this application, internal energy is defined as a function of temperature and the number of moles present in the mixture:

$$U(T, n) \tag{2.42}$$

Taking the derivative of internal energy with respect to time yields:

$$\frac{dU}{dt} = \frac{\partial U}{\partial T}\frac{dT}{dt} + \sum_{i=1}^{n} \frac{\partial U}{\partial n_i}\frac{dn_i}{dt} \tag{2.43}$$

For internal energy to be conserved, the rate of change must equal zero:

$$0 = \frac{\partial U}{\partial T}\frac{dT}{dt} + \sum_{i=1}^{n} \frac{\partial U}{\partial n_i}\frac{dn_i}{dt} \tag{2.44}$$

Rearranging to make the rate of change of temperature with respect to time the subject of the formula:

$$\frac{dT}{dt} = \frac{-1}{\frac{\partial U}{\partial T}} \sum_{i=1}^{n} \frac{\partial U}{\partial n_i} \frac{dn_i}{dt} \tag{2.45}$$

Recall the derivative of internal energy with respect to temperature is:

$$\frac{dU}{dT} = n_{tot} C_{v-mix} \tag{2.46}$$

Therefore, it follows:

$$\frac{dT}{dt} = \frac{-1}{n_{tot} C_{v-mix}} \sum_{i=1}^{n} \frac{\partial U}{\partial n_i} \frac{dn_i}{dt} \tag{2.47}$$

This differential equation for temperature solving together with the given differential equations for species solving encapsulate the FGAM. Solving this system of differential equations for the specified initial conditions determines the temperature-time trace predicted by the FGAM.

2.3.3 Solving for Kinetic Rate Parameters

In order to deduce the rate parameters used for describing a particular fuel without any prior knowledge, the following method has been suggested by Floweday as part of his doctoral thesis [19]:

Phase 1

The following steps must be completed sequentially:

1. Solve for the low temperature cool flame timing and low temperature pathway fuel consumption by adjusting the kinetic parameters of reactions 1b and 6. Make the speed of reactions 1a and 2 fast enough so that they do not hinder the function of 1b and 6. Close off pathways 3, 4, 5 and 7 by making the reaction rates small since these pathways are not relevant in this sub-phase.

2. Fit the cool flame hook behaviour by further adjusting the parameters of reaction rate 1b.
3. Fit the cool flame ceiling temperature by adjusting parameters in reaction rate 3.
4. The high temperature pathway will then be calibrated using parameters in reaction rate 5 and 7.
5. The post cool flame enhanced reactivity is achieved by adjusting parameters in reaction rate 4.
6. The parameters for reactions 8 and 9 are to be taken from literature.

Phase 2

Subsequent to phase 1, all of the Arrhenius A and B parameters are optimised in order to fit the behavioural characteristics relevant to the reactions.

Phase 3

The parameters for each equation are re-solved sequentially in order to optimise a fitness function.

Discussion of Solving Method

The method listed above is laborious, as all of the adjustments performed in the first two phases are to be performed manually. In addition, the final phase's sequential solving of each reaction is more computationally expensive compared to a multi-variable solver. Floweday acknowledged the computational expense of the sequential solving routine, but found it to be the most stable and robust method of solving for the kinetic rate parameters.

From the explanation as to the detailed workings of the model provided in section 2.3.2, it is clear that it is not possible to generate a coefficient set by simply initiating a multi-variable solver on a broad domain. The two main pathways are competing against each other with regard to reactant consumption. For example, by not halting the high temperature pathway at low temperatures, some of the reactants will be consumed by the high temperature pathway, hindering the ability of the low temperature pathway in achieving the required behaviour. In order for a multi-variable solver to be successful, it would need to be seeded with values nearby the optimal solution. For previously undefined fuels, this would require

working through the first two phases prescribed by Floweday. However, since it is likely that these "new" fuels will relate to existing ones, combinations of kinetic rate parameters for the known fuels can be used under these circumstances. For the purposes of this research, kinetic constants for many of the fuel surrogates most commonly used auto-ignition research have already been derived in previous work.

Table 2.3 shows the experimental design used by Floweday in the solving for the kinetic rate parameters. The temperature used in this experimental design ranged between 600 K and 1200 K. As mentioned previously, the model has not been validated in regions of rich equivalence ratio, as evidenced by the table. Interestingly, only one EGR (exhaust gas recirculation) containing experiment was used in the solving of the coefficients. This would indicate that the solved coefficients are weighted more towards conditions not containing EGR. As such, the model could be expected to perform weakly under conditions involving EGR.

Table 2.3: *Floweday's Experimental Design*

Case No.	Pressure(bar)	EGR (%)	Phi
1	30	0	0.75
2	20	0	1
3	20	0	0.5
4	40	0	0.5
5	40	0	1
6	20	40	1

2.3.4 Implementation

Currently , it has been found that most robust implementation of the FGAM is achieved by using forward Euler numerical integration with an adaptive time-stepping procedure [25]. The forward Euler method is an example of an explicit numerical integration scheme, meaning that it is only conditionally stable. Due to the stiffness of the FGAM's system of differential equations, the stability of the forward Euler integration was dependent on the size of the time-step taken, hence an adaptive time step sizing algorithm was included in the method. The adaptive time-stepping algorithm reduces the size of the time-step taken if the projected concentration of any species is negative, such that the minimum concentration of any species is zero. The size of the reduced time-step for each species is found via the following calculation:

$$S + \delta S \times \delta t = 0$$
$$\delta S \times \delta t = -S$$
$$\delta t = \frac{-S}{\delta S}$$

where,

S is the concentration of the species,
δS is the rate of change of concentration of the species,
δt is the time step.

The time-step used in the integration is the smallest one from those calculated for all of the species. An investigation was performed in previous work in trying to implement the FGAM using implicit (unconditionally stable for any time-step size) numerical integration methods such as the backward Euler [25]. Using an unconditionally stable method of numerical integration is desired for applications of previously untested fuels and in-cylinder conditions. The implicit methods were implemented without the adaptive time-step sizing algorithm. It was found that the time step size required for maintaining stability of the implicit method for fuels at conditions validated by Floweday resulted in significantly longer running times than those of the forward Euler method. One of the reasons behind the failure of the implicit integration methods is the non-integer nature of the concentration indices, some of which had magnitudes less than 1. Although it is not physically correct, the concentration of certain species in the FGAM may become negative before feedback from the solving routine shuts down the reaction depleting the species. This is an example of the use of abstract concepts in mathematical models. The adaptive time-stepping procedure avoided the possibility of negative concentrations entirely by reducing time-step size. Implicit methods cannot be implemented with the adaptive time-stepping procedure as they require information from a fixed future point (e.g. the future rate of change) in order to converge to a suitable solution. The adaptive time-stepping routine would continually shift this future point, increasing the convergence time. Since the implicit methods were implemented without the time-stepping procedure, at some point, the concentrations were allowed to become negative due to difficulties encountered in converging to a suitable solution (a suitable solution being one where all of the concentrations have real values). A negative concentration raised to a non-integer index results in complex numbers which can cause many solvers to become unstable. Other more accurate explicit integration methods such as the Runge-Kutta 4th order, which used multiple minor time-steps, were also investigated. However, these methods proved unsuccessful as they were incompatible with the adaptive time-stepping procedure due to their requirement for information at multiple points along the time domain.

Although the temperature at each time step can be solved implicitly according to the

derivation given in section 2.3.2, it can also be solved explicitly using the conservation of internal energy. For internal energy to be conserved, the difference between the starting value and the current value must equal zero:

$$0 = U(T) - U_0 \tag{2.48}$$

where,

$U(T)$ is the internal energy at the new time step,
U_0 is internal energy of the system at the start.

The roots of the above equation can be found using Newton's iterative scheme, remembering that:

$$\frac{dU}{dT} = nC_v \tag{2.49}$$

This results in the following explicit equation for temperature solving:

$$T_j^i = T_j^{i-1} - \frac{U_j(T_j^{i-1}) - U_0}{n_{total}C_{v-mix}} \tag{2.50}$$

where,

T_j^i is the temperature at the current time-step and current iteration,
T_j^{i-1} is the temperature at the current time-step and previous iteration,
$U_j(T_j^{i-1})$ is the internal energy of the mixture at the current time-step, evaluated at the temperature of the current time-step and previous iteration,
U_0 is the initial internal energy of the mixture.

The ideal gas law is used for the derivation of pressure:

$$PV = nR_uT \tag{2.51}$$

2.3.5 Calibration of Kinetic Rate Parameters

The first instance of optimisation of the reaction rate parameters was performed by Floweday during his development of the FGAM. This calibration was performed against the DKM (detailed kinetic mechanism) of Mehl et al. [3], for constant volume experiments of n-heptane, iso-octane, 1-hexene, toluene, methanol and a quaternary gasoline surrogate of iso-octane, toluene, hexane, and n-heptane in the ratio 44/30/18/8% by moles. The average ignition delay error between the FGAM and the DKM for these fuel surrogates ranged from 11% to 23%. The error was calculated as the relative difference between the ignition delay predicted by the FGAM and the DKM.

Perumal [4] developed further sets of reaction constants using the particle swarm optimisation technique for a range of PRF (Primary Reference Fuel) and TSF (Toluene Standardisation Fuel) blends. The calibration was also performed against the Mehl DKM at a constant EGR rate and equivalence ratio. The average ignition delay error of the calibrated coefficients was between 6% and 12% for the PRF blends and between 6% and 15% for the TSF blends. The error was once again calculated as the relative difference between the ignition delay predicted by the FGAM and the DKM.

2.4 Multi-Variable Optimisation Techniques

The FGAM can be fitted to fuels through the minimisation of an error function by adjustment of the kinetic coefficients. Due to the stiffness and complexity of the FGAM, it is possible for the error function to have multiple local minimums as shown in Figure 2.16, especially given the number of coefficients that can be adjusted.

A conventional gradient based solver (a root finding solver which makes use of the derivative of the function, e.g. Newtons method) solver will be able to find the global minimum C if it is initiated in the region around C. If a gradient based solved is initiated around and A or B, it will converge to a solution at one of the two local minimum values. However, this is not to say that gradient based solvers are entirely unsuitable for this problem. If it was possible to ensure that the domain of the root finding function was always nearest to the global minimum, or perhaps the problem was broken into pieces such that only one global minimum existed, gradient based solvers could possibly prove more useful due to their simplicity. In fact, Floweday chose this approach to solve for the kinetic parameters using a standard secant solver by sequentially optimising each equation of the FGAM. The main disadvantage of this approach is additional computational expense encountered when breaking the problem in pieces. A multi-variable solver would be inherently faster due to the effective parallelisation of the optimisation process when compared to a sequential

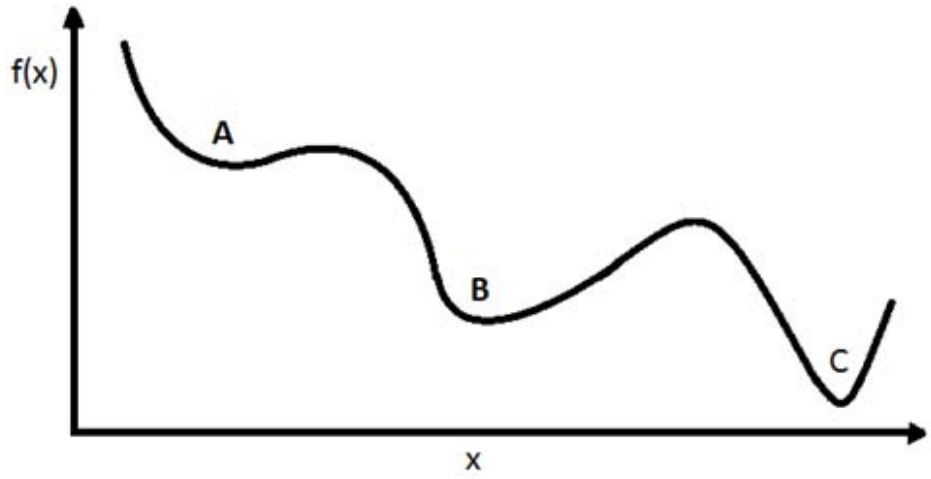

Figure 2.16: *Error function with 2 local minimums (A,B) and 1 global minimum (C)*

solving strategy.

One of the aims of this work is to find a method of robustly calibrating the FGAM which improves upon previously conducted work. The following sections will look at the two most commonly found heuristic (learning) methods that have found application in the optimisation of reaction rate constants in auto-ignition models.

2.4.1 Particle Swarm Optimisation

The basic method of the PSO algorithm as prescribed by Hassan et al. [26] is presented below:

Firstly, a set of possible solutions, called a swarm, is generated on the domain of the error function. Each of these solutions (called particles) in the swarm has knowledge of its position and velocity data. The following loop is then initiated to update the position of the particles:

1. Firstly, the fitness function is evaluated for each particle. This function grades particles closer to the global minimum of the error function as having a higher fitness value.
2. The velocities of the particles are updated so that the particles move toward the current best position in the swarm.
3. The position of the particles are updated according to the new velocities. Following this, the next iteration of the loop is initiated.

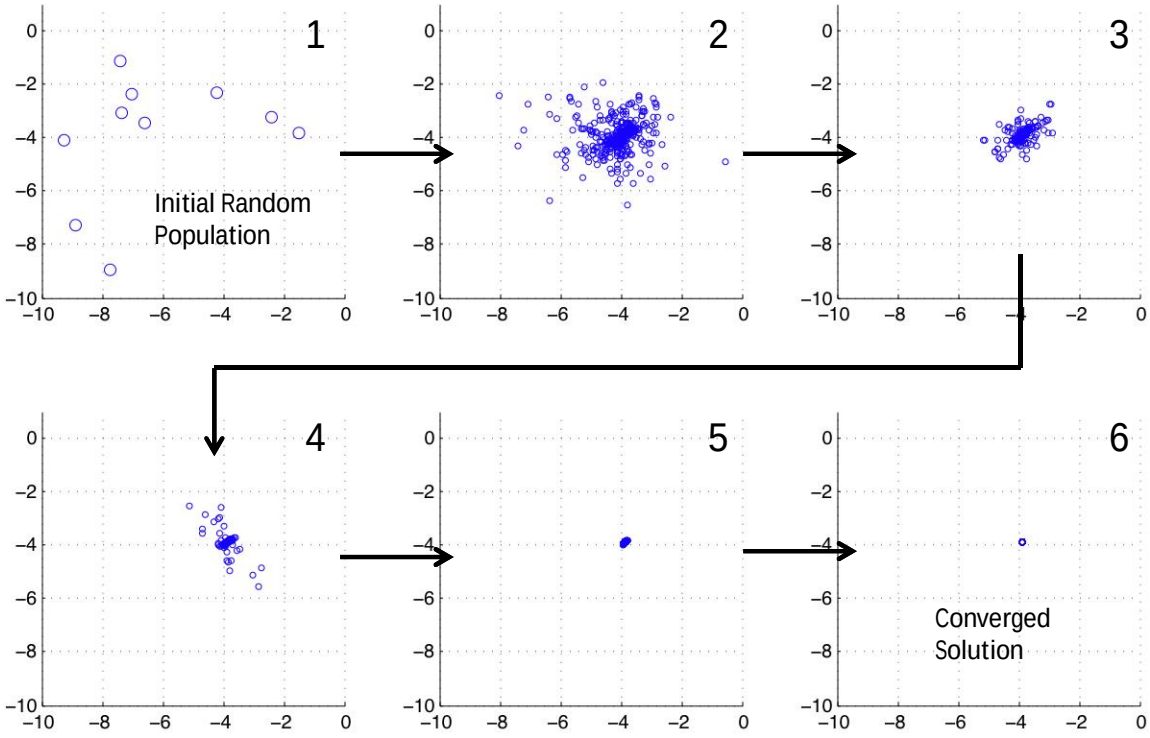

Figure 2.17: *A visualisation of Particle Swarm Optimisation (PSO), adapted from [27]. In frame 1, a set of random points is generated on the chosen domain. Frames 2 to 6 display the movement of the swarm as the particles as the fitness of each particle and the swarm as a whole is evaluated. The number of particles in the first frames is lower than that of the subsequent frames as some particles are outside of the chosen domain range. Note that for the PSO method, it is possible for the all of the points in the swarm to converge on a single solution.*

The loop is exited when either the points converge to a global minimum of the error function, or the chosen number of iterations has been exceeded. A visualisation of the process is given in Figure 2.17 adapted from [27]. The size of the swarm used is most commonly between 20 and 50 points according to Hassan et al. [26] and Poli et al. [28]. Poli states that dynamic problems which have fitness functions that change with time can prove difficult to solve with PSO due to the nullification of the previous generation characteristics of the particle. In addition, it is mentioned that PSO algorithms tend to converge to optima within the initialisation region, especially if this regions is smaller than that of the search space. Genetic algorithms, which are presented in the next section, overcome this limitation through a step called mutation.

The equation which governs the new velocity of the particle as found in Hassan et al. [26] is:

$$\vec{v_{k+1}^{i}} = w\vec{v_k^i} + c_1 r_1(\vec{p^i} - \vec{x_k^i})/\Delta t + c_2 r_2(\vec{p_k^g} - \vec{x_k^i})/\Delta t \tag{2.52}$$

where,

$\vec{v_{k+1}^{i}}$ is the new velocity of the particle,
w is the inertia of the particle,
$\vec{v_k^i}$ is the original velocity of the particle,
r_1, r_2 are random numbers between 0 and 1,
$\vec{p^i}$ is the best position found by the particle at the time,
$\vec{p_k^g}$ is the best position found by the swarm at the time,
$\vec{x_k^i}$ is the current position of the particle,
c_1, c_2 are the constants which relate the confidence that the particle has in itself to the confidence that the particle has in the swarm.

The three constants terms in the equation above, namely c_1, c_2 and w usually range between 0.4-1.4, 1.5-2 and 2-2.5 respectively. Venter et al. [29] states that the parameters c_1, c_2 and w are largely problem dependent, and that, for example, the modification of the inertia parameter w can significantly impact the convergence speed of the algorithm. Both Venter and Hassan had to modify these parameters from suggested/commonly used values in order to suit their individual problem.

As mentioned previously, this optimisation technique was implemented successfully for the FGAM by Perumal [4] for PRF and TSF blends. The model was optimised against auto-ignition behaviour predicted by the detailed kinetic mechanism developed by Mehl et al. [3], by minimising the area between the temperature time traces of the DKM and FGAM simulations. The conditions under which the calibration was performed included pressures from 10 bar to 40 bar and temperatures from 600 K to 1200 K. The equivalence ratio and exhaust gas dilution ratio were kept constant at 1 and 15% respectively. The average error margin of the FGAM using the optimised kinetic parameters lay between 6-15%. This is an improvement upon the Flowedays average error between the FGAM and DKM of 11-23%. However, it should be noted that this optimisation was performed for a single equivalence ratio and EGR rate, and such an improvement should not be expected when calibrating the model for a wider range of conditions. No mention is made as to the weightings used for the particle velocity calculation.

2.4.2 Genetic Algorithms

Genetic algorithms appear similar to particle swarm optimisation; however, they have fundamental differences with regard to data selected by the solver for each iteration. This

can be illustrated through the basic method given in [30]:

As with particle swarm optimisation, a set of solutions, called a generation, is generated in the domain of the error function. Each solution (called a parent) of the generation has knowledge only of its location. The following routine is then initiated to converge to a solution:

1. The fitness of the parents is evaluated.
2. A selection process takes place which chooses the parent which will breed in order to form the children of the new generation. There are a number of different methods by which this selection process can take place. Three common selection methods, taken from [31], have been given below:
   - **Elitist**: the parents with the best fitness value are guaranteed to be chosen.
   - **Roulette wheel**: the fitness of the population is summed until its value exceeds that of a randomly generated limit, at which point the prevailing parent is chosen for breeding. The parents with better fitness have a higher likelihood of being chosen, but it is not guaranteed.
   - **Tournament**: a subgroup is selected from the population, of which, the fittest member is chosen for reproduction.
3. In an attempt to ensure that the parents of the next generation of the cycle have a better fitness value than the current parents, crossover is initiated. Crossover facilitates combination of the best characteristics of the current set of solutions so as to propagate the features of good surviving designs in the next generation. At its simplest, crossover combines the characteristics of the parents on either side of a crossover point in order to create a child as shown in Figure 2.18:

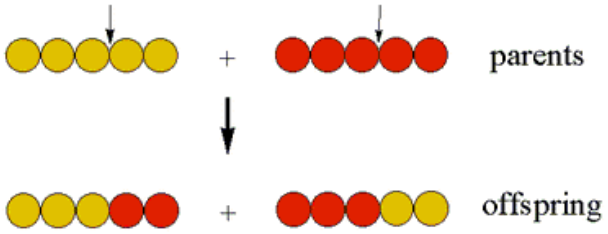

Figure 2.18: *A simple crossover process which combines the different characteristics of each parent on either side of the crossover point in order to create a child. Adapted from [32]*

4. The final process is called mutation. This process allows for searching of the global space of the error function in order to ensure that this solver is not converging to a local minimum. This can be achieved by either introducing a randomly generated solution set, or by modifying specific parameters of the newly formed children. The choice in this regard is problem dependent.

5. The newly formed offspring then either replace those parents in the current generation who have poor fitness, or can be used to form an entirely new generation.

As with PSO, this iterative process is completed when either the population converges to a solution or the maximum number of iterations is reached. This heuristic method is most commonly used in work of the same nature as this research, i.e. optimisation of kinetic parameters of reaction rate based auto-ignition models. Hamosfakidis and Reitz [33] successfully used this method to improve the useful temperature and pressure range of the Shell model. This optimisation was performed as part of an investigation into combustion in diesel engine environments. As such, the kinetic parameters of the model were only optimised for n-heptane and tetradecane, two diesel surrogate fuels. The conditions under which the optimisation was performed ranged from an equivalence ratio of between 0.5 and 4.0, a pressure from 40 to 120 bar and a temperature between 650 K and 1175 K. In addition, dilution from recycled exhaust gas ranged between 0-75%. The authors made changes to the structure of the Shell mechanism before initiating the optimisation process. The model was optimised against curve fits of CHEMKIN®predictions at constant pressure and enthalpy of the n-heptane mechanism developed by Curran et al. [34]. The error bound of the Shell model prior to the optimisation was as high as 56% in under certain conditions. The optimisation process decreased the average error to just 11%. This is however a comparison of a peak error value to an average error value - and it is therefore possible that one of the error values used in the calculation of the average error could have been as large of the peak values prior to optimisation. No description is given as to the specific operations used in the genetic algorithm.

Toulson et al. [35] also used genetic algorithm searching to optimise the twenty-six reaction parameters of the Shell model whilst modelling the auto-ignition of dimethyl ether (DME) in a rapid compression machine. DME is an alternative to petroleum based fuels, specifically diesel, as DME has a high cetane number. The conditions under which the optimisation was performed ranged from an equivalence ratio of between 0.43 and 1.5, a pressure between 10 and 20 bar and a temperature between 615 and 735 K. The range of investigation for this research is considerably smaller than that of Hamosfakidis and Reitz; the chosen upper pressure bound is only 20 bar when modern diesel engine vehicles can have compression ratios approaching 20 [36]. The chosen temperature range is also relatively low, below the point at which DME begins to exhibit NTC behaviour. The model was optimised against experimental data obtained from rapid compression machine (RCM) experiments. RCMs have limited operating ranges, which explains the narrow temperature and pressure range used in this optimisation. Toulson made use of modifications to the original Shell model presented by Hamosfakidis and Reitz [33] and Schapertons and Lee [37]. The modelling took into account heat loss as well as the compression stoke of the RCM. The average error between the experimental data and the optimised model was less than 30%. No description is given as to the specific operations used in the genetic algorithm solving strategy.

Kim et al. [30] implemented genetic algorithm optimisation for a detailed kinetic model for gasoline HCCI combustion consisting of 101 species and 592 reactions, as well as a reduced mechanism consisting of 28 species and 45 reactions for DME. The pressure and temperature conditions under which the optimisation took place were not clearly stated although the temperature can be inferred from one of the ignition delay curves as ranging between 600 K and 1200 K. The DME simulations were performed at an equivalence ratio ranging between 0.07 and 0.26, whilst the gasoline simulations used an equivalence ratio between 0.5 and 1.9. Although improvement was made to the accuracy of these mechanisms which is visible in the various plots presented in the paper, the improvement was not quantifiably stated. The detailed mechanism against which the optimisations were performed was poorly referenced and unable to be investigated further. However, Kim did present insight into the methods behind the GA. At each step, an entirely new population was created from the parents of the old generation.

Of all of the papers mentioned above, only one gave minor insight into the workings behind the genetic algorithm used. The other researchers made use of pre-existing genetic algorithm software. Even so, very little mention is made as to areas of difficulty encountered when implementing a genetic algorithm to solve a reaction-rate-based chemical mechanism. This is of particular concern for the FGAM system as the set of differential equations describing the model is stiff.

In a paper by Whitley [38], the following common pitfalls among genetic algorithms were highlighted:

- The solution space can become dominated by a few members of the population who have good fitness early on. This problem can be addressed with implementation of a selection method that is not fitness based, such as roulette-wheel selection.
- Stagnation of the searching function can occur after multiple iterations as the points converge on the optimum values. This is due to a decrease in variation of the fitness of the points in the population.

Both of these areas of concern highlight the need for an element of randomness in the three main operations of the genetic algorithm. Without the randomisation, dominance and stagnation will occur which can prevent the algorithm from finding better solutions.

It is mentioned by Hassan et al. [26] that genetic algorithms are potentially more computationally expensive when compared to particle swarm optimisation, although this is dependent not only on the problem itself, but also the different methods used to execute the selection, crossover and mutation operations in the case of the genetic algorithm. For example, a tournament selection may help to avoid dominance of a particular solution occurring early on, but the additional computational effort required to rank the members

of the population means that it will be slower than an elitist based selection which chooses only the best members of the population for breeding. A PSO is comparable to an elitist GA as it is only concerned with the particle which has the best position in the swarm, and speculatively, could therefore be viewed as less computationally expensive compared to a tournament selection GA.

2.5 Validation of the FGAM

One of the advantages of the FGAM is supposed to be its ability to fit the auto-ignition behaviour of any given fuel over a wide-range of operating conditions. This is to be achieved through the optimisation of model calibration coefficients. It is therefore important to understand which range of operating conditions is of interest, what type of data is available and what is required in order to fit the model to this data.

2.5.1 Regions of Interest

This section determines which ranges of fuels, temperature, pressure, equivalence ratio and exhaust gas recirculation are most applicable for use in the calibration of the FGAM.

Fuel

Due to the fact that in this work, the FGAM will be tested in regions not previously validated, it would be sensible to use fuels for which auto-ignition data is readily available. In fact, in order to conduct error analysis in the development of the calibration methodology, it is preferable to use fuels for which the model has been partially validated. These fuels are listed below:

- n-Heptane
- iso-Octane
- PRF blends
- TSF blends
- 1-Hexene

- Toluene
- Methanol
- Quaternary gasoline surrogate of iso-octane, toluene, hexane, and n-heptane in the ratio 44/30/18/8% by moles

Temperature

The temperature region chosen for validation needs to allow the fuel to exhibit high temperature, low temperature and NTC behaviour. This will allow for the two-stage fuels to form the characteristic S-curve when plotted on an inverse temperature versus a logarithmic ignition delay curve as shown in Figure 2.7. From the previous literature discussed of section 2.4.1, all of the fuels for which the FGAM has been partially validated display all of the required auto-ignition behaviour in a temperature range between 600 K to 1200 K. In order to further motivate this choice of temperature range, an isentropic relation can be used to estimate the end of compression temperature for spark ignition and diesel engines:

Heywood [39] states that compression ratios range between 8 to 12 for spark ignition engines and 12 to 24 for compression ignition engines. However, the peak compression ratio of 24 is decreasing for diesel engines due to the increased cost of components designed to withstand high peak pressures over components designed for lower pressures. Nevertheless, modern diesel engines still have compressions ratios approaching 20, an example of which is given in [36]. In order to ensure that the temperatures used in the calibration are representative of end of compression temperatures experienced in contemporary internal combustion engines, the lower and upper compression ratios of 8 and 20 will be used in the isentropic relation. Assuming a start of compression temperature of 300K, the maximum possible end of compression temperature for an internal combustion engine is:

$$\begin{aligned} T_{CI,EOC}/T_1 &= (V_1/V_2)^{\gamma-1} \\ T_{CI,EOC}/300 &= (20)^{1.4-1} \\ T_{CI,EOC} &= 994.3K \end{aligned}$$

where,

$T_{CI,EOC}$ is mixture temperature in a compression ignition engine at the end of compression,
T_1 is the starting temperature,
V_1 is the displacement volume,

V_2 is the clearance volume.

Using the same start of compression temperature, the lowest possible end of compression temperature in a spark ignition engine is:

$$\begin{aligned} T_{SI,EOC}/T_1 &= (V_1/V_2)^{\gamma-1} \\ T_{SI,EOC}/300 &= (8)^{1.4-1} \\ T_{SI,EOC} &= 689.2K \end{aligned}$$

where,

$T_{SI,EOC}$ is mixture temperature in a spark ignition engine at the end of compression.

Since hydrocarbons have lower specific heat ratios compared to pure air, the final temperatures actually achieved will be slightly lower than these estimations. However, it can be seen that the chosen temperature range of 600 K to 1200 K includes both of the temperatures derived above.

Experimental devices have limitations regarding their range of use, as seen the research conducted by Toulson et al. [35], where the end of compression temperatures achieved by their RCM ranged between 615 K and 735 K. This is considerably lower than the estimated end of compression temperature for compression ignition engines. As such, Toulson could only validate the low temperature behaviour of DME. Nevertheless, the FGAM can still be validated in regions outside of the testing range of experimental devices using detailed kinetic auto-ignition mechanisms.

Pressure

In order to determine the pressure regions to be investigated, another simple isentropic calculation of the compression of pure air was used. This calculation overestimates the final pressure as it does not take into account heat loss of the specific heat capacity of the fuel. For the upper pressure bound, a calculation will be performed based on the compression ratio of a diesel engine. The same compression ratio values of 8 and 20, used in the temperature calculations, will be used for the pressure calculation. Assuming pure air enters the combustion chamber at atmospheric conditions:

$$\begin{aligned} P_{CI,EOC}/P_1 &= (V_1/V_2)^{\gamma} \\ P_{CI,EOC}/1 &= (20)^{1.4} \\ P_{CI,EOC} &= 66.3bar \end{aligned}$$

Considering that this calculation is idealised and does not take into account any inefficiencies or heat loss in the compression process, a upper pressure bound of 60 bar was chosen for this research. Calculation of the lower pressure bound was performed in a similar manner, using a compression ratio of 8 instead of 20. The lower pressure bound for this work was chosen to be 20 bar.

Recycled Exhaust Gas

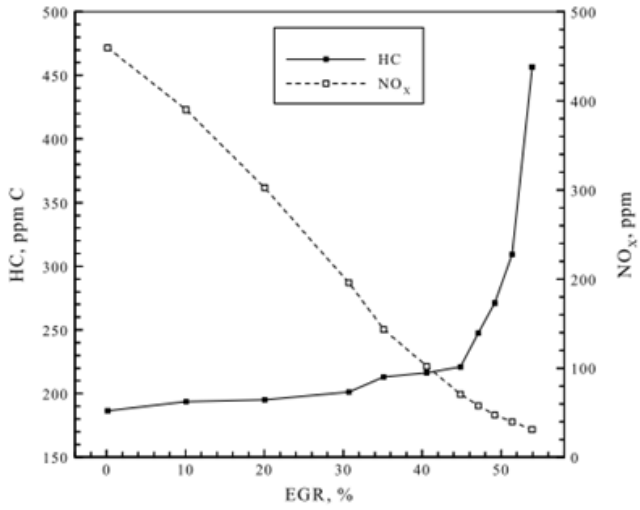

Figure 2.19: *Exhaust gas dilution effects on emissions in diesel engines. Adapted from [41]*

Exhaust gas recirculation is aimed at reducing emissions through the lowering of peak combustion temperatures [40]. The components of the exhaust gas mixture have a higher specific heat capacity compared to the fuel air mixture. This means that more heat is required to raise the temperature of the exhaust gas compared to the fresh charge. The heat released during combustion will therefore results in a lower peak temperature when the air-fuel charge is diluted with exhaust products. Recall from section 2.1.2, the regulated soot and NOx emissions form under high temperatures. The optimum ratio of exhaust gas dilution for spark ignition engines lies between 15 and 30% [40], depending upon the engine's operating characteristics. For diesel engines, an investigation was performed by Wagner et al. [41] into extending the exhaust gas recirculation limits of diesel engines. Figure 2.19 shows the optimum reduction in both hydrocarbon and NOx emissions occurs at just over 40% dilution.

To include ranges in which EGR is beneficial to the emissions characteristics of for both spark and compression ignition engines, a dilution range of between 0-50% will be used for this validation.

Equivalence Ratio

The FGAM has previously not been validated for rich equivalence ratios. Hamosfakidis and Reitz [33] investigated the Shell model for equivalence ratios ranging from a lean value of 0.5 to a super-rich value of 4. The super-rich validation was necessary due to implementation of the Shell model into a CFD code where localised rich regions can occur. This range of equivalence ratios encompasses the upper (UFL) and lower (LFL) flammability limits of the most common fuel surrogates as seen in Table 2.4 [42] [43]. If the FGAM is to become widely adopted so that it may also be implemented into CFD code, validation of the model for this range of equivalence ratios may also be necessary.

Table 2.4: *Equivalence Ratios at the Flammability Limits of Common Surrogate Fuels.*

Fuel	**LFL(%vol)**	ϕ **LFL**	**UFL(%vol)**	ϕ **UFL**
n-heptane	1.05	0.56	6.7	3.77
iso-octane	1.1	0.66	5.64	3.13
toluene	1.2	0.52	7.1	3.57

2.5.2 Experimental Validation

The following sub-section discusses two machines available at SAFL able to provide experimental auto-ignition data, namely the RCM and Shock Tube. Note that in this work, experimental validation of the model has not been performed. This section aims to illustrate the approach that needs to be taken when calibrating the FGAM to experimental data.

It should be noted that for real fuels, the only way to obtain accurate auto-ignition data is through experimental techniques - DKM's are not usually a feasible option for real fuel applications. Surrogates can be used in a DKM, but these would first need to be validated experimentally against there real world equivalent to hold proper value.

Rapid Compression Machine (RCM)

The RCM is similar in nature to an engine which operates for one four-stroke cycle. The combustion chamber is filled with the desired fuel-air mixture, a piston is rapidly ac-

celerated, compressing the mixture, until it comes finally to rest, through the use of a momentum trap. The temperature and pressure seen at the end of compression can be controlled by adjusting the initial temperature of the mixture, introducing dilutants to the mixture or by adjusting the compression ratio of the machine. A schematic of the SAFL RCM that was designed and developed by Everzard [44] is given in Figure 2.20.

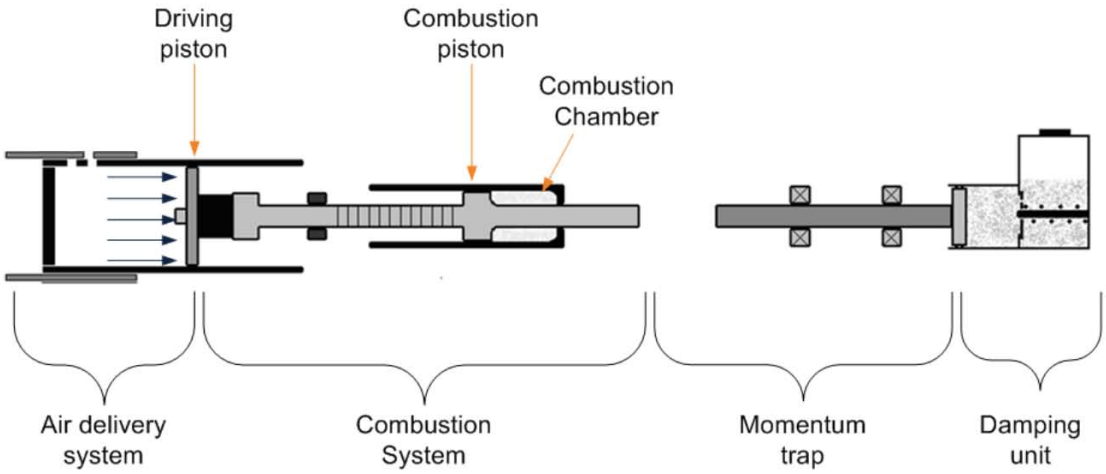

Figure 2.20: *A schematic of the SAFL RCM adapted from [44]. The air delivery system builds pressure to move the driving piston which compresses the mixture in the combustion chamber. The kinetic energy of the combustion piston is transferred to the damping unit via the momentum trap, causing it to come to a standstill.*

The machine requires a fuel with high volatility, with a boiling point in the gasoline range in order to operate. The high volatility of the fuel is needed to keep it suspended in the air, ensuring a consistent fuel-air mixture. This requirement could be circumvented by heating the fuel, but the maximum allowable temperature of the initial mixture is 130 °C. Therefore, fuels with higher boiling points compared to gasoline, such as diesel, cannot currently be used in this RCM. The maximum testing capability of parameters of the machine are given in Table 2.5.

Table 2.5: *Maximum Testing Capability of SAFL RCM*

Parameter	Maximum Value
Initial Temperature of Mixture	403 K
Initial Pressure of Mixture	1 atm
Compression Ratio	18

Figure 2.21, is an example of the type of data recorded during rapid compression machine experiments. The experiment was performed at a compression ratio of 16, with a distinct ignition delay, occurring between the end of compression and the main heat release. From Figure 2.21, it can be seen that the pressure trace from the end of compression until ignition, i.e. the ignition delay, contains noise. The pressure trace from the RCM would need to

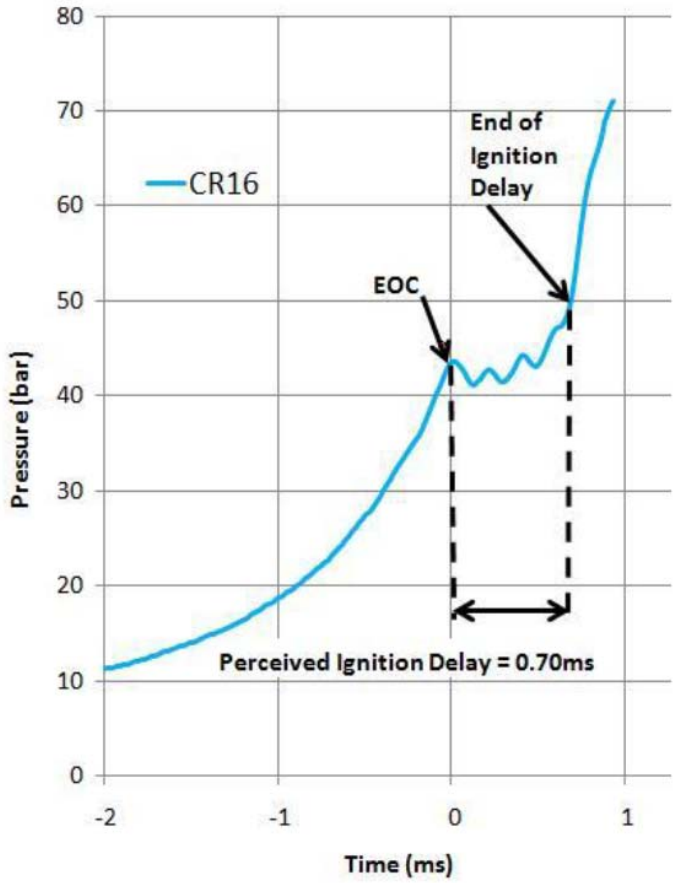

Figure 2.21: *Pressure trace obtained from RCM experiment for n-heptane at 1 bar, 318 K and* $\Phi = 0.4$*, adapted from [45]. EOC indicates end of compression. The compression ratio used was 16:1 and the ignition delay recorded was 0.7 milliseconds.*

be smoothed prior to the commencement of the calibration process in order to allow for recognition of key low temperature auto-ignition behaviour. When trying to fit the FGAM to this data, either the pressure readings from the RCM can be converted to temperature through assumption of the ideal gas law, or alternatively, the FGAM's temperature traces can be converted to pressure traces. A compression model would need to be incorporated when trying to model the ignition delay in an RCM due to the fact that it is possible for the ignition delay to complete during the compression period, depending on the state of energy of the mixture.

Shock Tube

Shock tubes are used to measure very short ignition delays which occur at high temperatures and pressures. The device is limited to measure ignition delays equal to or shorter than 5 ms [46]. At its most basic, a shock tube is a long tube separated into two parts, a

driver and driven section, by a diaphragm or piston. On the driver side of the diaphragm, high pressure gas is stored, whilst on the driven side, the fuel-air mixture is stored. When the diaphragm is burst (or the piston is displaced), the high pressure gas moves toward the driven section, creating a shock wave which compresses the fuel air-mixture. A schematic of the SAFL shock tube designed and developed by Downey [47] is given in Figure 2.23. Notice the SAFL shock tube uses a piston to separate the driver section from the driven section, with the aid of a supply of compressed gas. The compressed air forces the auxiliary piston to seal the actuating chamber, which itself contains sufficient pressure to ensure that th
al
tu
th
ac

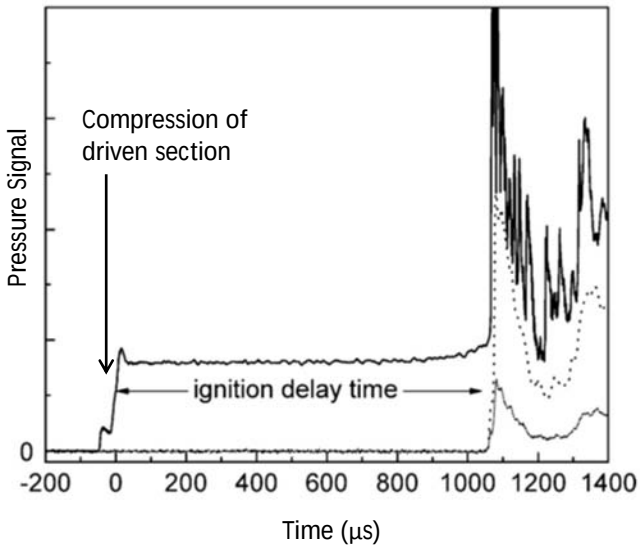

Figure 2.22: *Gasoline/air ignition data collected from a shock tube. Adapted from [48]*

An example of the output of a shock tube experiment is given in Figure 2.22. Note its similarity to the RCM pressure trace in Figure 2.21, barring the compression phase. The compression in the shock tube occurs on a much shorter time scale when compared to compression in a RCM. In fact, due to the rapidity of the compression in a shock tube, it can more than likely be ignored in the modelling process. As with the trace from the RCM trace, the signal from the shock tube will require smoothing prior to use for calibration of the FGAM.

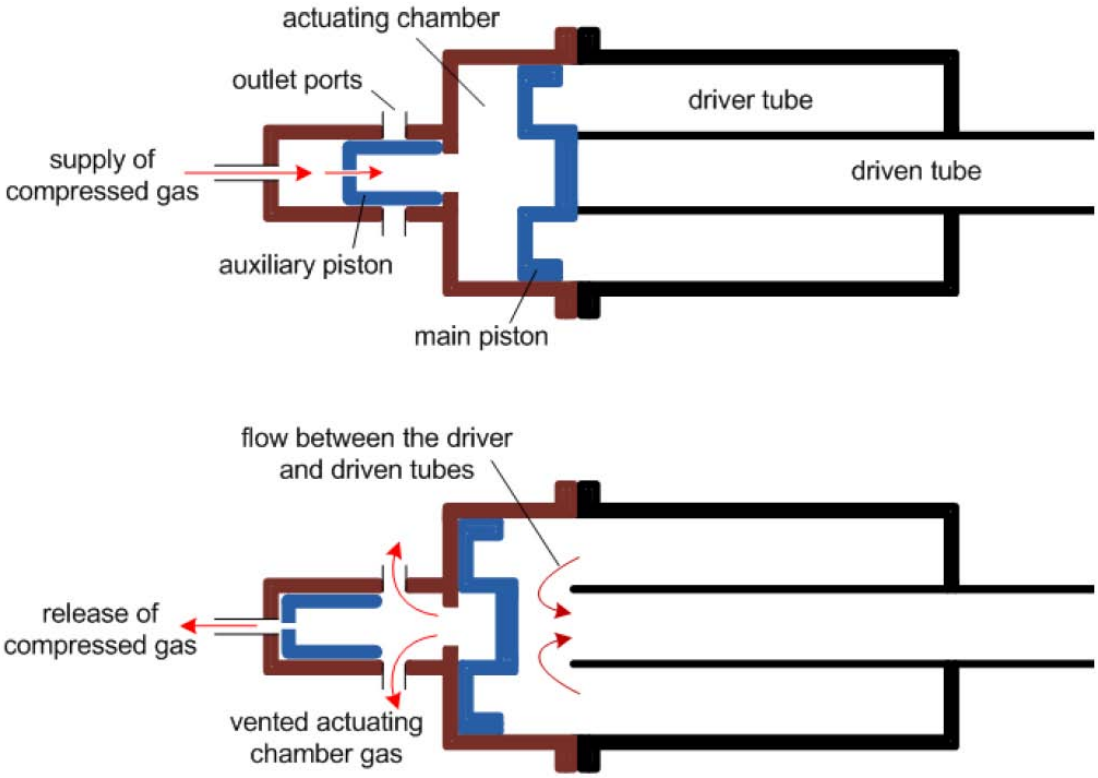

Figure 2.23: *A schematic of the SAFL shock tube adapted from [47]. The top schematic shows the shock tube in with the driver and driven section separated by the main piston. The bottom picture demonstrates the gas flow when the pressure from the supply of compressed air is relaxed.*

Table 2.6: *Operating Capability of SAFL Shock Tube*

Parameter	Tested Range	Potential Range
Test Temperature	973 K	1518 K
Test Pressure	27.1 bar	20 bar
Ignition Delay Duration	1.3 ms	0.9 ms

2.5.3 Validation Against Other Models

Detailed Kinetic Mechanisms(DKM)

In a paper by Griffiths [23], it is mentioned that it is preferable to validate a reduced kinetic mechanism against a detailed kinetic mechanism rather than directly against experiments. The reason for this ideology developed from the need for the reduced mechanism to be as robust as possible, which requires validating it for as many different types of practical systems and as wide a range of conditions as possible. Detailed mechanisms are able to produce data for a relatively large range of auto-ignition experiments compared to the limited operating windows (as discussed in the previous section) of the experimental apparatus. A RCM is able to perform low temperature ignition delay experiments until the temperature becomes high enough that the ignition delay becomes too short to measure. The shock tube is able to operate at high temperatures, with the maximum possible ignition delay measured determined by the length of the tube. Therefore, in order to collect enough experimental data points to generate a full S-curve for two-stage fuel ignition delay, as shown in Figure 2.7, a combination of data collection from the shock tube and RCM is required. However, it should be noted that there are difficulties associated with the combination of data from multiple machines due to differences in heat loss characteristics and other factors which affect the heat release rate of an auto-igniting mixture. These factors, along with the ever present variances that occur between identical experiments, may result in an ignition delay curve which does not follow the characteristic S-curve, in the case of a two-stage fuel, due to the fact that it uses data from both machines. Alternatively, running a set of experiments using a detailed kinetic mechanism will produce a well formed "S"-curve, and because the mechanism can be chosen to work for a wide range of fuels, it does not encounter the same operating restrictions as the physical apparatus.

Floweday [1] and Perumal [4] both used the detailed mechanism developed by Mehl et al. [3] for the purposes of model validation. The Mehl mechanism is applicable to gasoline surrogates, namely PRF mixtures (including pure iso-octane and pure n-heptane), 1-hexene and toluene. Hamosfakidis [33] made use of the mechanism developed by Curran et al. for n-heptane oxidation. Curran et al. also developed a detailed mechanism describing iso-octane auto-ignition [49]. Since the Mehl mechanism allows for ignition prediction of mixtures rather than the single component surrogates and is a newer DKM from the same research group which developed the Curran n-heptane mechanism, it was chosen as the DKM against which the FGAM would be optimised for this research.

Floweday noted that discrepancies between the Mehl [3] and Curran [34] mechanism for prediction of ignition delay for n-heptane auto-ignition can be as large as 38% under certain conditions. Instinctively, the Mehl mechanism may be thought of as the less accurate of the two in this case since it will have had to compromise on its structure to ensure a

good fit for across the range of gasoline surrogates, whereas the Curran mechanism is purely focused on n-heptane combustion. However, the Mehl mechanism was published in 2010, whereas the Curran mechanism was published in 1998, meaning that the Mehl mechanism has twelve years of development over the Curran mechanism. Since neither paper quantitatively states the accuracy achieved by each of the mechanism in matching experimental data, the question of which mechanism is more accurate cannot so easily be answered. From this, it is understood that even detailed mechanism are flawed in terms of accuracy, and thus calibrating the FGAM to a detailed mechanism is more of an exercise in investigating the flexibility of the FGAM, than a pursuit of increased model accuracy.

2.5.4 Modelling Tools

CHEMKIN®

CHEMKIN®will be used to solve the detailed kinetic mechanism used in the validation of the model. The code uses a backwards differencing method for time integration incorporating a modified version of a software package called DASPK [50], details of which can be found in Li and Petzold [51]. This modified backward differencing method was likely chosen as it was found to be most robust in dealing with the generally stiff systems of differential equation used to describe most reaction-rate-based models.

GT-Suite

GT-Suite, developed by Gamma Technologies, is a virtual engine/power train platform, for integrated simulations of engines and vehicles. GT-Suite allows for the modelling of various vehicle systems, ranging from electrical control circuits, acoustics, vehicle mechanics, valvetrain kinematics, lubrication and in-cylinder combustion. According to the General and Advanced Simulation and Application Manual [52] provided with the software, there exists three possible methods of implementing the FGAM into the GT-Power engine modelling environment under GT-Suite:

- Using of the provided global reactions templates
- By creating a user subroutine
- Through the use of the MATLAB®/Simulink® coupling with GT-Suite

The creation of the user subroutine requires an Intel Fortran and C++ compiler in order for the created routine to be compatible with pre-compiled components in the software.

The MATLAB/Simulink coupling requires that the end user has access to a MATLAB and Simulink license. This is likely to hinder the widespread adoption of the FGAM in the application due to the increased cost. Using the global reactions templates is the most appropriate method moving forward for the following reasons:

1. This template allows for the use of non-standard reaction rates for auto-ignition models. This is ideal for the implementation of the FGAM into GT-Suite due to the non-standard form of reaction rate 1.
2. The template does not require the user to have access to additional software licenses which can be costly.

The global reactions template is available in two different forms, based on the modelling application [53]. The first, `GlobalReactions` is made for use in exhaust after-treatment applications, whilst the second, `EngCylChemGlobal`, is designed to describe combustion in engine simulations. Figures 2.24 to 2.26 demonstrate the user interface provided in the global reactions templates. The ability for the user to customise the solving process while using these templates is limited. Essentially, the only control given to the user is the entering of the reactions rate equations and solver selection. Use of the adaptive time-stepping forward Euler routine used previously by Floweday and Perumal would therefore not be possible.

Available solvers are:

1. Adaptive RK (Adaptive Runge-Kutta): recommended for non-stiff problems concerning 1 or 2 reactions in which case it is said to be more efficient than the other in-built solvers.
2. BDF (Implicit Backward Differential Formulations): recommended for stiff problems, BDF's use the information at the current time step to predict the variable's derivative with respect to time at the future time step. This future derivative can then be used in numerical integration to predict the future variable value at the future time step.
3. Adpative RK/BDF(Combination of Adaptive Runge-Kutta & Backward Differential Formulations).
4. RADAU (Implicit Runge-Kutta, 3rd/5th order): recommended if all other solvers fail in solving the model.

The solving process can be tweaked by adjustment of the tolerance and step size parameters shown in Figure 2.24 - although not all of the parameters shown apply to each of the solvers

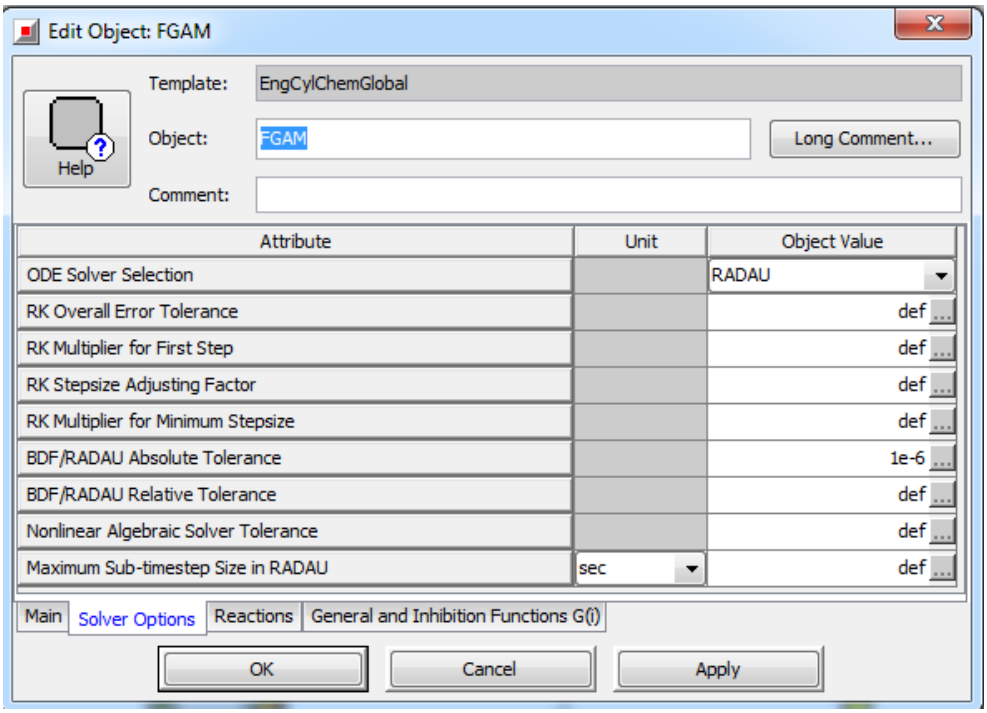

Figure 2.24: *The solver options available in the* `EngCylChemGlobal` *template. Notice the solver currently selected is the RADAU and the absolute tolerance value is limited to the maximum value of* $1e-6$ *recommended by the support team at Gamma Technologies.*

(i.e. the first four options under the solver selection box only apply to the adaptive RK method and therefore do not apply when the RADAU solver is being used). Through correspondence with the support team at Gamma Technologies, it was recommended that the absolute convergence tolerance was not larger than $1e-6$, as shown in the figure, in order to limit the error introduced in the solving process. The convergence scheme used by the built-in solvers was described by the support team as similar to the Newton's iterative solving of the backward Euler method derived in appendix B, thus increasing the convergence tolerance should facilitate faster solving. However, in its current state, the original form of the FGAM was unable to converge to a solution using the most robust RADAU solver. Further increase of the size of the convergence tolerance was deemed as unacceptable due to the loss of accuracy which would occur. Since the FGAM was also not able to be successfully solved by implicit methods implemented in previous work (as mentioned in section 2.3.4), it was obvious that the issues surrounding the solving of the FGAM were attributed to the structure of the model, and not the solvers used. Therefore, one of the main objectives of this work will be to determine, and if possible, correct the source of stiffness which prevents successful solving of the model by implicit methods.

Figure 2.25 is the interface used for entering of the reaction rate expressions and Figure 2.26 is the interface used for entering of non-standard reaction rate terms. From these screen captures, it is seen that the user has minimal input with regard to the solving of the

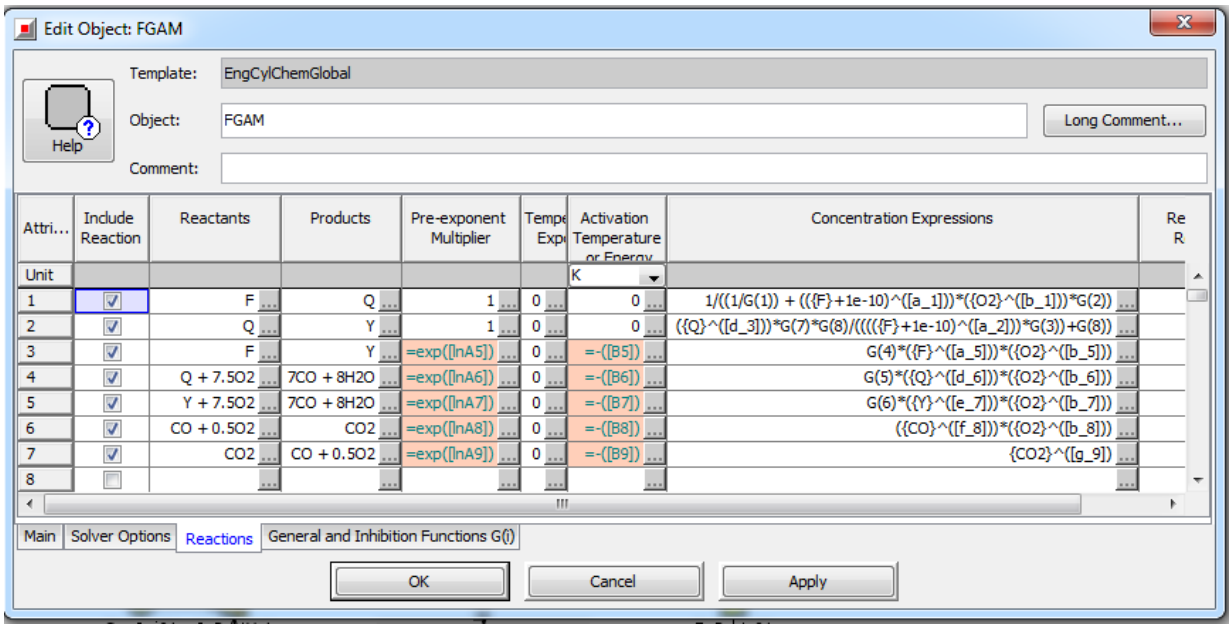

Figure 2.25: *The Reactions tab of the* `EngCylChemGlobal` *template. The G terms under concentration expression are referring to functions in the General and Inhibition Functions tab.*

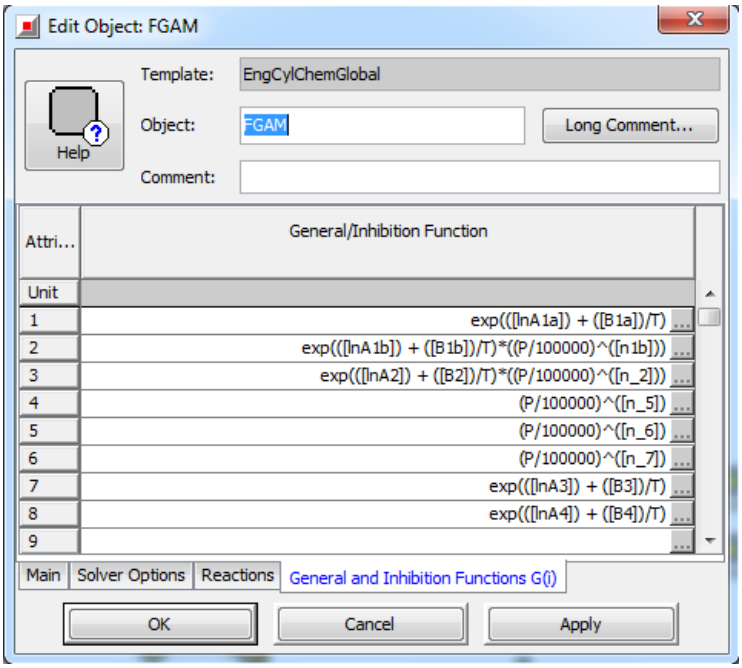

Figure 2.26: *The General and Inhibition Functions tab of the* `EngCylChemGlobal` *template. This facility is used for entering the non-standard reaction rates, and is called from the Reactions tab.*

model when using the global reaction templates. This can be seen as a disadvantage over the other two methods of implementing the FGAM into GT-Suite mentioned above. By creating a user subroutine route or using the MATLAB®/Simulink®coupling, the user would be able to write their own solving strategy for the FGAM. However, this would need to compiled with the solver GT-Suite uses for the rest of the simulation, which would be non-trivial. Furthermore, using one of these alternative methods would mean that the cause of stiffness in the FGAM would not be properly investigated. Addressing the stiffness of the model is key for its wider adoption in the field of auto-ignition research and will serve to streamline the process of implementing the model in future work. It is intended that GT-Suite be used as a test case to show how the FGAM could be implemented in a generic simulation software, therefore, the more generic the implementation strategy, the better.

2.6 Conclusions from Literature Review

The background into the auto-ignition of fuels gives insight into key characteristics and behaviour that needs to be captured by a model such as FGAM. As such, it is important the calibration routine developed in this work improves upon the accuracy of the FGAM with regard to the timing of the cool flame ignition delay, overall ignition delay and the extent of the cool flame heat release. Using a PSO or GA should optimise this process, however, both require a set of seeded values in order to provide a useful solution. Additionally, performance of the FGAM with regard to the effects of EGR and equivalence ratio on ignition delay needs to be thoroughly investigated since the model has not yet been validated in regions of rich equivalence ratio, and previous work has involved fixed or little variance in EGR rates. For this work, the validation of the FGAM will be performed against the DKM of Mehl et al. [3], and the same validation technique can be used when fitting the FGAM to experimental data in future work.

Currently, the FGAM has only been successfully solved using a forward Euler integration method with an adaptive time-stepping procedure. In previous work [25], difficulties were encountered in implementing the model with implicit integration methods without the use of the adaptive time-stepping procedure. Therefore, one of the main areas of focus when investigating the stiffness of the model will be to pinpoint the cause of failure of the implicit methods. Addressing this issue could potentially allow for successful implementation of the model in engine simulations in GT-Suite. This is especially critical due to the limited input that the user has with regard to the solving of the FGAM when using the templates provided in the GT-Suite software.

Chapter 3

Investigation into the Stiffness of the FGAM

The stiffness of the FGAM is one of the main obstacles preventing widespread implementation of the model. Stiffness is a common trait for all auto-ignition models due to the fact that certain reactions need to take place at a faster speed than others in order to ensure that the correct behaviour is captured. In addition to this, one reaction in a reduced mechanism between two species can represent hundreds of reactions between hundreds of species in a detailed mechanism. As such, the speeds at which the reactions occur in a reduced mechanism need to be representative of the combined speeds of the reaction pathways in the DKM - increasing the stiffness of the reduced mechanism. The purpose of this investigation is to determine which reaction(s) in particular are responsible for the stiffness of the FGAM.

Since CHEMKIN®, GT-Suite and other engine simulation software use fairly basic BDF type solvers, it is imperative that the FGAM be solvable by such generic solvers, without artificial interventionist techniques. Even if the FGAM was able to be solved by a sophisticated canned solver, it is preferable to address the underlying issues of numerical stability and stiffness to allow for it to be solved by simple solvers.

3.1 Probable Causes of Stiffness in the FGAM

From inspection of the set of kinetic rate parameters for the FGAM derived by Floweday for n-heptane and iso-octane, shown in Table 3.1, it is seen that the order of magnitude of coefficients $A3$ and $A4$ are far greater than any other "A" value in the table (bearing in

mind that the values given in the table are natural logarithms of coefficients, and still need to be raised by base e). This is indicative that these reaction rates are most likely to be the fastest once activated, and the most probable cause for failure due to stiffness. The speed of reaction rate 4 cannot be decreased as this reaction is responsible for the increased post cool flame reactivity. Decreasing the magnitude of reaction rate 4 would result in a longer post cool flame ignition delay period and subsequently a longer overall ignition delay period. Reaction 3 is responsible for controlling the cool flame heat release in order to for the model to adhere to the correct ceiling temperature. Decreasing the magnitude of reaction rate 3 would result in higher ceiling temperatures and an under prediction of the of the final ignition delay. If either of these reaction rates are found to be the source of the stiffness, it may be possible to replace these fast reactions with multiple slower reactions. This should reduce the contrast in speeds of reaction rates in the mechanism and thereby reduce the degree of stiffness seen by the numerical solving strategy.

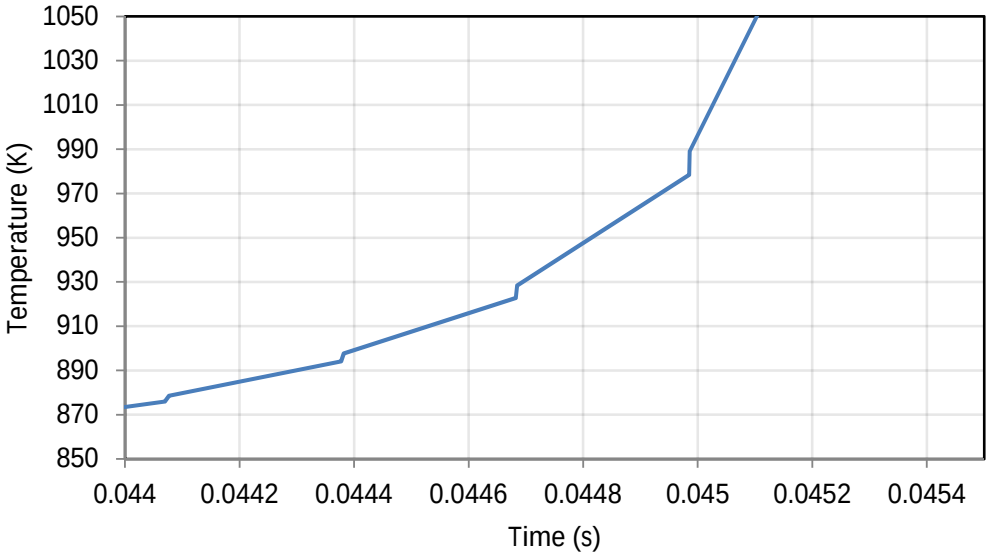

Figure 3.1: *A section of a temperature-time trace produced by the FGAM for iso-octane at 600K, 20bar using forward Euler numerical integration. Notice the steps which manifest as a result of the adaptive time-stepping procedure.*

Currently, the FGAM has been most robustly implemented using a forward Euler numerical integration with an adaptive time-stepping procedure. As mentioned previously, the forward Euler integration is explicit, meaning that it is only conditionally stable, hence the use of the adaptive time-stepping procedure. However, this method of implementation still exhibits some numerical instability, which manifests as a step-like graph profile, shown in Figure 3.1. The adaptive time-stepping procedure limits the minimum value of the concentration of species in the model to zero. This ensures that the solving routine does not encounter imaginary numbers, which can cause a simple integration method such as the

Table 3.1: *Floweday's original kinetic rate parameters for iso-octane and n-heptane*

Coefficient	**n-Heptane**	**iso-Octane**
ln(A1a)	23.09	25.98
B1a	-12300	-14900
a1	-0.14	-0.15
b1	0.922	0.702
ln(A1b)	20.87	20.1
n1b	-2.72	-2.71
B1b	-21300	-15200
a2	0.986	1.191
c2	0.638	0.603
ln(A2)	24.92	22.94
n2	-1.17	-1.17
B2	-8120	-8110
d3	2.853	2.858
ln(A3)	43.66	42.09
B3	-29900	-27800
c4	0.05	0.016
ln(A4)	52.27	37.61
B4	-41300	-24400
a5	0.983	0.927
b5	0.855	0.854
ln(A5)	21.83	21.42
n5	-0.61	-0.58
B5	-17700	-16600
d6	5.92	5.742
b6	0.145	0.166
ln(A6)	26.59	25.53
n6	-0.04	-0.03
B6	-15800	-16000
e7	5.792	3.22
b7	0.141	0.152
ln(A7)	12.42	11.52
n7	1.804	1.804
B7	-13600	-14900
f8	3.823	2.727
b8	0.164	0.229
ln(A8)	17.27	16.92
B8	-12900	-14000
g9	1	1
ln(A9)	21.74	21.39
B9	-44900	-46000

forward Euler to fail.

Once the concentration of a certain species has been reduced to zero, over the consecutive time step, the reactions dependent on these species are shut off. During this time step, these species are allowed to accumulate as the reactions which deplete them are non-functioning. If the species in question is involved in a heat releasing reaction, this accumulation will manifest a steep temperature rise in the next time step, resulting in a step-like graph profile. Due to this displayed numerical instability, it is desired to implement an implicit (unconditionally stable) integration method which does not require the adaptive time-stepping procedure and will thus not exhibit any "step" instability.

As mentioned in the literature review, implementing the FGAM with an implicit integration method has not proved successful thus far. Therefore, an understanding is needed as to the cause of the stiffness in the FGAM which should address the problems with implementation of an implicit solver. Finding the cause of the stiffness may allow for minor modifications made to the structure of the model, such as reducing a single fast reaction into two slower ones, which does not change the model's behaviour, but allows for it to be solved more easily. Reducing the stiffness through a minor structural change will also prove useful when integrating the FGAM into software packages such as GT-Suite and CHEMKIN®, which have built-in solvers. Both the solver used by CHEMKIN®as well as the solvers suited to stiff systems in GT-Suite are implicit.

Implicit solvers are ordinarily much better at solving stiff systems . The particular problem in this case is two-fold; firstly, the non-integer exponents on the concentration terms of the reaction rate equations and secondly, the very small exponents on some of the concentration terms, e.g. $c4$. The non-integer exponents do not allow for momentary negative concentrations, which can occur whilst the solver is converging to a solution. The very small concentration terms result in very small, but definitely non-zero concentration values. The combination of these two effects can cause numerical instability of the solving algorithm rather than instability of the final solution. Any solver should actually work if the time-steps are made to be small enough; what is required is one that solves in a reasonable time.

3.2 Method of Investigation

The standard method of analysing a mechanism to determine the cause of stiffness is by interrogating the Jacobian matrix to see if any elements dominate. Specifically large negative elements on the diagonal can lead to instability. For a normal elementary reactions with the reaction rate given by equation 3.1:

$$\mathrm{RR} = Ae^{\frac{B}{T}}[X] \tag{3.1}$$

the corresponding differential equation for a generic species is given by equation 3.2:

$$\frac{d\mathrm{RR}}{d[X]} = Ae^{\frac{B}{T}} \tag{3.2}$$

The Jacobian matrix for this system is made up of the partial derivatives of the differential equations for each species (given on page 27) with respect to each species in the model. The Jacobian terms corresponding to the individual concentration are relatively easy to compute as they do not contain the concentration values and the temperature sits inside a defined range. For the FGAM, interrogating the Jacobian becomes problematic. Firstly, as the A's and B's change for different calibration fits, so the most volatile element may differ from system to system. Still, for a given set of coefficients, this is not a problem, however, for the non-linear behaviour introduced by the non-integer exponents, the differential equation of a generic species will include concentration terms, as displayed in equation 3.3. Therefore, without running the simulations, it is particularly difficult to determine which term will be the largest.

$$\frac{d\mathrm{RR}}{d[X]} = Ae^{\frac{B}{T}}c_j[X]^{c_j-1} \tag{3.3}$$

An interesting case is where an exponent has a value far smaller than 1. For very small concentrations and exponents, the Jacobian terms can become extremely large. Again though, it is not possible to know before the time how low the concentration will drop and how large the terms will become. It does highlight that such terms may be the source of the problems. An example which exists in the FGAM is reaction 4. In this reaction, the exponent, $c4$, is 0.05 for n-heptane and 0.016 for iso-octane, and therefore, a small concentration of I will cause these terms to dominate in the Jacobian.

In order to determine the cause for the stiffness, the model was implemented using a backward Euler integration scheme whilst monitoring the behaviour of the reaction rates and species concentrations at each time step. The backward Euler method is an example of a backward differential formulation (BDF), such as that used in the GT-Suite global reactions templates. The backward Euler scheme is a relatively simple BDF as it only uses one additional data point for the integration. Comparatively, the RADAU solver also found

in the global reaction templates uses a 3rd to 5th order implicit Runge-Kutta, meaning information is needed at an additional three to five points. If the FGAM can be made solvable for a backward Euler, then it should be solvable by the more sophisticated solver. Forward Euler integration uses the rate of change at the current time step to predict the future position, as per the formula:

$$\vec{S_{i+1}} = \vec{S_i} + \delta t \times f(\vec{S_i}, t_i) \tag{3.4}$$

where,

δt is the time step,
$\vec{S_{i+1}}$ is the future species concentration vector,
$\vec{S_i}$ is the current species concentration vector,
$f(\vec{S_i}, t_i)$ is the rate of change of species concentration vector based on the current species concentration vector and current time.

Backward Euler integration uses the rate of change at the future position to predict the future position, as per the formula:

$$\vec{S_{i+1}} = \vec{S_i} + \delta t \times f(\vec{S_{i+1}}, t_{i+1}) \tag{3.5}$$

where,

$f(\vec{S_{i+1}}, t_{i+1})$ is the rate of change of species concentration vector based on the future species concentration vector and future time.

Obtaining the future rate of change is not a trivial exercise and the method has been included in the Appendix B.

With very small time steps, of the order of one millionth of the ignition delay, the backward Euler integration is able to solve the FGAM. However, using such a small time step means that the FGAM loses its computational advantage over a DKM. The forward Euler algorithm is able to robustly solve the FGAM for a time step size one hundredth of the ignition delay (not including the additional time steps taken due to the adaptive time-stepping procedure). This equates to the FGAM predicting the auto-ignition of a fuel under fifty unique conditions in less than one second. An implicit method needs to come close to this computational performance in order to be useful for the purposes of calibration of the kinetic rate parameters.

Another major reason for implementation of an implicit method is to increase the time-step

size further than the maximum stable size of the forward Euler method, thereby increasing the computational efficiency of the FGAM. When very small time steps are used, the convergence tolerance can be relatively small and the solver is still able to find a good solution because the changes that have occurred to the system between the time steps are relatively small. However, as the time steps are made larger, the changes to the system that occur between the steps are more significant. Due to the issues with stiffness in the FGAM, the iterative procedure of the backward Euler method (described in Appendix B) now takes longer to converge to a solution. One method to overcome this problem would be to increase the size of the convergence tolerance to facilitate faster solving. However, the solver eventually reaches a point at which the time step size is still not large enough for the backward Euler to be computationally competitive, yet the solver is not able to converge to a solution at the current time step inside of the required tolerance.

In order to find the problematic species/reaction rate that causes the stiffness, the convergence tolerance of the solver was relaxed to such that the backward Euler was able to complete its solve of the FGAM, albeit providing an inaccurate solution. The species and reaction rates at this time were monitored. This investigation was carried out for iso-octane at 20 bar, 665 K, 0% EGR and stoichiometric air-fuel ratio. A temperature time trace for

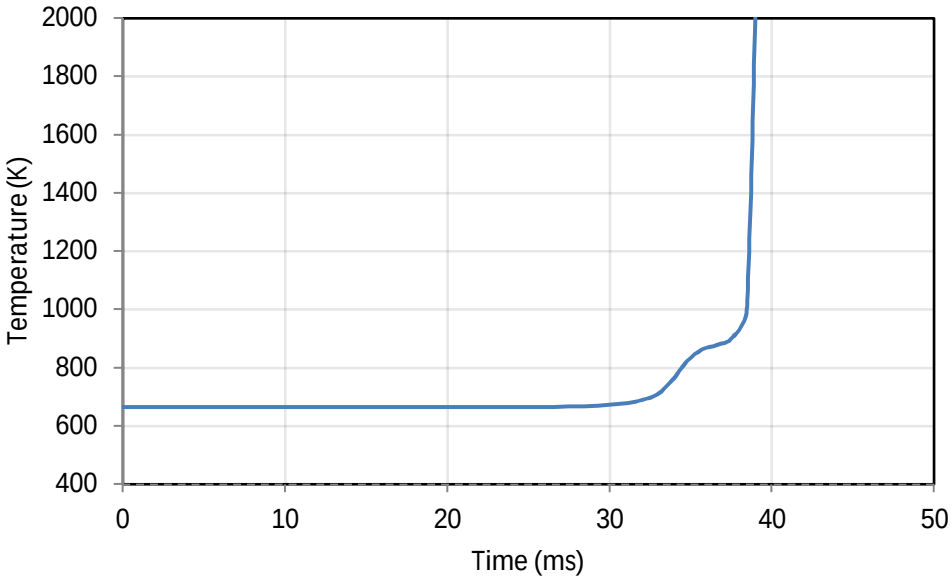

Figure 3.2: *Temperature-time auto-ignition trace of iso-octane at 665 K, 20 bar produced by the Mehl DKM [3].*

In order to more easily identify the source of the problem, the sequence of dominant reaction activations in the FGAM for this condition is given below, with reference to the plots in Figure 3.3 in which the development of temperature and concentration is shown as solved

by the forward Euler method:

1. The fuel is converted into intermediate species I via reaction 1.
2. I is converted to intermediate species Q via reaction 2.
3. The cool flame heat release occurs as Q is converted into CO via reaction 6, reaching a maximum rate at the point at which $[Q]$ is maximum, as displayed in Figure 3.3.
4. After the desired cool flame heat release is achieved, reaction pathway 3 activates. This reaction takes place at a much quicker rate compared to reactions 6 and 2, halting the formation of Q, converting residual Q to I, and ultimately shutting down low temperature heat release. Around this time, reaction 1b cuts off the fuel consumption to the low temperature pathway.
5. The residual of intermediate species in the low temperature pathway, which has by now accumulated at I, as shown in Figure 3.3, is converted to intermediate species Y via reaction 4. Additionally, F is converted to Y via reaction 5.
6. The high temperature heat release then occurs via reaction 7. Reactions 8 and 9 control the peak flame temperature.

3.3 The Source of Stiffness in the FGAM

The point at which the backward Euler integration fails when the convergence tolerance is decreased under these conditions is slightly over 0.034 seconds, or just after the cool flame event. At this time, reaction 3 should have activated, shutting down the feed to Q, and the species remaining in the low temperature pathway are being driven to the high temperature pathway via reaction rate 4. Upon closer inspection of the actual species concentration values, species I seems to have the most difficulty solving at the time of failure. Up until the point of failure, species I carries a small negative concentration, of the order of one hundredth of the initial fuel concentration. The concentration of any species in the model should not become negative due to constraints imposed in the solver. This is therefore indicative of stiffness in the reactions surrounding I. Directly before the failure, species I goes from having a small positive concentration to a large negative concentration of the order of one fifth of the initial fuel concentration. None of the other species in the model exhibited this instability at the point of failure. Corresponding to this relatively large change in concentration of I, was the sudden activation of reactions 2 and 4, which had a combined magnitude twenty times greater than that of reactions 1 and 3 combined. When the feeding reactions are smaller in magnitude than the depleting reactions, this creates

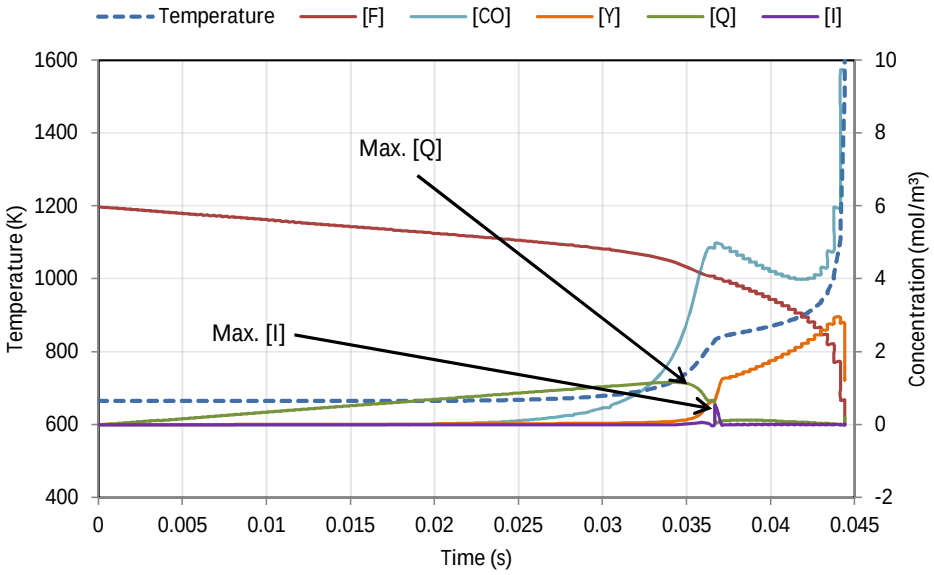

Figure 3.3: *Temperature-time and species concentration traces as predicted by the FGAM using forward Euler integration with adaptive time-stepping for of iso-octane at 665 K, 20 bar. Temperature is plotted against the left vertical axis; the species concentrations are plotted against the right vertical axis. The species O_2, N_2, H_2O and CO_2 were not included in the plot for easier reading of the graph.*

stiffness in the model as the solver has difficulty converging to a point where the species has a sensible concentration value.

Species I is involved in four reactions, the most of any species in the model. The first proposed method of reducing the stiffness of the FGAM was to reduce the number of reactions seen by species I by introducing a dummy species , thereby reducing the complexity encountered by the solver when converging to a solution. This new scheme for the FGAM is presented in Figure 3.5. For reference the original form of the model is included in Figure 3.4. Species I has effectively been split into two parts, species I_1 and I_2, both of which have the same thermodynamic properties as I. Species I_1 acts as a gateway between F and Q via reactions 1 and 2 respectively; species I_2 acts as a gateway between Q and Y via reactions 3 and 4 respectively. Although a dummy species has been introduced, the actual form of the original model has not been significantly altered. The new version is simply a manipulation of the solving of the FGAM in order to reduce mathematical complexity. It is important to not lose any of the original interactions between the reactions in order to ensure that the model has the same level of accuracy as the original form.

However, this revised formulation was not able to solve the problem regarding the stiffness of the FGAM. Since reactions 4 and 2 were of a far greater magnitude compared to reactions 1 and 3, the same problem seen in the original model regarding species I was seen in the revised formulation with species I_1 and I_2. Similar to species J in the QSSA form of reaction

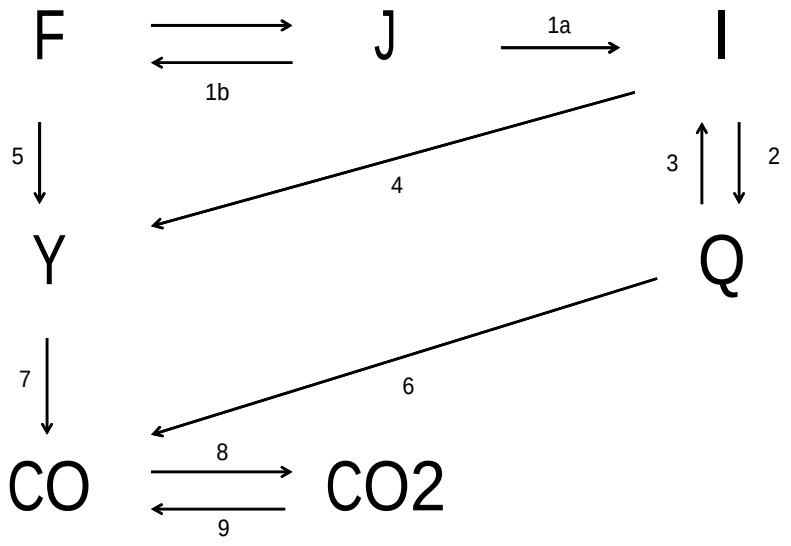

Figure 3.4: *The original form of the FGAM.*

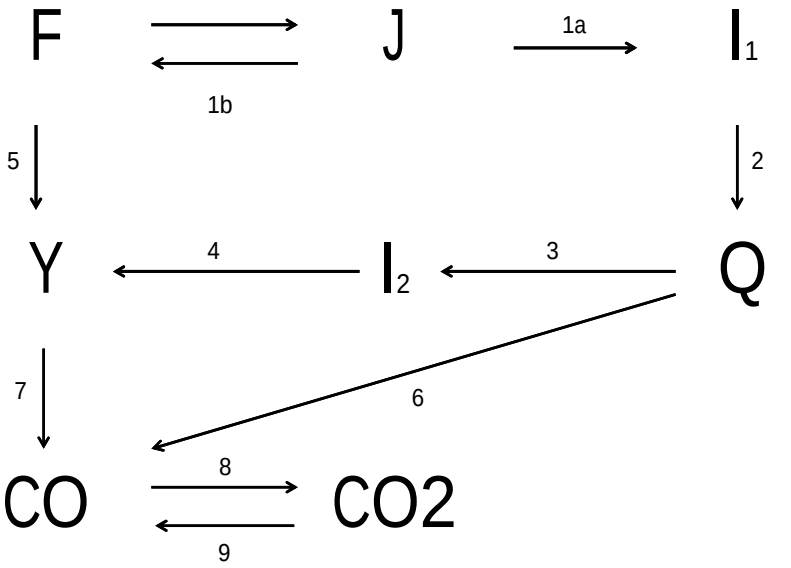

Figure 3.5: *Version 2 of the FGAM which uses a dummy species to reduce the number of reactions involving species I from 4 to 2. The dummy species have the same thermodynamic properties as species I.*

rate 1, species I is difficult to solve for as it is fed by slow reactions and depleted by much faster reactions. Another similarity between species J and I is that the concentration of both species remains relatively small throughout the course of the predicted auto-ignition.

3.4 New Formulation of the FGAM

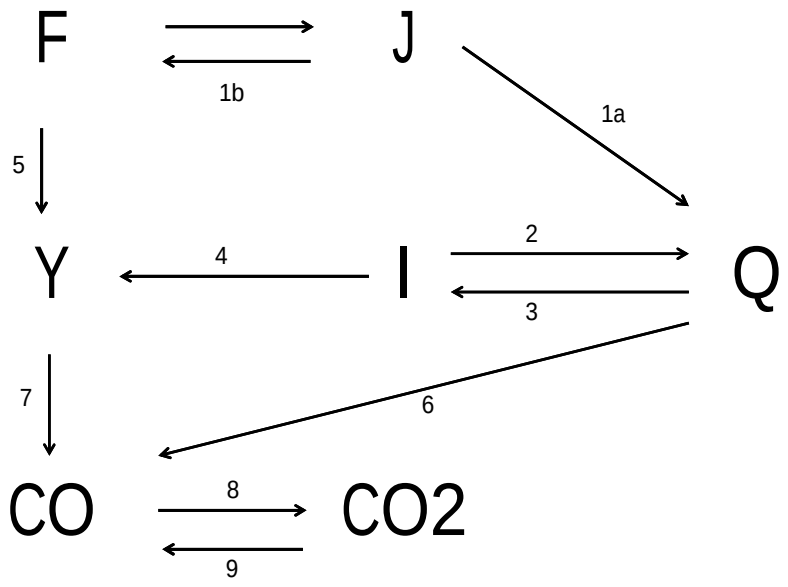

Figure 3.6: *Version 3 of the FGAM. The final modified form of the FGAM which uses a pseudo-QSSA assumption for the reactions 2, 3 and 4.*

The second proposed method of reducing the stiffness in the FGAM is the contraction of species I via a QSSA scheme, similar to that used in reaction rate 1. Since I is actually an accumulation species (and reaches a maximum magnitude), this QSSA scheme, similar to that involving F, J and I, will not strictly follow the QSSA form due to the non-integer exponents.

The interaction between reactions 2 and 3 is responsible for achieving the cool flame ceiling temperature. From the observation made by Floweday presented in section 2.3.1, the cool flame ceiling temperature is dependent on the fuel-air ratio, and for this reason, reaction rate 2 has an included F term. In order to maintain accuracy in the region surrounding the cool flame, which was one of the key development principles for the FGAM, these two reactions need to be preserved in the new formulation. For the most part during the auto-ignition event, species I acts as a gateway between the fuel, F, and species Q, only reaching a significant magnitude in concentration when reaction 3 activates. During the movement of fuel from F to Q via I, reaction 1 is the limiting reaction. Theoretically, a direct link

between F and Q could be made, without the need for the reaction 2 and I. The proposed new form of the FGAM, shown in Figure 3.6, retains all of the original reaction pathways, maintaining their original directions, except for having reaction 1 directly feeding into Q rather than I. Species I will then be involved in a "reversible" reaction consisting of reactions 2 and 3 as well as the fast reaction 4, which will allow for it to be reduced into a QSSA form.

The pseudo-QSSA derivation involving species I is given below:

$$\begin{aligned} RR2 &= [F][I]K_2 \\ RR3 &= [Q]K_3 \\ RR4 &= [I]K_4 \end{aligned}$$

For QSSA, d[I]/dt = 0, therefore:

$$\begin{aligned} RR3 &= RR2 + RR4 \\ [Q]K_3 &= [F][I]K_2 + [I]K_4 \\ [Q]K_3 &= [I]([F]K_2 + K_4) \\ [I] &= [Q]K_3/([F]K_2 + K_4) \end{aligned}$$

Substituting for [I], RR4 becomes:

$$RR4 = [Q]K_3K_4/([F]K_2 + K_4) \tag{3.6}$$

In order to ensure that the original accumulation effect of I was preserved, the concentration indices were preserved. This new form of the model allowed for its to be successfully implemented using backward Euler integration for all of the conditions in which the model was previously validated. The reactions included in this new formulation of the FGAM are:

$$
\begin{aligned}
F &\rightarrow Q \\
I &\rightarrow Q \\
Q &\rightarrow I \\
I &\rightarrow Y \\
F &\rightarrow Y \\
Q + ((x + y/2)/2)O_2 &\rightarrow xCO + (y/2)H_2O \\
Y + ((x + y/2)/2)O_2 &\rightarrow xCO + (y/2)H_2O \\
CO + 0.5O_2 &\rightarrow CO_2 \\
CO_2 &\rightarrow CO + 0.5O_2
\end{aligned}
$$

where **x** and **y** are the number of **C** and **H** atoms in the hydrocarbon fuel respectively. The corresponding reaction rate equations for new formulation of the FGAM are:

$$
\begin{aligned}
RR1 &= 1/(1/K1a + [F]^{a1}[O_2]^{b1}K1b) && (3.7)\\
RR234 &= [Q]^{d3}K_3K_4/([F]^{a2}K_2 + K_4) && (3.8)\\
RR5 &= [F]^{a5}[O_2]^{b5}K5 && (3.9)\\
RR6 &= [Q]^{d6}[O_2]^{b6}K6 && (3.10)\\
RR7 &= [Y]^{e7}[O_2]^{b7}K7 && (3.11)\\
RR8 &= [CO]^{f8}[O_2]^{b8}K8 && (3.12)\\
RR9 &= [CO_2]^{g9}K9 && (3.13)
\end{aligned}
$$

Where the Arrhenius K terms are defined:

$$
\begin{aligned}
K1a &= A1_a e^{B1a/T} \\
K1b &= A1_b P^{n1b} e^{B1b/T} \\
K2 &= A2P^{n2} e^{B2/T} \\
K3 &= A3e^{B3/T} \\
K4 &= A4e^{B4/T} \\
K5 &= A5P^{n5} e^{B5/T} \\
K6 &= A6P^{n6} e^{B6/T} \\
K7 &= A7P^{n7} e^{B7/T} \\
K8 &= A8e^{B8/T} \\
K9 &= A9e^{B9/T}
\end{aligned}
$$

The rate of change of the species in the model:

$$
\begin{aligned}
d[F]/dt &= -RR1 - RR5 && (3.14)\\
d[O_2]/dt &= -(x+y/2)RR6/2 - (x+y/2)RR7/2 \\
&\quad - 0.5RR8 + 0.5RR9 && (3.15)\\
d[N_2]/dt &= 0 && (3.16)\\
d[CO_2]/dt &= RR8 - RR9 && (3.17)\\
d[H_2O]/dt &= (y/2)RR6 + (y/2)RR7 && (3.18)\\
d[CO]/dt &= xRR6 + xRR7 - RR8 + RR9 && (3.19)\\
d[Q]/dt &= RR1 - RR234 - RR6 && (3.20)\\
d[Y]/dt &= RR234 + RR5 - RR7 && (3.21)\\
dT/dt &= \frac{-1}{n_{tot}C_{v-mix}} \sum_{i=1}^{n} \frac{\partial U}{\partial n_i}\frac{dn_i}{dt} && (3.22)
\end{aligned}
$$

Figure 3.7 gives the trace of the important species concentrations for the temperature time trace predicted by the revised FGAM for iso-octane at 665K, 20bar when solved by the backward Euler method. Although there exist minor differences in the species concentration levels predicted by the revised model compared to the original form, the concentration traces predicted by the revised model are still smooth and continuous in shape. This indicates that changes to the structure have not further jeopardised the numerical stability of the model.

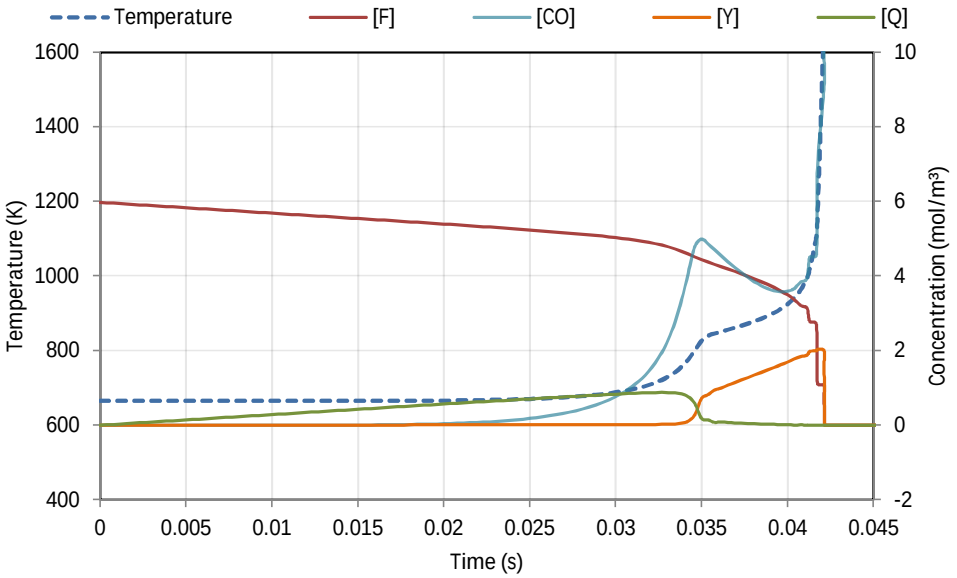

Figure 3.7: *Temperature-time and relevant species concentration traces as predicted by the revised FGAM for iso-octane at 665K, 20 bar when solved by the backward Euler method. Note that the revised FGAM does not include species tracking for I. Temperature is plotted against the left vertical axis; the species concentrations are plotted against the right vertical axis. The species O_2, N_2, H_2O and CO_2 were not included in the plot for easier reading of the graph.*

The modifications did not significantly alter the performance of the model, evidence of which is given in the ignition delay curves for n-heptane and iso-octane in Figures 3.9 and 3.8 respectively. For the ignition delay curves, ignition delay and cool flame ignition delay are plotted against the left vertical axis, and cool flame ceiling temperature is plotted against the right vertical axis. Note that for these plots, the new FGAM used Floweday's set of coefficients for the fuels, and the behaviour of the old and new mechanism can be seen as near identical.

The new formulation of the FGAM performs similarly to the original FGAM for iso-octane (Figure 3.8) with both versions predicting a higher cool flame ceiling temperatures at 665 K (1.5 on the horizontal scale) than the DKM. Single-stage fuels are unaffected by this modification to the model as they only make use of the high temperature pathway (reactions 5 and 7) for ignition delay prediction [19]. Temperature-time traces for the n-heptane at 600 K, 770 K and 1000 K representing the performance of the new formulation of the FGAM in the low, intermediate and high temperature regions have been included in Figures 3.10, 3.11 and 3.12 respectively.

The modification allowed for the model to be successfully implemented and solved in the global reactions templates in GT-Suite, detail of which is provided in chapter 5. Although the original form of the FGAM could be implemented into the global reactions templates, none of the built-in solvers were able to converge to a solution for a single auto-ignition event owing to its stiffness.

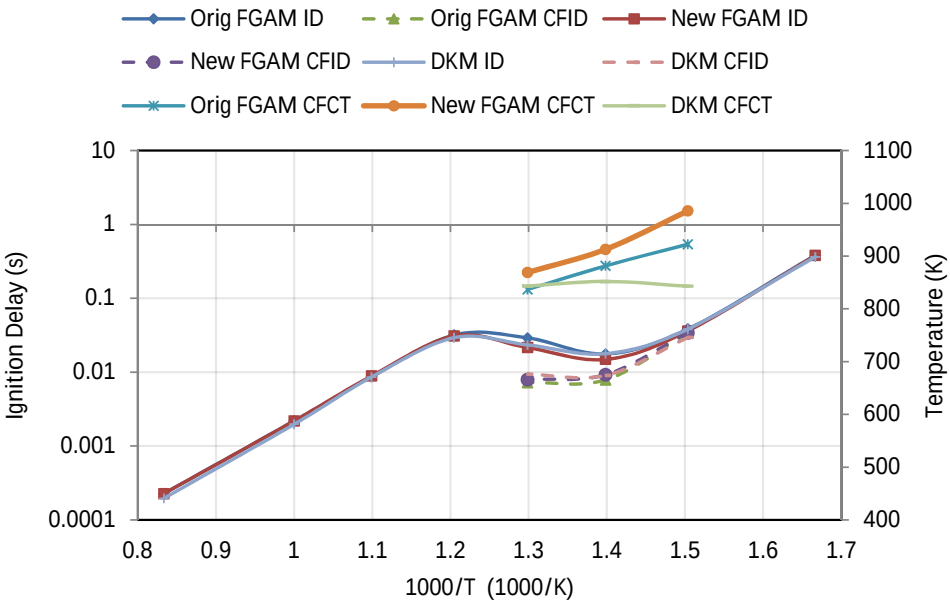

Figure 3.8: *Performance of the new formulation of the FGAM for iso-octane at 20 bar, $\Phi = 1$, EGR = 0%. Notice that both versions (Original and New) of the FGAM perform similarly with reference to the Mehl DKM [3].*

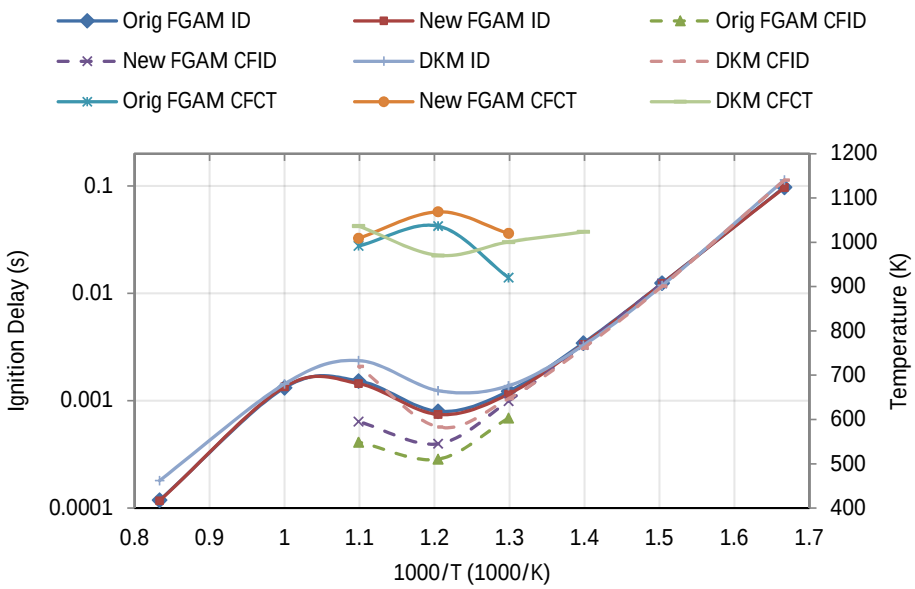

Figure 3.9: *Performance of the new formulation of the FGAM for n-heptane at 20 bar, $\Phi = 1$, EGR = 0%. Notice that both versions (Original and New) of the FGAM perform similarly with reference to the Mehl DKM [3].*

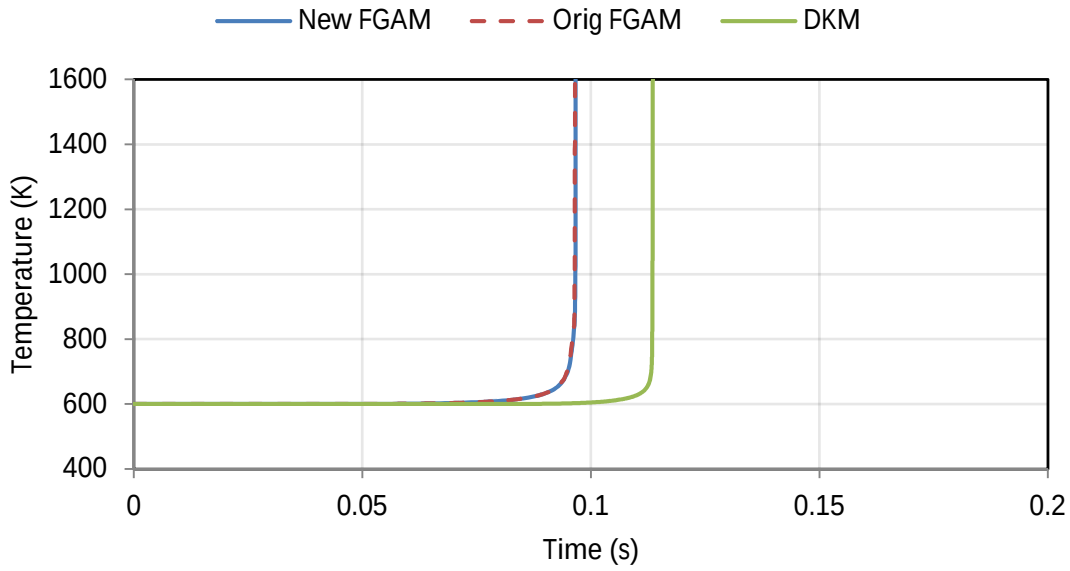

Figure 3.10: *Temperature-time traces of both the original and new formulation of the FGAM against the Mehl DKM [3] for n-heptane at 600 K, 20 bar, Φ = 1, EGR = 0%.*

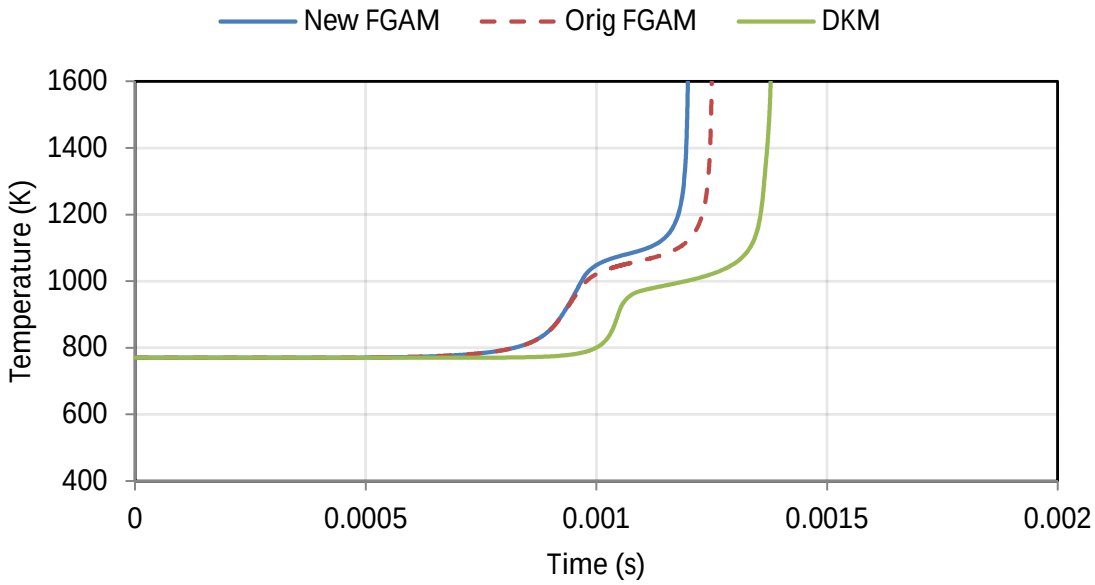

Figure 3.11: *Temperature-time traces of both the original and new formulation of the FGAM against the Mehl DKM [3] for n-heptane at 770 K, 20 bar, Φ = 1, EGR = 0%.*

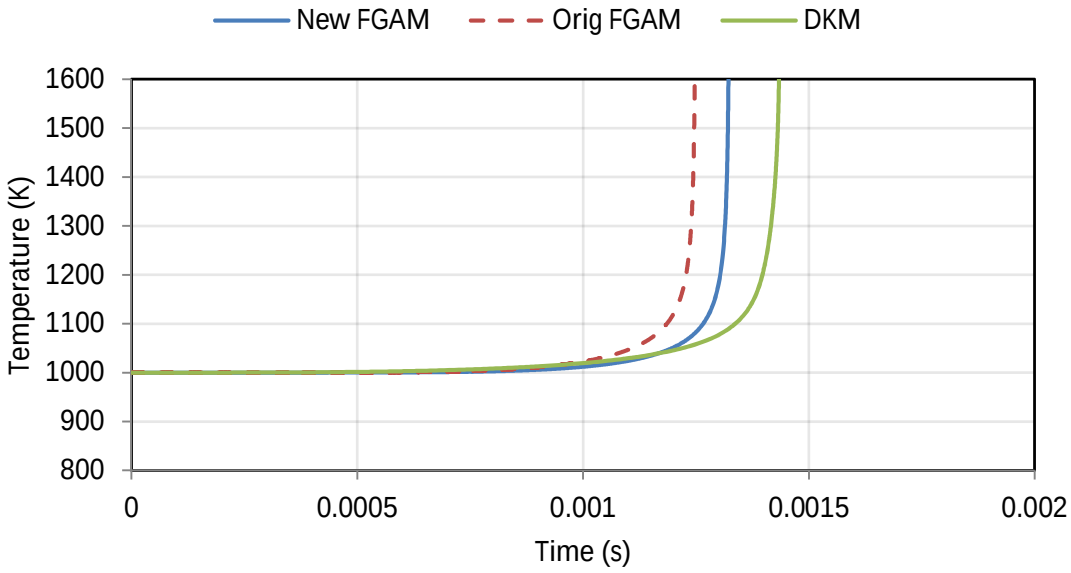

Figure 3.12: *Temperature-time traces of both the original and new formulation of the FGAM against the Mehl DKM [3] for n-heptane at 1000 K, 20 bar, $\Phi = 1$, EGR = 0%.*

3.5 Summary of FGAM Stiffness Investigation

The source of the stiffness in the FGAM was found to be the difficulty encountered in solving for the transient concentration of species I. This problem was overcome by reducing reactions feeding and depleting I in a pseudo-QSSA form. This reduction removed the requirement for calculation of the transient concentration of the species. This new revision to the model allowed for it to be solved by standard implicit Backward Euler integration, something that could not be achieved with the original form of the model (a fact also noted in previous work [25]). Further demonstration of the reduction in stiffness is displayed in chapter 5 where only the revised model was able to be implemented successfully in GT-Suite engine simulations. In order to demonstrate that the introduction of the pseudo-QSSA from had not significantly altered the behaviour of the model, both the revised and original form were benchmarked against the Mehl DKM [3] for two common fuel surrogates, n-heptane and iso-octane. Both forms of the FGAM preformed similarly with respect to the detailed kinetic mechanism. However, it should be noted that the revised form of the model used coefficients calibrated for the original model in these simulations - greater accuracy with regard to the heat release rates and cool flame timing is expected once the coefficients have been calibrated via the process developed in the next chapter.

Chapter 4

Calibration of the FGAM

This chapter describes the methods used in calibrating the FGAM to reference data and discusses the results obtained from the calibration process.

4.1 Development of Calibration Methodology

The FGAM has 40 kinetic rate parameters which can be modified in order to change the behaviour of the model to fit a particular fuel. Modification of these parameters against a chosen fitness function is to be achieved through the use of a multi-variable heuristic solver. This section gives background into the workings of the calibration methodology, from the choice of solver to the defined fitness function.

Although the modifications made in the chapter 3 have made the model easier to solve, these changes have not impacted on the solving process for the kinetic constants. Finding suitable constants using a heuristic solver with a completely random seeded solution is unlikely. Therefore, the heuristic algorithm will make use of the existing set of kinetic rate parameters for the fuels and aim to improve upon them based on the fitness function.

4.1.1 Heuristic Solver Selection

The PSO (particle swarm optimisation) and the GA (genetic algorithm) heuristic solvers were presented in the literature review. In order to determine which solver was best for the application of calibrating the FGAM to reference data, a comparison between the two

solvers needed to be drawn. The challenge encountered with directly comparing these solvers lies with the fact that the GA has numerous options with regard to implementation since each of the procedures used (i.e. selection, crossover and mutation) can be executed by several different methods. In contrast, the PSO has a standard method of implementation, with constants that can be modified to fit the problem, as detailed in section 2.4.1. In order to most fairly represent and compare the performance of both solvers without favouring either one, the GA was implemented using the most straightforward of the most commonly used techniques. This structure was to be amended if it was found that either method far outperforms the other.

The GA made use of roulette-wheel selection; each new generation formed entirely out of combinations selected from the old generation (i.e. no parents will be directly carried through to the new generation). This type of selection method should have prevented the occurrence of domination of good solutions early on. Midpoint crossover was used to combine the genes from the selected parents, where the midpoint was allowed to randomly move along the length of the solution vector. This use of this type of crossover should further help to avoid the dominance of certain solutions early on. Mutation was introduced via the randomisation of a single kinetic constant in the solution vector. For the PSO, the following values for weighting factors c_1, c_2 and w of 2, 2.5 and 0.4 were found to give good results for the for the calibration problem. Each solver was seeded with values 10% either side of coefficients derived by Floweday.

During the comparison of the two heuristic solvers, employing the same fitness function used by Floweday [19] and Perumal [54], it was found that whilst both methods performed similarly to one another, the repeatability of results obtained was poor. Additionally, when allowed to run for over 500 iterations, both methods produced results which smoothed out key low temperature auto-ignition behaviour such as the cool flame temperature rise. As mentioned previously, it is important for the FGAM to maintain accuracy in the regions surrounding this low temperature heat release as this was one of the primary objectives in the development of the model. The cause of this "smoothed" behaviour was found to be the fitness function used in the optimisation process - more detail of which is given in section 4.1.2. Whilst trying to compare the heuristic methods to be used for the calibration, the classic "chicken and egg" situation was encountered. The fitness function was clearly not performing sufficiently which needed to be addressed, but a new fitness function for the problem could not be chosen without a heuristic solver in place. Emphasis also needed to be placed on developing a fitness function which could identify and preserve the required auto-ignition characteristics. Another important aspect of the calibration that needed priority was the analysis of the results post-calibration due to the fact that the FGAM was to be validated in previously untested regions. Therefore, since neither solver significantly outperformed the other, the choice was made to use the PSO for this application due to the uniformity and simplicity of its implementation which would enhance the reproducibility of this work.

4.1.2 Fitness Function

The fitness function will be used to compare the data produced by the FGAM to reference data. During the development of the FGAM, its ability to accurately capture cool flame and NTC behaviour was given highest priority, along with ignition delay timing. In order to maintain this focus, particularly the accurate modelling of the cool flame, the data used in the comparison should be in the form of temperature-time traces in order to allow for comparison of required data.

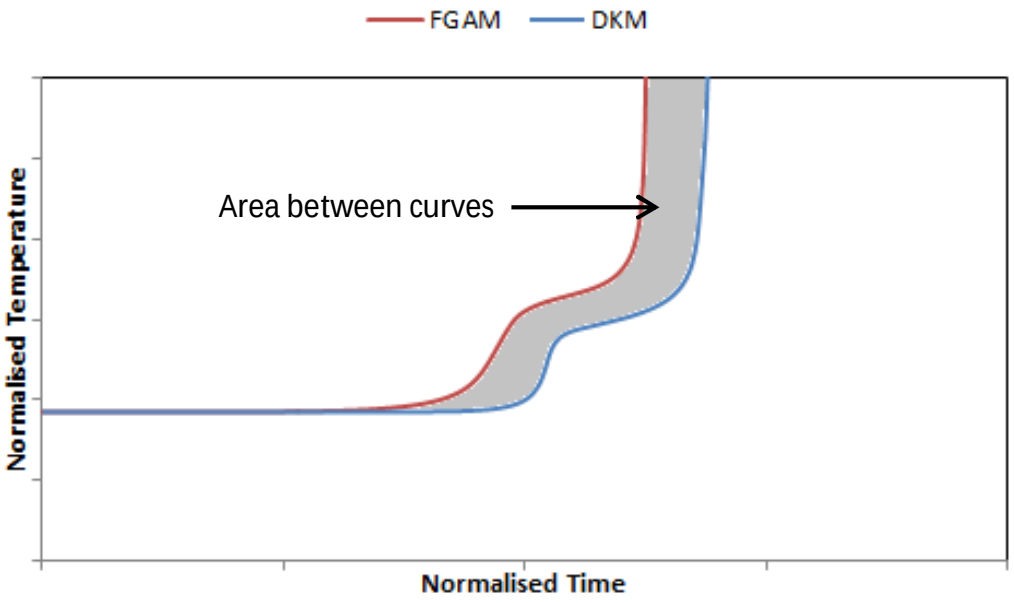

Figure 4.1: *A visualisation of the area between the curves calculated by the Shape-Area fitness function.*

The Shape-Area fitness function will approximate the area between two sets of temperature-time data by calculating the Riemann sum integral, as shown in Figure 4.1. The solution

which has better fitness will result in a smaller area value. Each rectangle in the Riemann sum will be a product of difference in temperature in Kelvin and difference in time in seconds. Due to the rapidity of auto-ignition events, the difference in temperature will be several order of magnitudes larger than the difference in time. Therefore, the time and temperature components of the each piece of the Riemann sum needs to be normalised to prevent the temperature component from dominating the outcome of the calculation. Perumal [4] implemented a normalisation technique which divided the temperature term by the auto-ignition cut-off temperature and the time term by the overall ignition delay. This resulted in the following form of the Riemann sum integral:

$$err = 1/(T_{AI} \times ID) \times \int_{t=0}^{ID} |T_{DKM} - T_{FGAM}|dt \tag{4.1}$$

where,

T_{DKM} is the temperature predicted by the detailed kinetic model,
T_{FGAM} is the temperature predicted by the FGAM,
dt is the change in time,
T_{AI} is the temperature at which auto-ignition is assumed to have occurred,
ID is the overall ignition delay.

This fitness function was used by both Floweday [19] and Perumal [54] in the previous calibration and derivation of the kinetic constants. However, the inherent problem with a Shape-Area fitness function is that it is purely focussed on reducing the error value, without regard for the retaining key auto-ignition behavioural elements. For example, in the case of a well-defined two-stage reference temperature-time trace, it is preferable that the FGAM also predicts well defined two stage auto-ignition trace with a slight error in overall ignition delay timing as opposed to indiscernible two-stage behaviour with a smaller error in overall ignition delay prediction. Due to the structural limitations of the model which restrict its ability to fit all temperature-time traces exactly, the Shape-Area error function will begin to smooth out the effects of significant low temperature chemistry in the pursuit of minimisation of the area between the curves. This "smoothing" was noticed in the comparison of the two heuristic solvers which used of the Shape-Area fitness function.

The low repeatability of results occurred because the Shape-Area function would sacrifice accuracy in one area in order to minimise the total overall area, depending upon which area had greater seeded accuracy. An example of this is shown in Figure 4.2, which demonstrates the optimised curve sacrificing overall cool flame ignition delay accuracy in order to minimise the area between the curves in the post cool flame region. Two unique solutions derived using this fitness function can have the same average error value, with one solution showing good accuracy in the overall ignition delay timing and another displaying

better cool flame heat release accuracy. The fitness function should not sacrifice accuracy in one particular area to achieve greater accuracy in another area. The error should be reduced in all regions simultaneously, else smoothing of key behavioural elements can occur. The Shape-Area fitness function does not have provision for that type of control. These concerns can be addressed by introducing weighting of components in certain temperature and time regions, so as to preserve the chemistry in certain regions. However, since different fuels exhibit different auto-ignition behaviour in different regions, this requires the end user to have detailed auto-ignition knowledge. For this reason, the Shape-Area fitness function was not used in the calibration process.

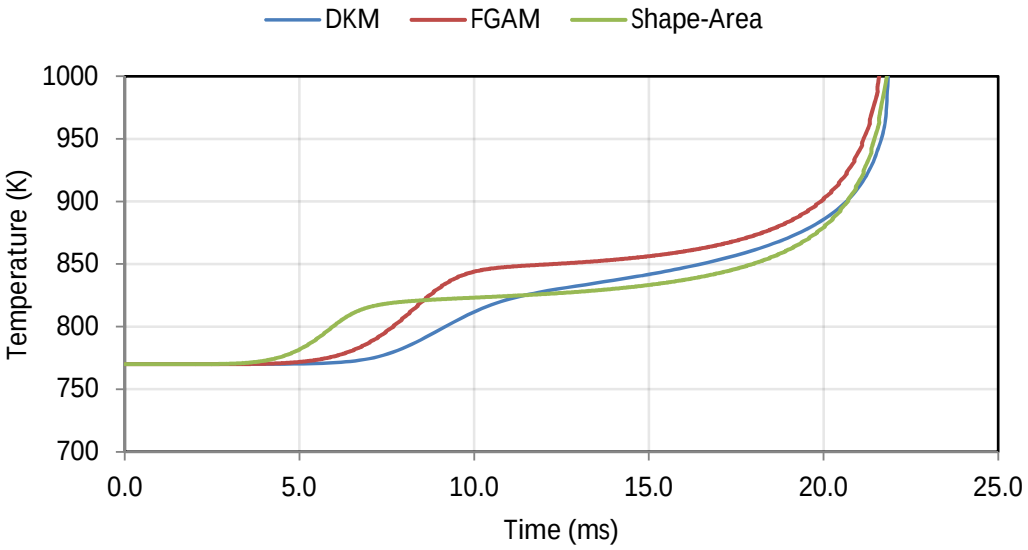

Figure 4.2: *The auto-ignition predictions of the Mehl DKM and the FGAM for iso-octane at 725k, 20bar. For the predictions made by the FGAM, Floweday's original constants as well as a set optimised using the Shape-Area fitness function were used. Notice how the Shape-Area function sacrificed cool flame ignition delay timing in order to obtain a better fit in the post cool flame region.*

Five Point

Due to the fact that the Shape-Area function does not prioritise the importance of the correlation of specific key behavioural events in the model and reference data, poor agreement between the two data sets can occur. Since accuracy in the cool flame and NTC region was one of the main philosophies behind the development of the model, it follows that a suitable fitness function for calibration process should directly compare these behavioural characteristics.

A fitness function has been developed that is based upon the comparison of five key data

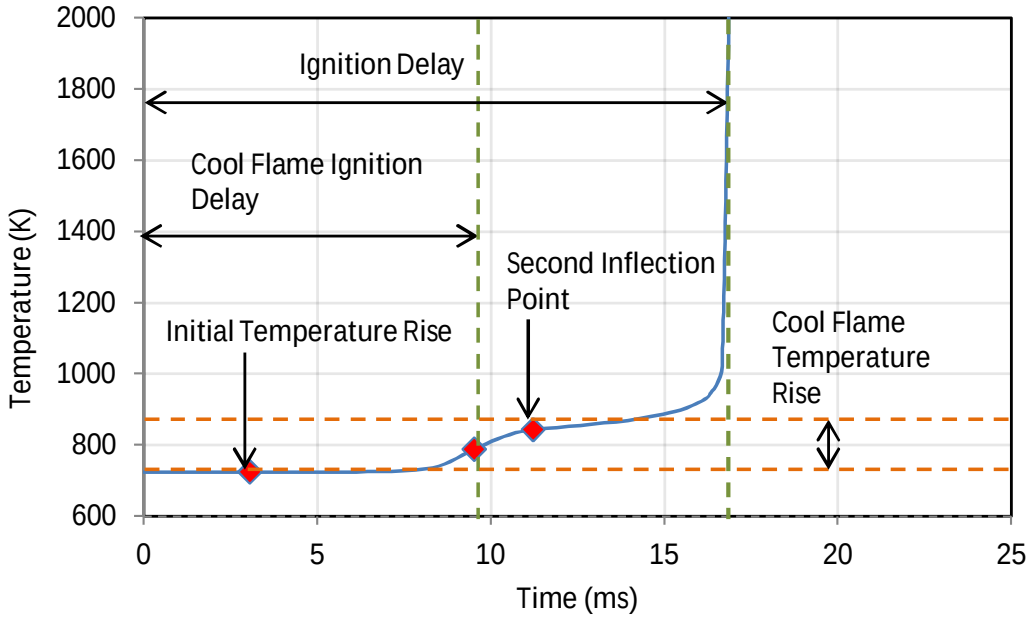

Figure 4.3: *The five data points used in the "Five Point" fitness function*

points typical of any two-stage auto-ignition event. The five points, displayed in Figure 4.3, are described as:

1. **Initial Temperature Rise**: the point at which the temperature has risen 5 K above the starting temperature. Chosen as the point at which the auto-ignition chemistry has activated.

2. **Cool-Flame Ignition Delay**: the point at which the cool flame event heat release rate is at its maximum. During the cool flame event, the heat release initially has a positive slope of increasing gradient, which transitions into an inflection point, after which it moves into a positive slope of decreasing gradient. The inflection point at which the cool flame heat release rate is at a maximum is the chosen point to which the cool flame ignition delay will be measured.

3. **Second Inflection Point**: this is the point at which the cool-flame event has ended and the temperature begins to level off toward the cool flame ceiling temperature. In this region, the heat release begins with the same slope as that which existed at the end of the cool flame event, a positive slope with decreasing gradient. After this point, the mixture is accepted to have settled at constant cool flame ceiling temperature. However, the ceiling temperature is not constant and the heat release in this region has a minor positive slope of increasing gradient. Therefore, the heat release must have undergone a point of inflection to go from a slope of decreasing gradient to a slope of increasing gradient.

4. **Cool Flame Temperature Rise**: the temperature of the mixture subsequent to the cool-flame event but prior to the main ignition event.

5. **Ignition Delay**: the overall ignition delay of the auto-ignition event

For a single-stage auto-ignition event, the comparison will reduce to two-points as the cool-flame ignition delay, second inflection point and cool flame temperature rise data will be inconsequential. The challenge with the implementation of this method is finding a way of identifying these sets of points for an auto-ignition event. In the case of a reaction-rate-based model, this can be accomplished by tracking certain species whose reaction rates or concentrations coincide with certain events. However, data obtained from experimental apparatus is usually on in the form of temperature-time or pressure-time traces. Therefore, a method needs to be derived which can identify these points from temperature/pressure-time data only, making the fitness function applicable for a range of applications. The following methods will be used to determine each of the five points:

1. **Initial Temperature Rise**: This is a relatively simple to identify as the time at which the temperature has increased 5 K above the starting temperature.

2. **Cool Flame Ignition Delay**: In order to monitor the inflections point that occur during the heat release, the second derivative of the temperature with respect to time is needed. The time at which the first instance of the second derivative of temperature is zero after the activation of the auto-ignition chemistry is classified as the cool flame ignition delay.

3. **Second Inflection Point**: Following from the cool flame ignition delay, the time at which the second derivative of the temperature-time trace is zero subsequent to the cool flame ignition delay will be classified as the second inflection point.

4. **Cool Flame Temperature Rise**: The ceiling temperature will be defined as the temperature at the time halfway between the cool flame ignition delay and overall ignition delay. The temperature rise is the difference between the ceiling temperature and the initial temperature.

5. **Ignition Delay**: This is another relatively simple calculation and is the recorded time at which the temperature exceeds the auto-ignition cut-off temperature.

One foreseeable issue with the implementation of this technique is the weightings given to the each of the five points during the evaluation, specifically the events relating to the cool flame. The accuracy of the FGAM for events relating to the cool flame is only desirable in the intermediate temperature regions where the cool flame manifests. Although a very minor cool flame heat release may occur close to the ignition delay at low temperature and

very early on at high temperature, the ability of the model to match these cool flame events in not as useful as matching the easily discernible cool flame events in the intermediate temperature zone. Furthermore, weightings given to the various components of this error function should be based on the importance and usefulness of the data point in question. For this application, the overall ignition delay ranks as the most important event as it is the point at which the main heat release occurs, and was accordingly given a normalised weighting of 1. The next three components from most to least important are the cool flame ignition delay, cool flame temperature rise and second inflection point. Lastly, the initial temperature rise ranks of least importance as it was included in this fitness function purely to indicate the activation of auto-ignition chemistry. The cool flame ignition delay and cool flame temperature rise were given a normalised weighting of 0.5, whilst the second inflection point and initial temperature rise were given a weighting of 0.25.

Another advantage of the Five Point method is that it only requires the five data points, not a full temperature trace for each calibration experiment. These point could even be determined from pressure traces and input directly directly into the calibration code if adequate smoothing cannot be performed on the raw data.

Comparison of the Fitness Functions

Table 4.1 displays a comparison in the average error of the set of kinetic constants optimised by the PSO using the Shape-Area and Five Point fitness functions, against the accuracy achieved by Floweday's original set of kinetic constants for stoichiometric iso-octane at 20 bar with 0% EGR. Figure 4.4 displays to the eight temperatures used in this optimisation. Notice from the table, that although the average error of the cool flame and overall ignition delays is approximately equivalent for both fitness functions, the cool flame temperature rise error of the Shape-Area solution is double that of the Five Point solution. Consequently, the total average error of the Five Point solution is 6.67% less than that of the Shape-Area solution. It should also be noted that the Shape-Area function did not produce a consistent optimisation, always indirectly favouring one particular feature of auto-ignition behaviour. The temperature-time traces presented here show the Shape-Area function favouring the overall ignition delay. In other optimisations, the accuracy in capture of the cool flame temperature rise was favoured, at the expense of the cool flame and overall ignition delay timing. However, the Five Point function was able to consistently reduce the average errors across all of the categories, as per the assigned importance of each of the features discussed in section 4.1.2. From a research based standpoint, repeatability and consistency of experimental results is highly important. Due to the fact that the Five Point function outperformed the Shape-Area function in terms of solution consistency and overall accuracy, it was chosen fitness function to be used in the calibration routine.

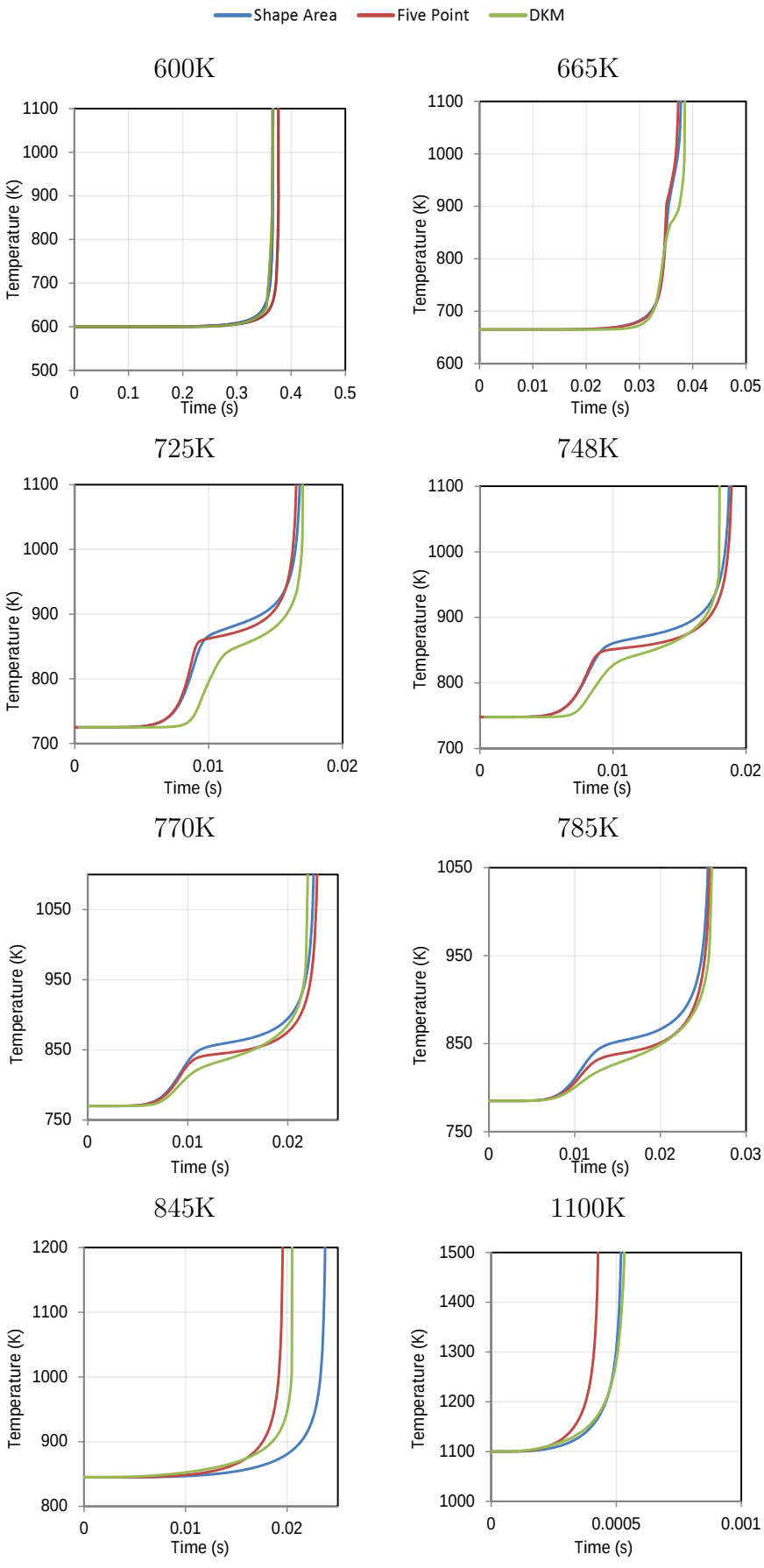

Figure 4.4: *Iso-Octane at 20bar, EGR = 0%, ϕ = 1.*

Table 4.1: *Comparison of Performance of Shape-Area and Five-Point fitness function with a PSO routine*

	Average Error			
	ID	CF ID	CFdT	Average
Floweday	12.12%	14.81%	64.47%	30.47%
Shape-Area	4.04%	3.53%	40.14%	15.90%
Five Point	5.30%	2.55%	19.85%	9.23%

Integration Method

Although the modification to the structure of the FGAM has reduced its stiffness and allowed for it to be solved via implicit methods, the stiffness of the system is still affected by set of kinetic rate parameters. If a particular solution inside a heuristic solver were to have a particularly stiff set of kinetic constants that caused the implicit integration method to crash, the optimisation routine may also crash in this instance. For this reason, the forward Euler with adaptive time-stepping integration will be used as part of the optimisation process due to the fact that it will still be able to evaluate the FGAM regardless of the stiffness of the set of kinetic constants.

4.2 Results & Discussion of the Calibration of the FGAM

Now that the optimisation routine has been shown to work at constant EGR and equivalence ratio conditions, the task moves to fitting a more complete description of fuels. In this section, the results of the calibration of the model to a DKM using the routine chosen in previous section are presented. Prior to the optimisation, a major area of weakness in the model was discovered, which required changes to be made to the experimental design in order to ensure a useful solution set. Following this, the results of the calibration based on the amended experimental design is presented, along with an investigation into the regions where the fit of the FGAM was poor against the DKM.

4.3 Investigated Conditions

In the literature review, the target range of fuels and conditions to be used in the kinetic rate parameter calibration process were presented. Ideally, one set of coefficients would allow the FGAM to describe one fuel for a wide range of pressures, temperatures, equivalence ratios

and EGR rates. However, as more variables are introduced into the calibration process, the achievable accuracy of the model for one specific variable is reduced. Compromises are made by the calibration algorithm in order to reduce the overall error, at the cost of the sensitivity of the model to a specific parameter. The focus of the optimisation process depends on the application for which the model is used. For example, if the EGR introduced into the fresh charge is to be fixed at 20%, it may prove more accurate to use a set of parameters that has been optimised with EGR fixed a 20%, as opposed to parameters which have been derived from an optimisation process which included a variety of EGR rates.

The FGAM has already been partially validated for a number of fuel surrogates; using any one of these fuel surrogates in the calibration process will suffice to demonstrate the possible accuracy increase achieved for all of them through this optimisation. For the development of the calibration routine, the coefficients for pure n-heptane and iso-octane will be optimised. There exists significant quantities of literature detailing the auto-ignition behaviour of these fuels under various conditions which will be useful in the event that the FGAM displays poor performance in previously untested regions. In addition, a set of coefficients will be developed for PRF50 (50% iso-octane and 50% n-heptane) in order to demonstrate that the calibration routine is able to find a good solution for a fuel without the aid of a good seeded solution.

The upper bound of the equivalence ratio limit has been chosen to be 1.5. According to the standard chemical balance for the combustion of hydrocarbons for rich equivalence ratios displayed in equation 4.2, n-heptane and iso-octane begin to form carbon for equivalence ratios greater than 1.46 and 1.47 respectively. Since soot is a regulated emission, engine manufacturers are likely to avoid using equivalence ratios beyond that at which carbon is formed.

$$C_xHy + a(O_2 + \frac{0.79}{0.21}N_2) \quad = \quad bCO_2 + cH_2O + dCO + eN2 + fC \tag{4.2}$$

where,

a, b, c, d, e, f are balanced chemical equilibrium coefficients,
x, y are the number of C and H atoms per molecule of the hydrocarbon fuel.

This upper equivalence ratio value also does not bias the model toward accuracy in the super rich regions at the expense of accuracy in the lean region, seeing as the range from the stoichiometric conditions to the upper flammability limit is greater than the range from the lower flammability limit to stoichiometric conditions according to Table 2.4. The lower bound has been chosen as 0.8, halfway between the lower flammability limit for the fuels used and stoichiometric conditions. Since the lower bound is closer to stoichiometric

conditions compared to the lower flammability limit, it should not restrict the optimisation algorithm as much as a leaner value when fitting the rich region.

From the literature review presented in section 2.5.1, pressures of 20, 40 and 60 bar, 8 temperatures from 600 K to 1200 K and EGR percentages of 0%, 30% and 45% will be used. This choice of conditions ensures that we have low, medium and high variation of the effect of each parameter represented in the experimental design. From these chosen ranges for temperature, pressure, equivalence ratio and EGR, the experimental design in Table 4.2 was developed representing a matrix of 72 constant volume experimental conditions (8 temperatures per case for 9 cases).

Table 4.2: *Investigated Conditions : 72 Experiments*

Case No.	Pressure(bar)	EGR (%)	Phi
1	20	0	0.8
2	20	30	1.5
3	20	45	1
4	40	0	1
5	40	30	0.8
6	40	45	1.5
7	60	0	1.5
8	60	30	1
9	60	45	0.8

4.3.1 Operating Limits of the FGAM

During the process of calibrating the FGAM, it was found that the mechanism is unable to robustly predict auto-ignition for mixtures with high equivalence ratios and high EGR rates. For the factorial design of experiments used in the calibration process, shown in Table 4.2, this resulted in a large error overall error for conditions 2 and 6. For all of these experiments, the constitution of the recycled exhaust gas was based on the equivalence ratio (i.e. lean mixtures contained excess O_2, stoichiometric mixtures contained CO_2 and H_2O, whilst rich mixtures contained CO_2, H_2O and CO). In an actual engine under real world conditions, the EGR constitution would be based on the properties of the in-cylinder mixture. The reason for the failure of the FGAM to predict ignition delay for mixtures with high equivalence ratios and high EGR rates is due to the presence of CO at the start of the auto-ignition event. Significant amounts of CO present at this time will result in the immediate activation of reaction 8, given by the following reaction rate:

$$RR8 = [CO]^{f8}[O_2]^{b8}K8$$

This reaction is responsible for initiating heat release in the model and should only be activated after fuel has been converted to intermediate species Q or Y. However, with a significant quantity of CO present at the start of auto-ignition combined with artificially accelerated CO to CO_2 conversion used in the model, heat is released early on, speeding up auto-ignition due to the temperature rise, whilst also stealing oxygen from the fuel and intermediate species. The combination of these conditions causes the model to either severely under-predict ignition delay or fail altogether due to numerical instability. An example of this is displayed in Figure 4.5, which shows the ignition delay prediction of the FGAM against the DKM at a 45% EGR rate for equivalence ratios greater than and equal to 1. Notice that the FGAM initially under predicts the ignition delay as the equivalence ratio is decreased before failing to predict a full ignition delay curve at a value of 1.2. In contrast, the DKM was able to predict ignition delays for 45% EGR rates for equivalence ratios as high as 3.

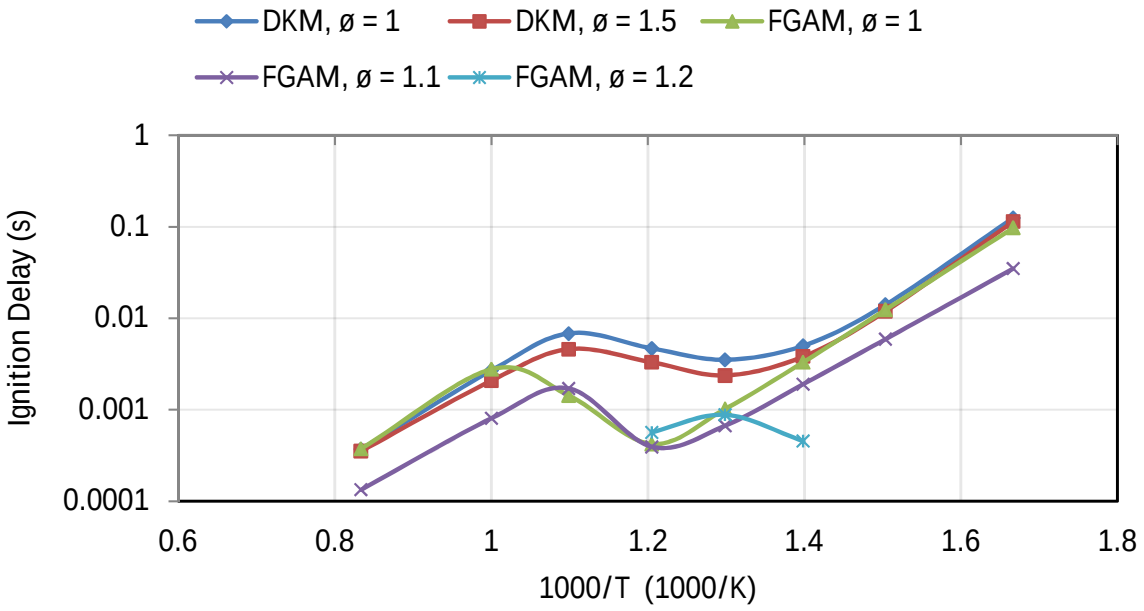

Figure 4.5: *The performance of the FGAM versus the DKM for rich mixtures of n-heptane with EGR rates of 45%. Notice that the FGAM is not able to predict a full ignition delay curve for an equivalence ratios greater than or equal to 1.2.*

In an attempt to solve this problem and possibly increase the range of operation of the FGAM, either the sensitivity of reaction rate 8 needed to be decreased or the activation of the reaction needed to be delayed by other means. Reducing the sensitivity of this reaction rate was achieved by reducing its pre-exponential multiplier value (i.e. lnA8 in Table 3.1). Although this alteration did allow the model to solve for all regions tested, the average error in ignition delay prediction rose to 41%, almost double that of Floweday's original upper bound error limit for the model of 23%. This increased error was the result of a slower ignition delay period due to slower heat release. To delay the activation of reaction rate

8 without modifying its speed, a dependency on intermediate species Y was introduced. Although, this did successfully delay the activation of the reaction, which resulted in better ignition delay timing, the peak temperature of the main heat release event was relatively low due to the depletion of Y occurring before enough CO could be converted to CO_2.

Literature was consulted in order to determine how other researchers were able to overcome this problems in other global and reduced auto-ignition model formulations. The Zheng model [20] was one of the existing global models to incorporate the CO-CO_2 equilibrium into its structure, as opposed to a fixed general end product mixture of used in the Schreiber [21], Müller [22] and Shell [18] models. However, the Zheng model was only used in extremely lean regions with equivalence ratios ranging between 0.4 to 0.5, and did therefore not encounter the same problem. During Hamosfakidis's [33] optimisation of the Shell model, the model was validated for rich regions and included EGR. However, the EGR was based on stoichiometric conditions, consisting of only CO_2 and H_2O, and was therefore not valid for all of the conditions in which it was used. Nevertheless, since the Shell model does not incorporate a CO-CO_2 equilibrium into its structure, it should theoretically not fail when CO is introduced at the start of the ignition delay.

It is useful to design in regions in which the model was originally validated (i.e. lean to stoichiometric equivalence ratios with minimal to high EGR rates) as these conditions promote a more efficient combustion. However, regions of high equivalence ratios and high EGR rates can occur locally in the cylinder, which may warrant investigation into this area in future research. Nevertheless, resolution in this area was not required for the scope of this research. Therefore, for this optimisation process, the conditions retained from the factorial design were all those with lean to stoichiometric air-fuel ratios as well as the rich mixtures without EGR. The amended experimental design is given in Table 4.3.

Table 4.3: *Amended Experimental Design : 56 Experiments*

Case No.	Pressure(bar)	EGR (%)	Phi
1	20	0	0.8
2	20	45	1
3	40	0	1
4	40	30	0.8
5	60	0	1.5
6	60	30	1
7	60	45	0.8

This represents a matrix of 56 constant volume experimental conditions (8 temperatures per case for 7 cases) which were used in the calibration process. In more detailed simulations of in-cylinder combustion where regions of high EGR and high equivalence ratio can occur locally, it is currently advisable to implement the FGAM with stoichiometric EGR. However, this assumption may prove inaccurate in regions where carbon is formed, and

for this reason, it is recommended that the structure of the CO-CO_2 equilibrium of the FGAM is amended in the future. Alternatively, the CO from the EGR should be made inert (i.e. a separate species used).

4.3.2 Results of Calibration Process

The comparative overall auto-ignition performance of the FGAM for the 56 experimental data points of Table 4.3 for n-heptane is presented in Figure 4.7. The plots for iso-octane and PRF50 are included in Appendix C. The calibrated coefficients for all three fuels have been included in Appendix A. It is important to note that the coefficients developed in this work are one of many possible sets of solutions for the FGAM under these specific conditions - the aim of this work was not to find all possible solution sets, but rather one which worked.

The graphs consist of overall ignition delay, cool flame ignition delay and cool flame ceiling temperature curves. Note that left vertical axis is plotted on a log scale, with the cool flame ignition delay and overall ignition delay plotted against the vertical ignition delay axis, and the cool flame ceiling temperature plotted against the vertical temperature axis. Table 4.4 demonstrates the improvement in accuracy made by the calibration routine for the new formulation of the FGAM for n-heptane, iso-octane and PRF50. Included in the table for reference is the accuracy achieved by Floweday for the original form of the model using the original sets of coefficients. Since Floweday did not derive a set of coefficients for PRF50, the calibration routine was seeded with an average of its coefficients of its constituent fuels (n-heptane and iso-octane). The average error in the final column of the table refers to the average of the ignition delay, cool flame ignition delay and cool flame temperature rise errors.

Table 4.4: *The Performance of the Calibration Methodology for the FGAM*

		Error (%)			
Fuel	**Coefficient Set**	**ID**	**CFID**	**CFdT**	**Average**
n-Heptane	Floweday	27.02%	29.57%	49.74%	35.44%
	Pre-Calibration	27.67%	21.46%	71.17%	40.10%
	Calibrated	24.73%	18.41%	44.82%	29.32%
PRF 50	Floweday	N/A	N/A	N/A	N/A
	Pre-Calibration	62.69%	38.04%	35.75%	45.49%
	Calibrated	22.66%	25.08%	35.42%	27.72%
iso-Octane	Floweday	24.58%	19.51%	37.46%	27.18%
	Pre-Calibration	23.83%	17.37%	39.44%	26.88%
	Calibrated	20.96%	14.90%	26.96%	20.94%

The calibrated set coefficients reduced the average error of the new formulation of the

model by between 5.94 % and 17.77% for the three fuels. Furthermore, the calibrated coefficients have an average error between 6.12% to 6.24% lower than Floweday's original model using his set of coefficients for the fuels. This demonstrates that the calibration routine successfully performs the function for which it was designed. The running time of the calibration for each fuel for the 56 conditions was between 2 hours 45 minutes and 3 hours, solved using MATLAB on a computer with a quad-core i5 processor and Windows 7. It was noticed that the average ignition delay error of n-heptane for both versions of the FGAM was above the error tolerance of 11-23% stated by Floweday in his original validation of the model. From inspection of the of all seven cases, it was seen that the FGAM performed weakest in cases 2 and 5. This is also true when consulting the ignition delay curves of iso-octane and PRF50. The poor agreement of ignition delay and cool flame ignition delay in the NTC region of case 2, as well as the poor agreement of the ignition delay in the high and NTC regions of case 5 were considered the most likely causes of the increased overall ignition delay error of the model.

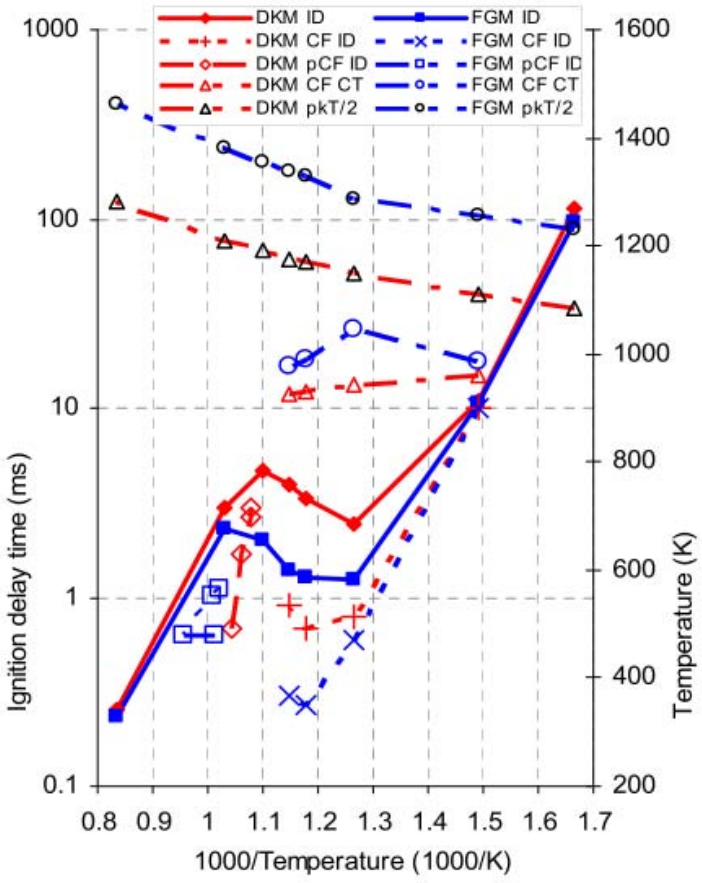

Figure 4.6: *A graph displaying the performance of the FGAM for n-heptane at 20 bar, 40% EGR, $\Phi = 1$ from Floweday's development of the model [19]. These conditions are similar to those of case 2, and display the same poor fit in the NTC region.*

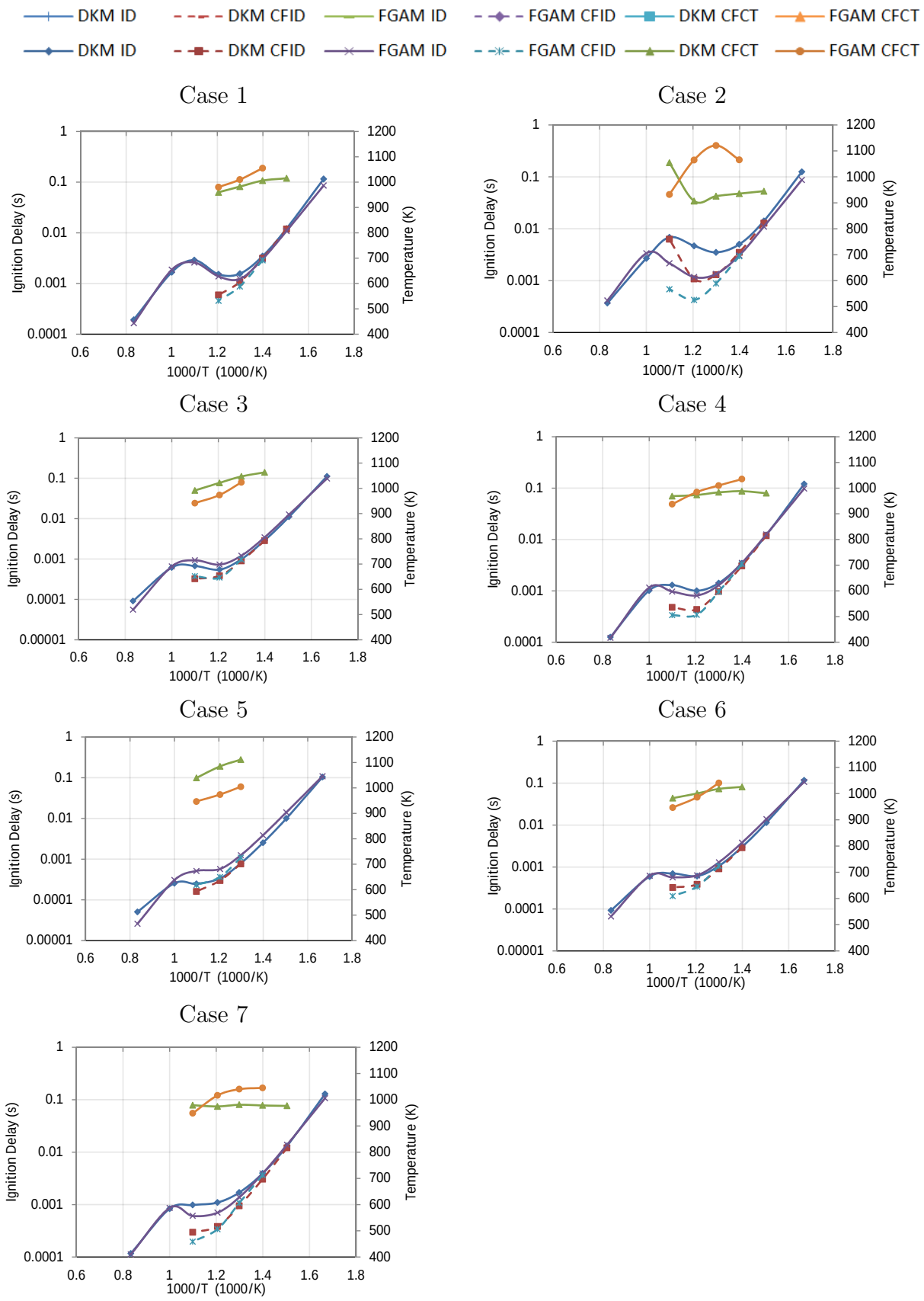

Figure 4.7: *Calibration of n-Heptane according to the cases described in Table 4.3.*

4.3.3 Sensitivity of FGAM to varying EGR Rates and Equivalence Ratios

Case 2 is representative of a high EGR condition. Floweday included an experiment similar to that of case 2 in his initial solving for the kinetic constants of n-heptane: 20 bar, EGR = 40% and $\Phi = 1$. The performance achieved by Floweday for this condition is displayed in Figure 4.6. Notice that in both Figure 4.6 and case 2 of Figure 4.7, the FGAM under predicts the ignition delay and cool flame ignition delay timing in the NTC region. Case 5 is representative of high equivalence ratio condition and it was not surprising that the model had performance issues in this area as it had not been previously validated for this region. In order to determine the reason for the FGAM's poor performance for each of these cases, it was decided to investigate sensitivity of the FGAM to varying EGR percentages and equivalence ratios. This investigation is presented in section 4.3.3.

EGR

As mentioned in section 4.3.2, the FGAM performs worst in cases 2 and 5. Case 2 is representative of a high EGR conditions, whilst case 5 is representative of high equivalence ration conditions. In order to determine the reason behind the model's performance in these regions, ignition delay sweeps for n-heptane for varying EGR rates and equivalence ratios were performed at 20 bar pressure and stoichiometric air-fuel ratio. The DKM's sensitivity to varying EGR rates is presented in Figure 4.8, along with the sensitivity of the modified model in Figure 4.9 as well as that of the original form of the model in Figure 4.10. Note that the FGAM does not display cool flame behaviour for temperatures below 770 K (greater than 1.3 on the horizontal scale of the ignition delay graph). This issue was mentioned previously in section 3.4 during the investigation of the cause of stiffness in the model. Since this issue was not corrected by the calibration routine, it is most likely a problem inherent in the structure of the model.

The DKM becomes sensitive to the effects of differing EGR rates for temperatures greater than 665 K. The trend displayed by the DKM is of increasing EGR rates resulting in an increased overall ignition delay, increased cool flame ignition delay and decreased cool flame ceiling temperatures. A pronounced difference between the ignition delay at the different EGR rates is found in the NTC region, which becomes less pronounced at higher temperatures.

The original and modified model display the same behaviour throughout these varying EGR sweeps, further validating the fact that the modifications made do not impact on the performance of the model. However, both forms of the FGAM do not display a significant sensitivity to varying EGR rates in the NTC region, but do display the correct trend

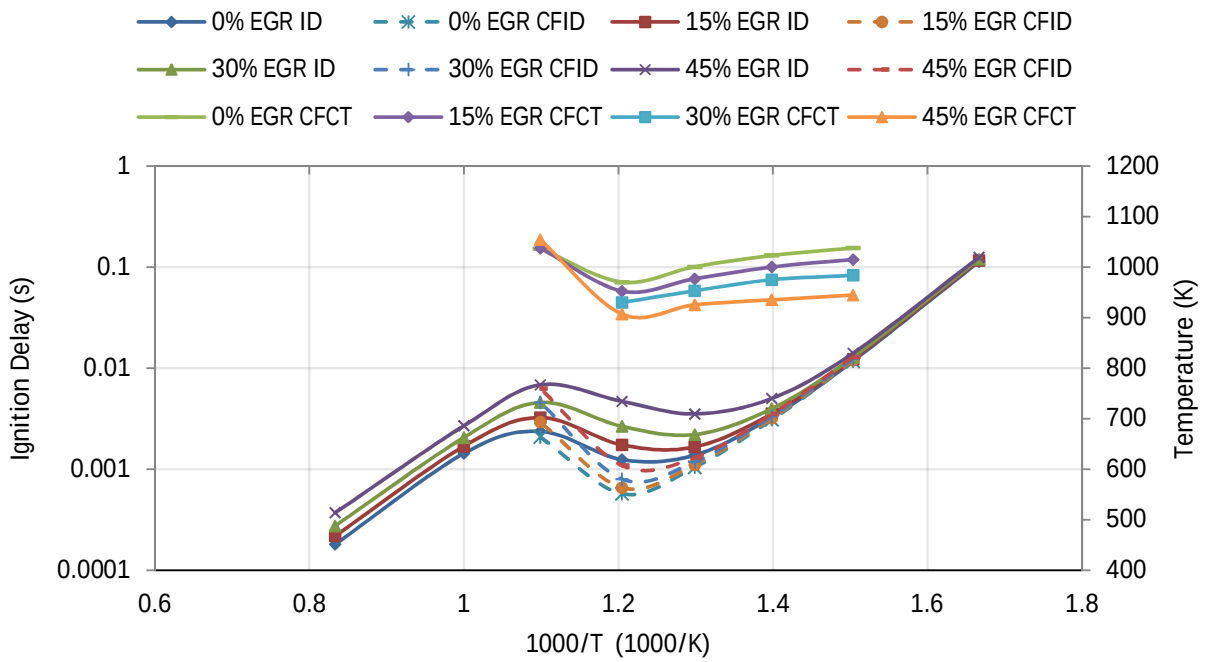

Figure 4.8: *The sensitivity of the DKM of Mehl, for n-heptane at 20 bar and stoichiometric air-fuel ratio, to varying EGR percentages.*

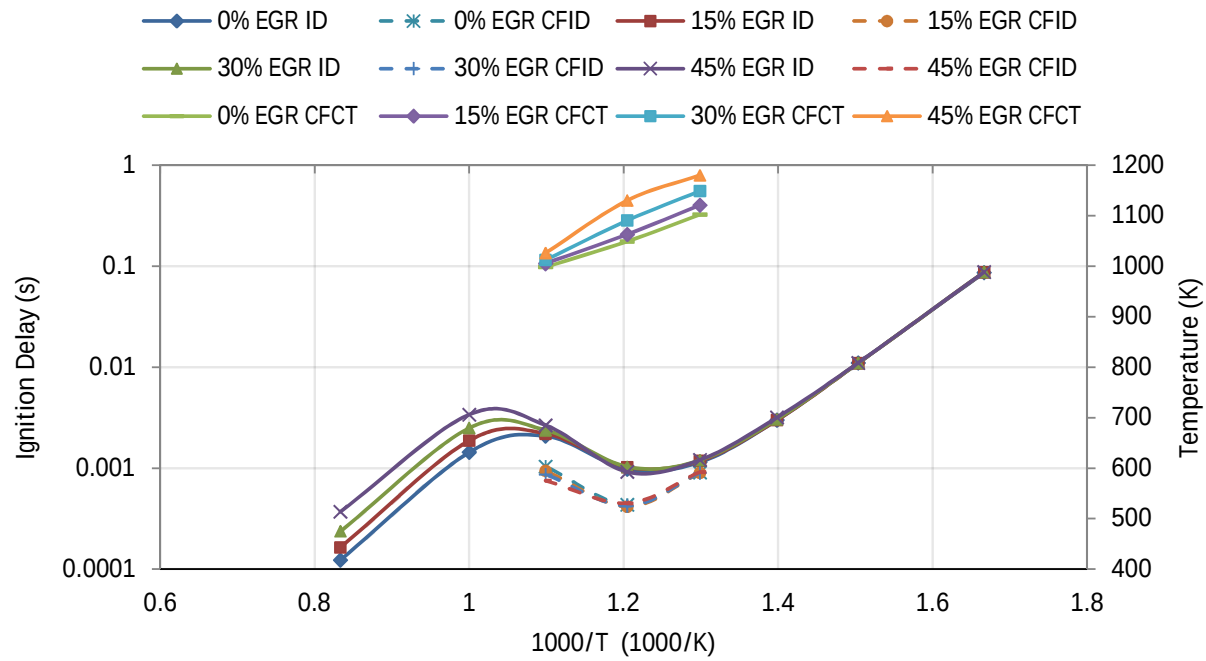

Figure 4.9: *The sensitivity of the modified FGAM using the calibrated coefficients, for n-heptane at 20 bar and stoichiometric air-fuel ratio, to varying EGR percentages.*

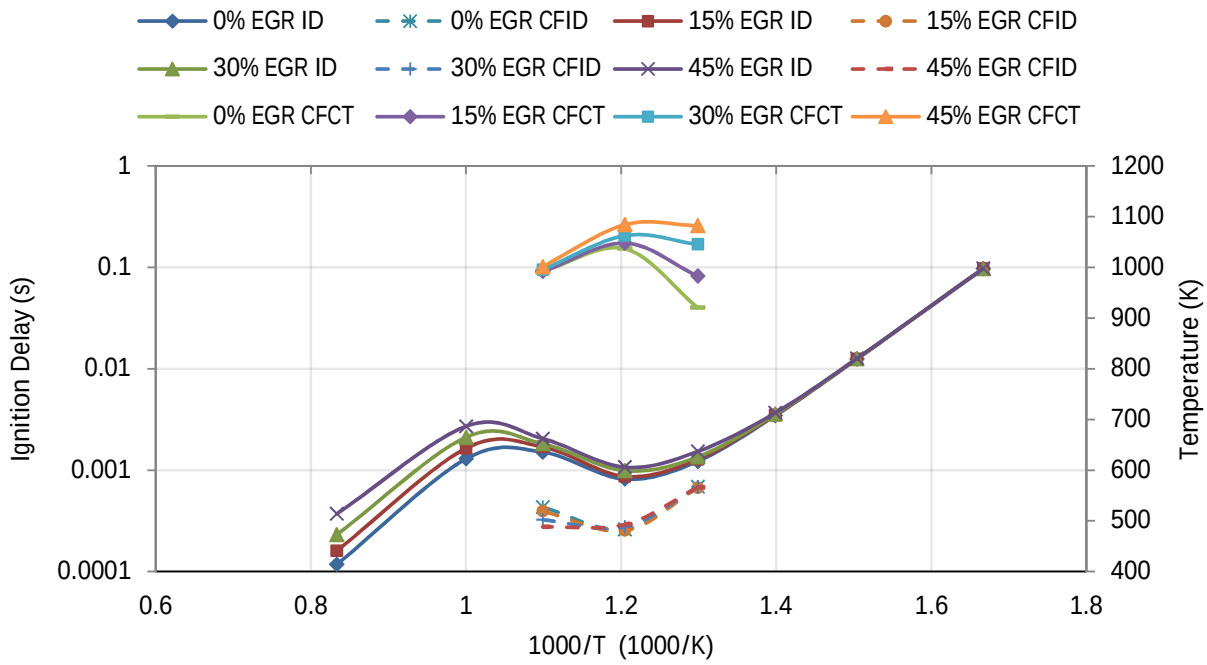

Figure 4.10: *The sensitivity of the original FGAM using Floweday's coefficients, for n-heptane at 20 bar and stoichiometric air-fuel ratio, to varying EGR percentages.*

concerning EGR and equivalence ratio in the high temperature region. As a result, in the NTC region, the FGAM with 45% EGR rate displays the same ignition delay behaviour as the DKM with 0% EGR, as shown in Figure 4.11. This explains the FGAM under predicting the ignition delay in the NTC region of case 2, resulting in a poor overall fit in this region. Another point to note from Figure 4.11 is that the FGAM does display correct EGR sensitivity in the high temperature region, which is also displayed in case 2 of Figure 4.7. This is reason for the FGAM being able to match the high temperature ignition delay in case 2. Recall that Floweday only included one experimental condition which included EGR in the initial solving of the kinetic rate parameter for the fuel, as mentioned in section 2.3.3. It was therefore expected that the FGAM would not display good sensitivity to EGR as the solution set of kinetic constants was dominated by non-EGR conditions.

Equivalence Ratio

The behaviour of the DKM for various equivalence ratios is displayed in Figure 4.12. From the figure, it is seen that the DKM is not sensitive to the changing of equivalence ratios in the low temperature region. Equivalence ratio effects only begin to significantly influence ignition delay for temperatures greater than 715K (less than 1.4 on the horizontal scale). Increasing equivalence ratio results in a decreased ignition delay, decreased cool flame ignition delay and increased cool flame heat release throughout the NTC region. The

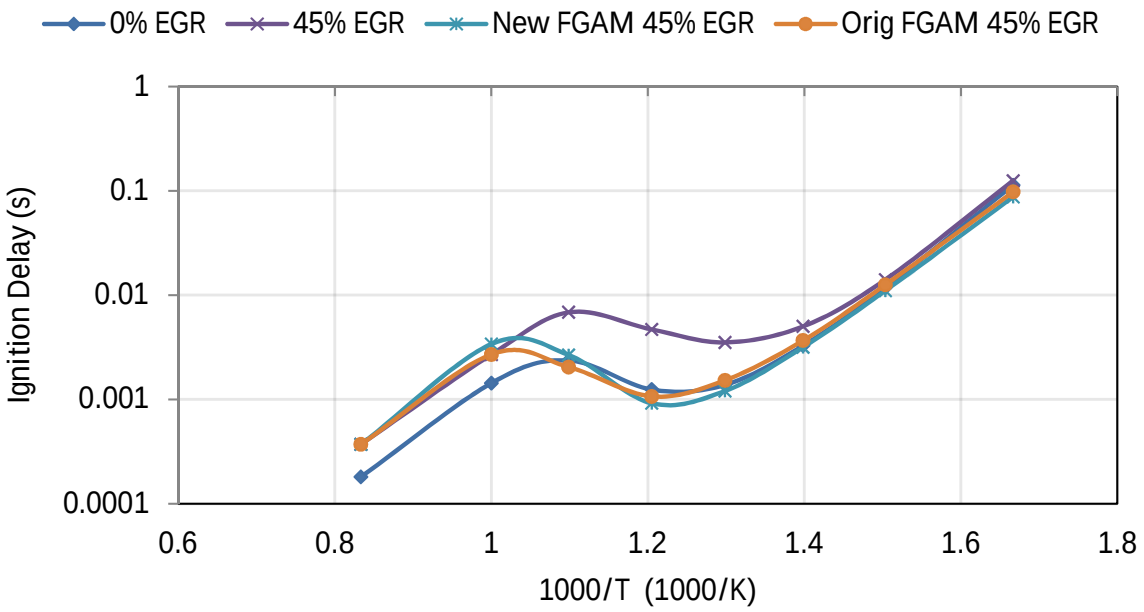

Figure 4.11: *The sensitivity of the DKM, for n-heptane at 20 bar and stoichiometric air-fuel ratio, to varying EGR percentages, with an overlay of the performance of both versions of the FGAM at 45% EGR. Notice that although both versions of the FGAM under predict ignition delay in the NTC region, they are able to fit both the high and low temperature region.*

nature of the sensitivity behaviour is similar to the DKM's response to EGR effects in the NTC region. An interesting point to note is that the ignition delay converges for all equivalence ratios in the high temperature region. In the high temperature region, EGR effects still significantly influenced ignition delay, whereas equivalence ratio effects do not. The FGAM however, displays no significant sensitivity to equivalence ratio effects until late in the NTC region, as displayed in Figures 4.13 and 4.14. In fact, the FGAM's cool flame ignition delay predictions are approximately equivalent for all equivalence ratios presented. It is also expected that higher equivalence ratios, as with lower EGR rates, result in higher cool flame heat releases (and therefore ceiling temperatures), as demonstrated by the DKM in Figures 4.12 and 4.8. However, the FGAM actually displays the reverse trend, with leaner mixtures having higher cool flame ceiling temperatures, which results in all equivalence ratios having the same final ignition delay. Furthermore, note that once again the FGAM does not display the same low temperature cool flame behaviour as the DKM (i.e. the low temperature cool flame seen in the DKM is not present in the FGAM under these conditions). Additionally, the FGAM still displays the influence of equivalence ratio effects at high temperatures, unlike the DKM. This fact is more clearly displayed in Figure 4.15, which shows that although for the case of $\phi = 1.5$ (similar to case 5), the FGAM is able to match the low and NTC temperature regions of the FGAM, it is unable to match the DKM at high temperatures.

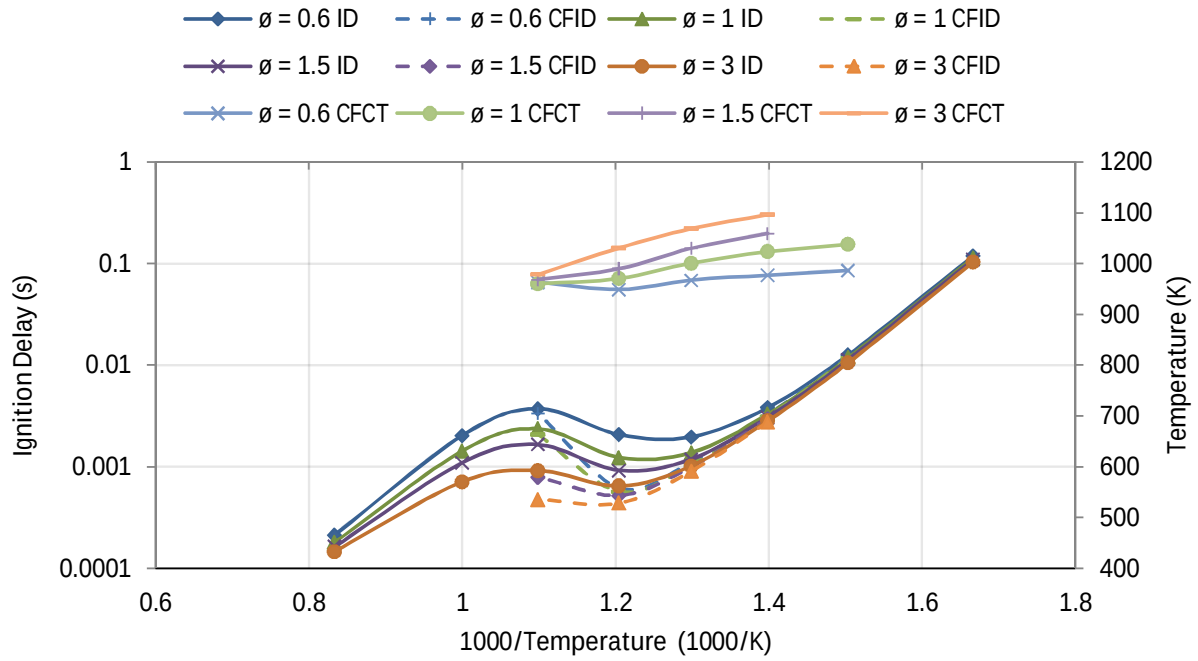

Figure 4.12: *The sensitivity of the DKM of Mehl, for n-heptane at 20 bar and stoichiometric air-fuel ratio, to varying equivalence ratios.*

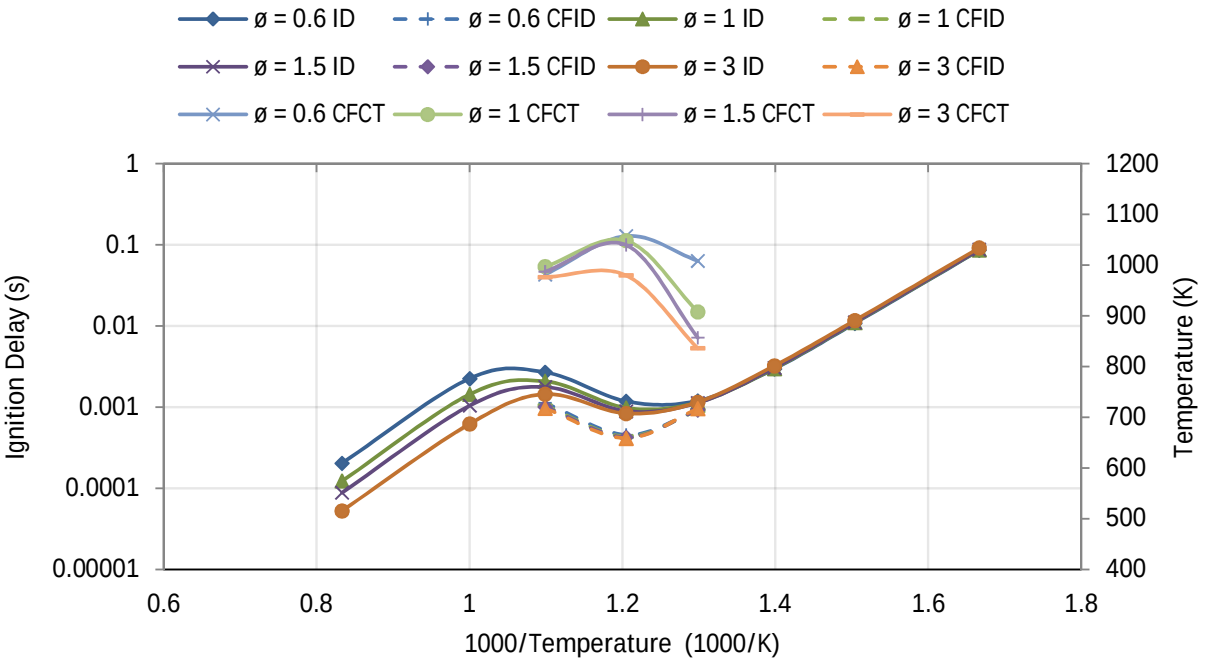

Figure 4.13: *The sensitivity of the modified FGAM using the calibrated coefficients, for n-heptane at 20 bar and stoichiometric air-fuel ratio, to varying equivalence ratios.*

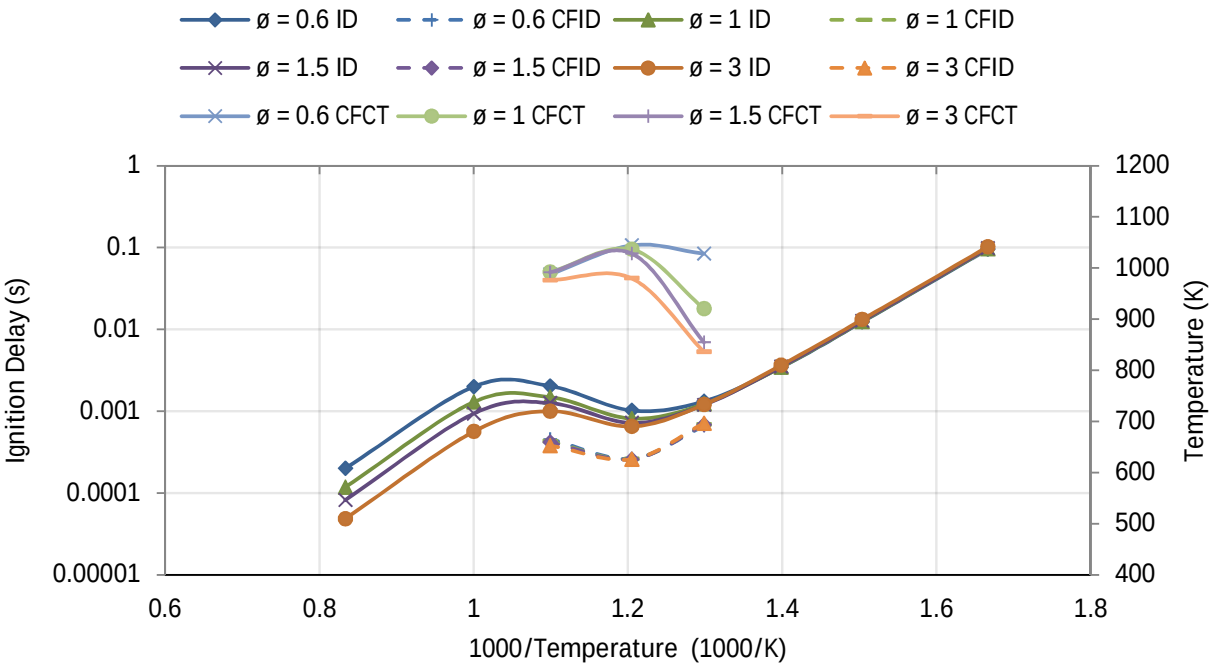

Figure 4.14: *The sensitivity of the original FGAM using Floweday's coefficients, for n-heptane at 20 bar and stoichiometric air-fuel ratio, to varying equivalence ratios.*

Discussion of the FGAM's Sensitivity to EGR and Equivalence Ratio

It is expected that any model will have a limited range of applicability, however, it is more important to determine whether or not these operating limitations affect the usefulness of the model. As mentioned in section 2.5.1, one of the main reasons behind the use of EGR in modern internal combustion engines is to reduce regulated emissions, such as soot and NOx, through lowering of the peak combustion temperatures. This was one of the key design philosophies behind the HCCI engine cycle. Due to the ever more stringent vehicle emission legislation being passed globally in an effort to reduce human carbon footprint, vehicle manufacturers are increasingly employing the use of EGR and other emission reducing techniques in contemporary internal combustion engines in order to comply with the legislation. As more modern engines adopt EGR subsystems, an accurate method of modelling the effect of EGR on ignition delay and combustion is needed in order to ensure that the engine runs as efficiently as possible. Unfortunately, due to the fact that the FGAM does not display correct sensitivity to EGR effects in its current state, it would not be useful as a modelling tool for engines running EGR. In its current form, this is a major obstacle that can prevent widespread adoption of the model.

In an internal combustion engine, the phenomenon of cycle to cycle variation means that in each cycle, the composition of the mixture in the cylinder differs slightly from the previous incarnation, which leads to differences in the combustion and heat release characteristics. The composition of the fuel air-charge is dependent on a variety of different factors, rang-

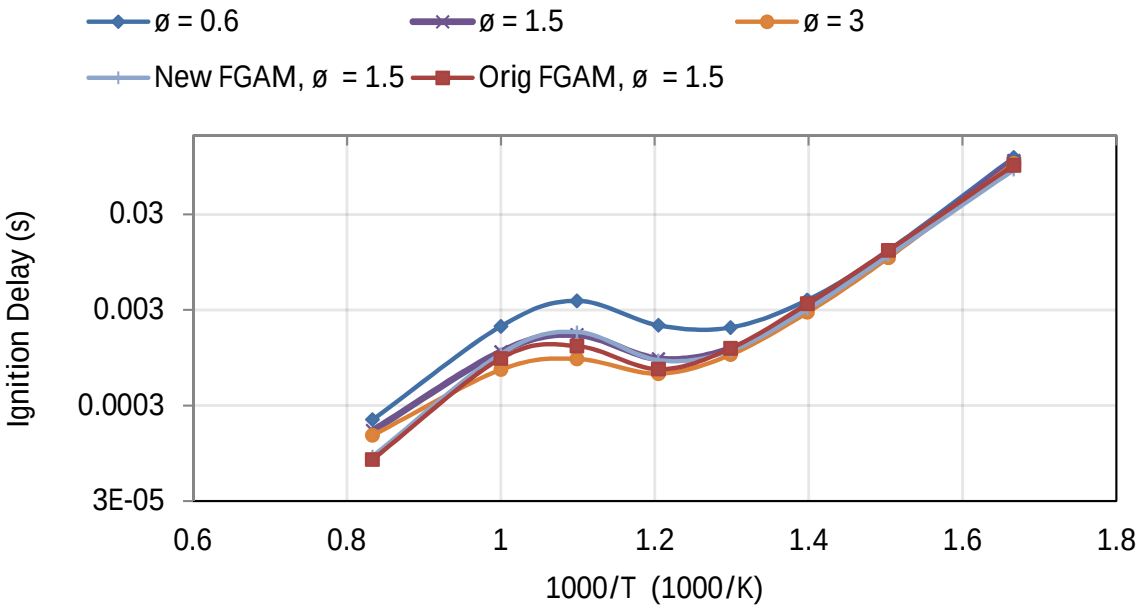

Figure 4.15: *The sensitivity of the DKM, for n-heptane at 20 bar and stoichiometric air-fuel ratio, to varying equivalence ratios, with an overlay of the performance of both versions of the FGAM at* $\Phi = 1.5$*. Notice that both versions of the FGAM do not converge to the same high temperature ignition delay prediction as the DKM.*

ing from the control systems of the engine to the environmental conditions and chemical composition of the fuel. In order to ensure that the engine is designed to cope with all applicable variations on the intake charge, each scenario needs to be modelled. Due to the FGAM's lack of sensitivity to equivalence ratio effects in the low to intermediate temperature zone, it would be unsuitable for modelling in this application. The lack of equivalence ratio sensitivity also means that the FGAM is not suitable for integration into complex CFD (computational fluid dynamics) simulations of spray and combustion events. In such a simulation, if the fuel is introduced to an environment where temperatures are close to that of the fuel's NTC region, the FGAM would predict the same ignition delay for the localised rich region surrounding a droplet as it would for leaner regions further away from the droplet. These errors would compound for the entire spray of droplets and decrease the likelihood of producing useful data.

One of the methods that can be used to overcome the FGAM's lack of sensitivity to these factors would be to calibrate the model for a fixed EGR and/or equivalence ratio condition. In order to validate this course of approach to the problem at hand, the fit of the FGAM was optimised for the above mentioned cases 2 (high EGR) and 5 (high equivalence ratio) for n-heptane. The fit achieved in the subsequent optimisation is presented in Figures 4.16 and 4.17. The running time of the calibration routine for each these fixed condition cases was approximately 20 minutes. Table 4.5 presents the accuracy achieved for cases 2 and

5 before and after this additional optimisation. Notice that the optimisation performed under these fixed conditions has drastically reduced the ignition delay, cool flame ignition delay and cool flame temperature rise errors. However, the cool flame temperature rise error of case 2 after the additional calibration is still greater than 50% (down from over 150%). This may not be critical depending on the application in which the model is used since the ignition delay error is less than 10%. Nevertheless, it may be possible to achieve even greater accuracy by rectifying the sensitivity of the FGAM to EGR and equivalence ratio effects through changes to the structure of the model.

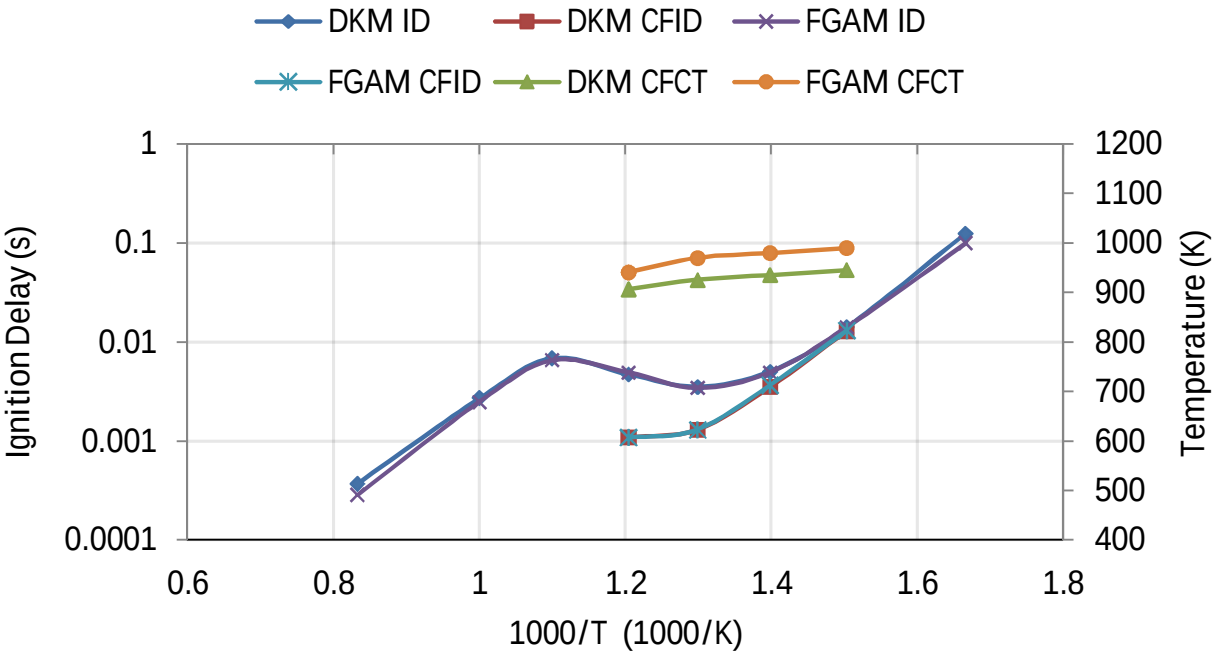

Figure 4.16: *FGAM calibrated for case 2 of experimental design only. Notice the better fit that is achieved compared to case 2 of Figure 4.7.*

Table 4.5: *Performance of Calibration for a Single Condition for n-heptane: Case 2 & Case 5*

		Error (%)			
Case	**Coefficient Set**	**ID**	**CFID**	**CFdT**	**Average**
Case 2	Pre-Calibration	41.61%	53.02%	153.94%	82.86%
	Calibrated	8.14%	26.78%	64.39%	33.10%
Case 5	Pre-Calibration	50.40%	16.46%	28.74%	31.87%
	Calibrated	10.62%	14.40%	3.36%	9.46%

The area of the model which needs most attention structurally is the low temperature pathway. Recall that the model did not display the same sensitivity as the DKM to EGR and equivalence ratio effects for low to intermediate temperatures, but did distinguish between variances in these values at higher temperatures. It was noticed from Figures 4.9, 4.10, 4.13 and 4.14 that the cool flame hook was unaffected by changes in EGR rates and equivalence ratios. Referring to Floweday's explanation of the function of each reaction in

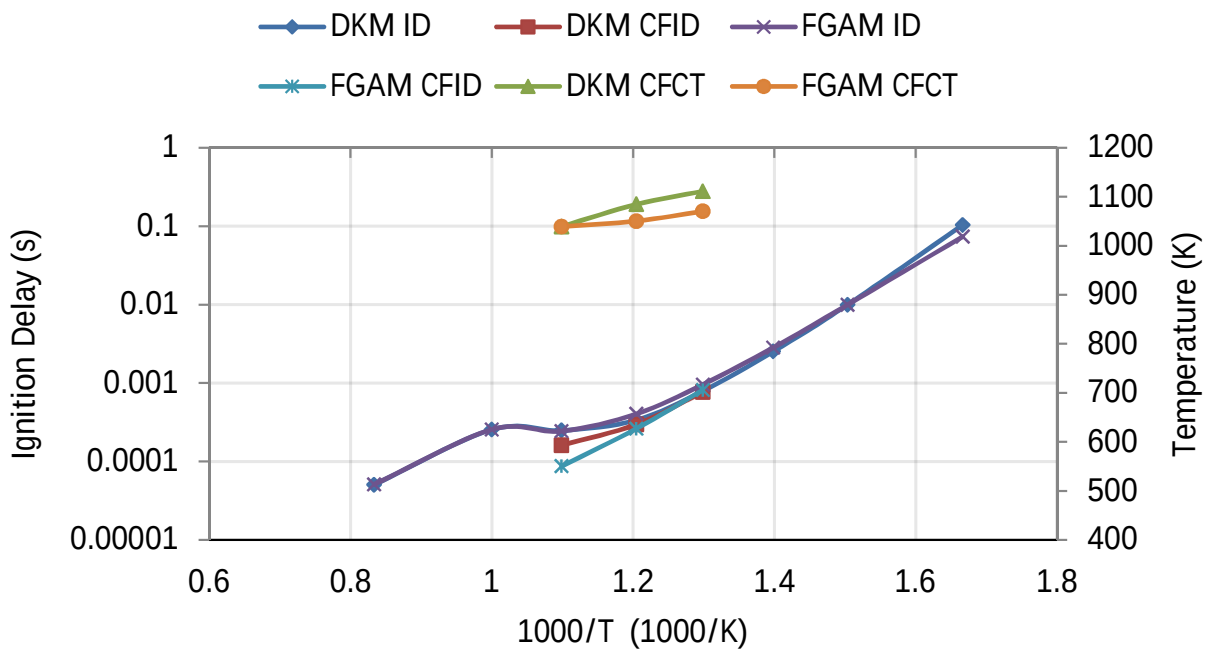

Figure 4.17: *FGAM calibrated for case 5 of experimental design only. Notice the better fit that is achieved compared to case 5 of Figure 4.7.*

the FGAM, presented in section 2.3.2, it is reaction 1b which controls the cool flame hook. Reaction rate 1 already contains both and oxygen and fuel terms, and should therefore already be sensitive to changes in EGR rates and the quantity of air to fuel. It may prove more effective to introduce a dependence on water, which is present in exhaust gas. However, this could potentially result in a shutting down of reaction rate 1 under conditions without EGR.

The cool flame timing in the FGAM coincides with the maximum concentration of species Q, and introducing the correct fuel and oxygen dependencies on the other reactions which interact with this species may result in the model displaying the same sensitivity as the DKM. In the new formulation of the model, reactions 2, 3 and 4 have been reduced via a pseudo-QSSA, as described in chapter 3, which uses the original forms of the individual reaction rates. From the original forms of these reaction rates, it is noticed that whilst only reaction 2 is sensitive to changes in air-fuel ratio through the inclusion of a fuel term in the reaction rate equation, none of the reactions rates equations allow for the reactions to be sensitive to varying EGR rates. Therefore, it should be investigated whether or not including an oxygen term in reactions 2, 3 and 4 and a fuel term in reactions 3 and 4, and then redefining the pseudo-QSSA assumption will cause the FGAM to display the desired sensitivity to EGR and equivalence ratio.

Reaction rate 6 contains an oxygen terms in its current form. However, due to the incorrect trend displayed by the FGAM regarding the cool flame heat release, with lower air fuel

ratios having higher heat release, it may prove necessary to include a fuel term in this reaction rate equation. Achieving the correct behaviour with regard to low temperature heat release magnitude and timing in the FGAM through changes to the structure of the low temperature pathway should correct sensitivity of the overall ignition delay timing in the low to intermediate temperature regions, since the high temperature pathway did display sensitivity to EGR and equivalence ratio effects. Once the changes to the structure have been made, further accuracy can be achieved through the use of the calibration routine.

4.4 Summary of the FGAM Calibration

A calibration methodology was developed in this chapter which incorporated a PSO algorithm with the Five Point fitness function. The Five Point function compares five key data points from the temperature time trace of the reference data and the FGAM. In this way, the fitness function could be tuned to focus on the cool flame ignition delay, overall ignition delay and cool flame heat release. Using a factorial experimental design, 72 data points were initially derived for the calibration process. However, upon initial inspection of the first set of calibration results, it was found that the FGAM encountered difficulty fitting to regions of rich equivalence ratios and high EGR rates. Upon further investigation, it was found that the FGAM did not display significant sensitivity to variances in EGR rates or air-fuel ratios, especially when compared to the experimentally validated DKM of Mehl et al. [3].

Given the issues the FGAM has with equivalence ratio and EGR, it was decided not to pursue the original calibration matrix which included EGR and equivalence ratio combinations even if this could be solved by using inert EGR. This reduced the number of data points in the calibration matrix to 56. The calibration was then performed using the revised data points and resulted in a decrease in average error over the cool flame ignition delay, overall ignition delay and cool flame temperature rise of over 6% compared to Floweday's original set with the original form of the model. Additionally, the average error reduction of the calibrated coefficients over the seeded values used in the revised model were as large as 18%. It is important to note that the coefficients developed in this work are one of many possible sets of solutions for the FGAM under these specific conditions - the aim of this work was not to find all possible solution sets, but rather one which worked. Furthermore, it was also shown that the calibration routine could reduce the error to acceptable limits when in the cases of high EGR rates and rich equivalence ratios when optimised for those specific conditions. Nevertheless, it was noted that calibrating coefficients for a single condition would be more time consuming for large scale experimentation. Therefore, recommendations were made as to possible changes that could be made to the model to improve its sensitivity to EGR and equivalence ratio effects.

Chapter 5

Integration of the FGAM into GT-Suite

This chapter details the implementation of the FGAM into GT-Suite. The chosen route by which this implementation was achieved was through use of the global reactions templates, mentioned in section 2.5.4. There were two templates available, `GlobalReactions`, for use with exhaust gas after-treatment simulations and `EngCylChemGlobal`, for describing in-cylinder chemical kinetics in an engine simulation. As mentioned previously, these built-in templates have facilities that allow for the entering of non standard reaction rate forms, of which there are two in the new formulation of the FGAM.

The modifications to the structure of the FGAM performed in chapter 3, allowed for the FGAM to be solved by the solvers built into the templates. It was noticed during implementation of the FGAM into GT-Suite that the model could be solved using the faster BDF solver when implemented with iso-octane, whereas implementation with n-heptane required the use of the slower, more robust RADAU solver. This is likely due to the considerably larger value of constant A4 for n-heptane compared to iso-octane, since this is the only significant difference between the implementation of both fuels. Nevertheless, both cases are an improvement over implementation of the original form of the model into GT-Suite, which was not able to be solved at all by the built-in methods due to its stiffness. The modifications made to the FGAM should translate to the model being more easily implemented in other chemical kinetic solvers in other software packages. Further details of the performance of the FGAM in GT-Suite is given in the sections that follow.

5.1 Constant Volume Adiabatic Reactor

A constant volume adiabatic reactor was constructed in GT-Suite making use of the `GlobalReactions` template. Although this template is aimed at exhaust gas after-treatment, it can be used in the configuration shown in Figure 5.1 for a constant volume adiabatic reactor. The `EngCylChemGlobal` template has the same inputs and solvers as the `GlobalReactions` template, but can only be invoked as part of the combustion mechanism in a full engine simulation. This would not allow for accurate comparison of the ignition delay and overall auto-ignition behaviour to the results derived from the optimisation routine of chapter 4.

In light of the findings in made in sections 4.3.1 and 4.3.3, the reactor conditions contained no EGR and maintained stoichiometric air-fuel ratio.

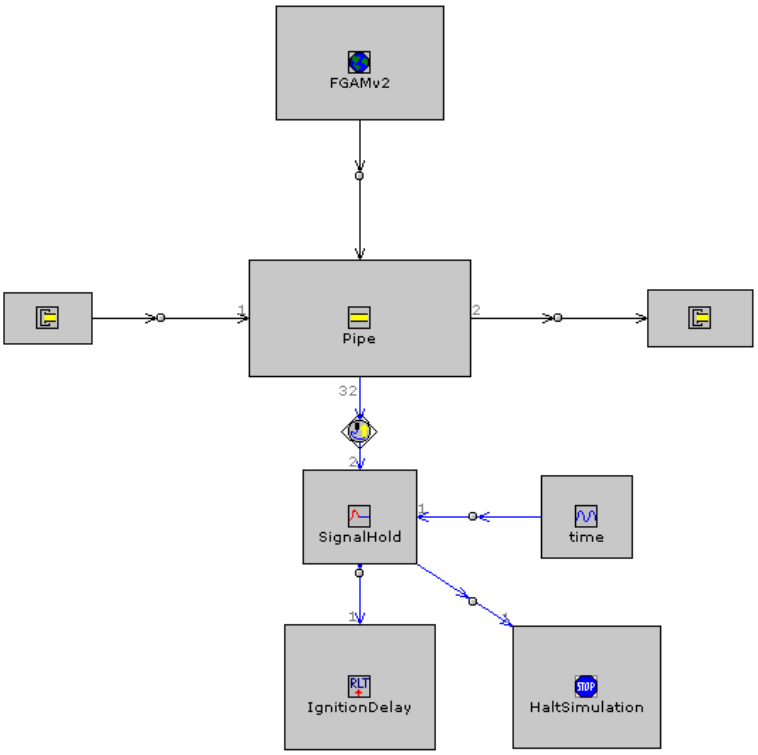

Figure 5.1: *A simple constant volume adiabatic reactor in GT-Suite. In its current configuration, the FGAM is responsible for the chemical kinetics inside of the closed pipe section.*

The reactor experiments consisted of temperature sweeps, consisting of 24 experiments in total, of n-heptane for the conditions shown in Table 5.1. The ignition delay as solved by GT-Suite's RADAU solver for these conditions is displayed in Figure 5.2. A comparison

of the auto-ignition behaviour of the FGAM predicted using the RADAU solver versus the forward Euler with adaptive time-stepping is presented in Table 5.2. The RADAU solver took approximately 7 seconds to complete the eight temperature experiments per pressure, which is longer than the 0.5 second time recorded by the forward Euler solving routine in MATLAB® (using a computer with a quad-core i5 processor and Windows 7).

From Table 5.2, it is seen that average difference in prediction of ignition behaviour for the FGAM when solved by the two different methods is no greater than 3%. This difference is insignificant in magnitude, and only exists at all due to the difference in time step taken by both of the solvers which affects the final time at which the various key aspects of auto-ignition are captured. This slight variation could also be caused by minor differences in the specific heat values used in the two implementations. This is a positive outcome which serves to demonstrate that the FGAM should provide the same results regardless of the solving technique used.

Table 5.1: *Constant Volume Adiabatic Reactor Conditions*

Case No.	Pressure(bar)	EGR (%)	Phi
GT1	20	0	1
GT2	40	0	1
GT3	60	0	1

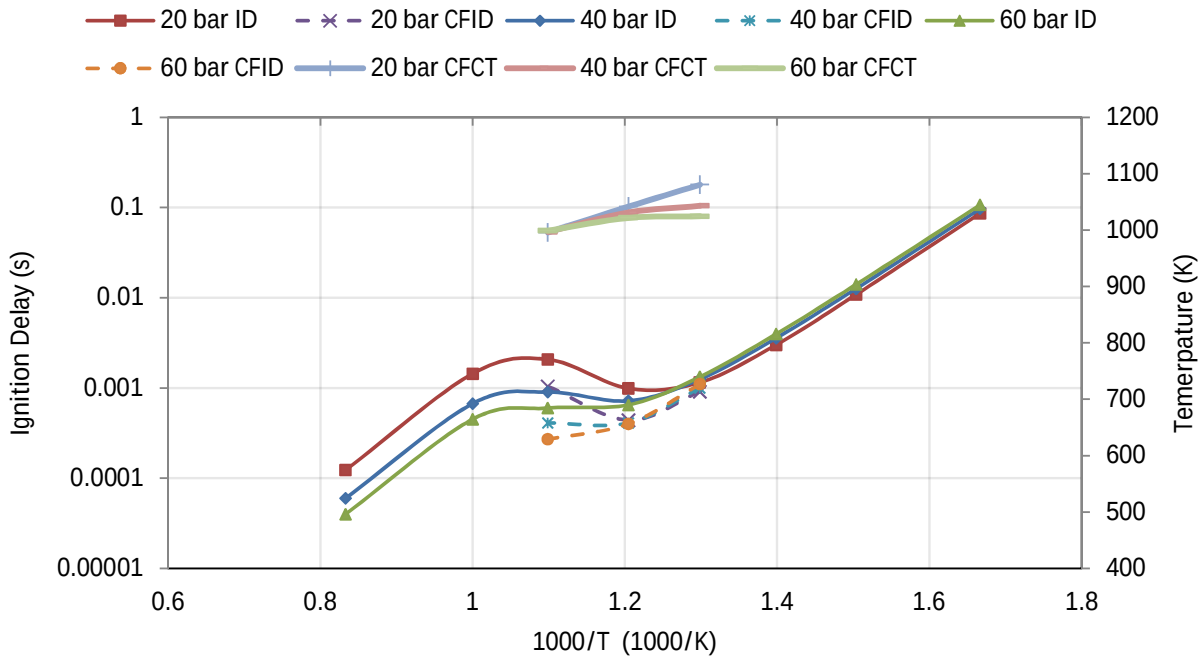

Figure 5.2: *The FGAM solved by the RADAU solver built into GT-Suite for n-heptane at 20, 40 and 60 bar, EGR = 0%, Φ = 1.*

Table 5.2: *Difference in auto-ignition prediction for the FGAM when solved by RADAU and Forward Euler*

	Error (%)		
Case No.	**Ignition Delay**	**Cool Flame Ignition Delay**	**Cool Flame Temperature Rise**
GT1	3.5	0.7	3.4
GT2	2.9	0.8	2.3
GT3	3.6	2.1	2
Average	3.4	1.2	2.6

5.2 Single Cylinder HCCI Model

This section serves to demonstrate that the FGAM can be used to describe chemical kinetics in an engine simulation. The schematic of the HCCI engine in GT-Suite is displayed in Figure 5.3. The FGAM was benchmarked against the auto-ignition model by Patel et al. [55]. The Patel model is a reduced kinetic mechanism (RKM), consisting of 29 species and 52 reactions, developed for HCCI engine simulations. As such, this reduced mechanism has been validated for equivalence ratios from 0.2 to 1 and EGR rates from 0% to 30%. It is important to note that the Patel model was not optimised for the particular conditions of this engine simulation, according to correspondence received from the support team at Gamma Technologies, but nevertheless should give a good indication as to the trends exhibited under varying conditions in an engine simulation. The parameters of the engine displayed in Table 5.3 are representative of actual HCCI engine operating conditions.

Table 5.3: *HCCI Engine Parameters*

Bore	86 mm
Stroke	86.07 mm
Conrod Length	175 mm
Clearance at TDC	1 mm
Compression Ratio	16
Engine Speed	3000 rpm
Ambient Temperature	298 K
Ambient Pressure	1 bar
Fuel	n-Heptane
EGR	0%; 30%
Equivalence Ratio	0.6; 0.8; 1

Figure 5.4 displays performance of the FGAM and Patel RKM in the engine simulations for equivalence ratios of 0.6, 0.8 and 1 with no EGR. Figure 5.5 displays performance of the FGAM and Patel RKM in the engine simulations for EGR rates of 30% and 0% at a fixed equivalence ratio of 0.8. The coefficients used for n-heptane were those derived in the

main calibration process of section 4.2.

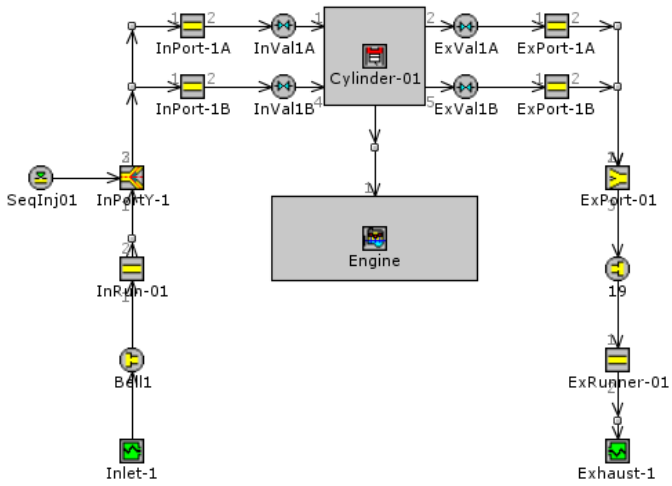

Figure 5.3: *The schematic of a single cylinder HCCI model implemented into GT-Suite*

In the case of changing equivalence ratios, as displayed in Figure 5.4, the FGAM does not displays the same degree of sensitivity as the Patel model. The crank angle degree difference in main heat release event when using the Patel model is approximately 4 degrees, whereas the difference when using the FGAM is less than one degree. The consequence of the lack of sensitivity displayed by the FGAM is that the peak pressure achieved by the global model is greater at stoichiometric conditions. Although the Patel model was not optimised for this specific engine simulation, it had been validated for equivalence ratios from 0.2 to 1. Since the FGAM was found to display poor sensitivity to changes in equivalence ratio compared to the Mehl DKM (section 4.3.3), it is likely that true pressure trace predicted using the Patel model is more accurate than when using the FGAM.

For engine simulations with and without EGR, the FGAM does not displays the same degree of sensitivity as the Patel model, as displayed in Figure 5.5. The FGAM also predicts a significantly later heat release event with 0% EGR, which means that the Patel model with 30% EGR has the same heat release timing as the FGAM without EGR. Both models achieve approximately equivalent peak pressures, but using the Patel model predicts in greater average pressure over the combustion event. The amount of sustained pressure may be an important fact to consider when designing the life span of internal engine components. Since the Patel model had been validated for EGR rates from 0% to 30% and FGAM was found to display poor sensitivity to changes in EGR rates compared to the Mehl DKM, it is unlikely that the FGAM is the more accurate model in this experiment.

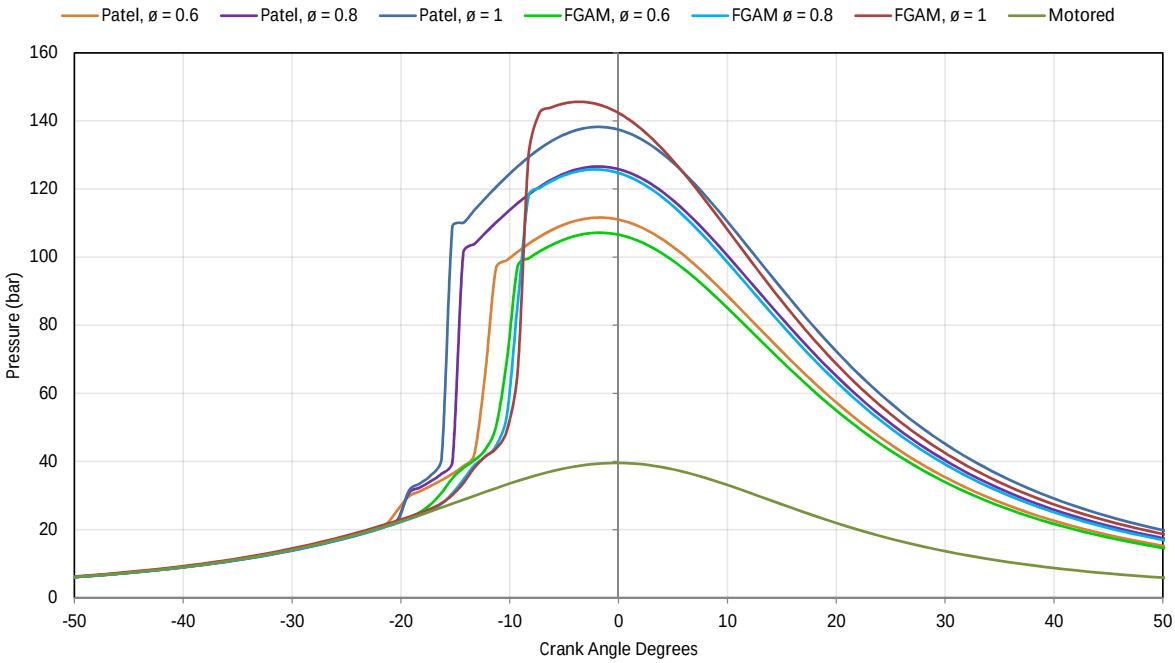

Figure 5.4: *Pressure traces for the single cylinder HCCI model using the FGAM and the Patel RKM for n-heptane at equivalence ratios of 0.6, 0.8 and 1. A motored trace has been included as well. Notice that the Patel model displays significant sensitivity to changes in equivalence ratio with regard to heat release timing whereas the FGAM does not.*

Since it has been shown in section 4.3.3 that the FGAM can be optimised for a specific EGR rate or equivalence ratio condition, the next step would be to implement the FGAM with a set of specially optimised coefficients which match the engine conditions. Before this is completed, there are certain practicalities which need to be noted with regard to total simulation time when using both models. For the simulations without EGR, the simulation time using the FGAM was approximately 3 seconds whilst using the Patel RKM resulted in a longer time of 9 seconds (using a computer with a quad-core i5 processor and Windows 7). For the simulations with EGR, the simulation time using the FGAM was approximately 8 seconds whilst using the Patel RKM resulted in a longer time of 23 seconds. The FGAM is therefore roughly 3 times faster than the Patel RKM when used in engine simulations. However, since the FGAM does not display the correct sensitivity to EGR and air-fuel ratio, it requires a optimised set of kinetic coefficients. From section 4.3.3, the time taken to calibrate the model for a fixed EGR rate and equivalence ratio is approximately 20 minutes. Engine design in particular often calls for experimenting with different EGR rates and air fuel ratios. Each time the user wants to see the effect of reducing the EGR rate or increasing the air-fuel ratio, they would have to re-calibrate a set of coefficients for the FGAM, costing another 20 minutes in total simulation time. Even if the end user is willing to budget in the extra time for the calibration, the FGAM is not as user-friendly in its current state compared to the Patel model as the user would need to keep track of the

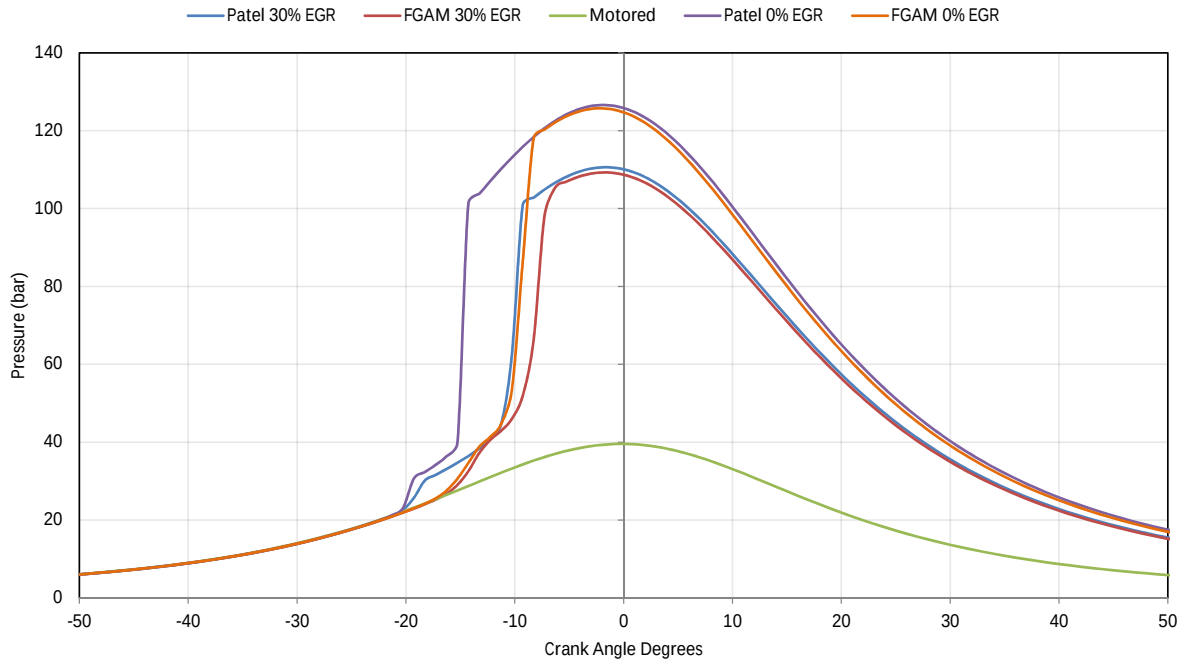

Figure 5.5: *Pressure traces for the single cylinder HCCI model using the FGAM and the Patel RKM to describe auto-ignition for n-heptane with $\Phi = 0.8$ and EGR rates of 0% and 30%. A motored trace has been included as well. Notice that the effect of EGR is far more pronounced by the Patel model compared to the FGAM.*

coefficients used for each simulation. Thus, the best way to improve the FGAM which will encourage wider adoption of the model would be to address the model's lack of sensitivity to EGR and air-fuel ratio through modification to its structure. Ideally, the final form of the FGAM retains the same computational speed, but requires no additional calibration of kinetic coefficients.

This implementation exercise does display that the FGAM can be used to describe combustion kinetics in an engine simulation in GT-Suite, which was one of the primary goals of this work. The method by which this implementation was performed is included in appendices.

5.3 Summary of GT-Suite Implementation

The FGAM was successfully implemented as a combustion kinetics descriptor for constant volume adiabatic reactor and single cylinder HCCI simulations in GT-Suite. For the constant volume experiments, the solving of the FGAM by GT-Suite's built-in solvers was checked against data obtained using the forward Euler method with the adaptive time-stepping procedure. The difference between the two solving routines across prediction of the cool flame ignition delay, overall ignition delay and cool flame temperature rise was less the 3%. This indicates a good repeatability of results obtained by the FGAM when solved using different techniques.

For the single cylinder HCCI simulations, the FGAM was benchmarked against the reduced kinetic mechanism of Patel [55], which itself had been validated for the regions used in these experiments. Again, as noticed during the calibration process completed in chapter 4, it was seen that the FGAM did not display significant sensitivity to the equivalence ratio and EGR effects, especially when compared to the Patel model. It was recommended that the lack of sensitivity of the FGAM be addressed prior to further use of the model in engine simulations. Recommended changes to be made to the model in this regard were given in section 4.3.3.

Chapter 6

Conclusions

An investigation was performed into the sources of stiffness in the FGAM. It was found that one of the main sources of stiffness in the model was the difficulty encountered in solving for species I for a given time step. Species I was linked to four reaction pathways, two feeding reactions and two depleting reactions. During solving of the model, there reached a point at which the two depleting reactions became much larger in magnitude compared to the two feeding reactions. At this point, implicit numerical solvers, such as those built into GT-Suite, were unable to converge to a solution for the concentration of species I. This problem was similar to one encountered during the development of the model regarding the solving for species J. As such, a similar solution method was used which removed the need to solve for the concentration of species I by using a pseudo-QSSA assumption. Implementing this assumption did not require major alteration to the structure of the model and hence did not significantly alter the performance of the model. However, it should be noted that the stiffness of the model is also a function of the set of kinetic constants used for the fuels.

An calibration routine was developed for the FGAM. The routine made use of a particle swarm heuristic algorithm. The fitness function used in this optimisation process compared five key points between the FGAM and the reference data provided by a DKM. The points used in the fitness function are explained in detail in section 4.1.2. The result of the optimisation was a decrease in the combined average error of the ignition delay timing, cool flame ignition delay timing and cool flame temperature rise of 6.12% for n-heptane and 6.24% for iso-octane compared to Floweday's original model. Additionally, a set of comparably accurate coefficients was developed for PRF50. However, the value of the average ignition delay error after calibration of the fuels was not within the quoted error tolerance of 11% to 23% established during development of the model. The reason for this increased average error was due to the fact that the calibration process included regions where the model had not previously been validated. Further investigation into these regions

showed that the FGAM displayed poor sensitivity to EGR and equivalence ratio effects in the low to intermediate (NTC) temperature region. In addition to this, it was found that the model is not stable under conditions of rich equivalence ratio and high EGR rates. At rich equivalence ratios, the EGR contains significant amount of CO, which immediately activated an exothermic pathway in the FGAM at the start of the ignition delay. As a result, for these conditions, the FGAM severely under predicted the ignition delay.

Due to the fact that increasing number of vehicle manufacturers are using EGR in order to comply with emission regulations, a useful auto-ignition model needs to display correct sensitivity to EGR effects in order to obtain widespread acceptance. Furthermore, manufacturers are also focused on reducing fuel consumption due to the rising oil prices. One of the ways in which this is achieved is through experimentation in changing equivalence ratio as well as modelling of in-cylinder gas dynamics. For this application, a useful auto-ignition model would need to display correct sensitivity to equivalence ratio effects. Unfortunately, due to the fact that the FGAM does not display correct sensitivity to either of these parameters in its current state, it is not suitable for applications with EGR or changing equivalence ratios.

The alterations made to the model allowed for it to be implemented into GT-Suite using the templates provided. In comparison, the original form of the model was unable to converge to a solution for a single auto-ignition experiment when implemented into GT-Suite for the regions tested. The revised formulations of the model was successfully integrated into the software for a constant volume adiabatic reactor and single cylinder HCCI engine simulation. For the constant volume adiabatic reactor experiments, it was found that the average difference in the predicted ignition delay timing, cool flame ignition delay timing and cool flame temperature rise of the FGAM when solved using GT-Suite's built-in RADAU solver and a forward Euler integration method with adaptive time-stepping was less than 3%. This is an indication of a good repeatability of auto-ignition predictions obtained from the FGAM when using different solvers. The FGAM was successfully implemented as a descriptor for combustion kinetics inside a single cylinder HCCI engine simulations. However, it did not display the same level of sensitivity to changing equivalence ratios and EGR rates as a contemporary reduced kinetic mechanism.

In conclusion, despite the fact that a robust calibration technique was developed for the FGAM and the major source of stiffness in the model was addressed, the FGAM has limited application due to its lack of sensitivity to EGR and equivalence ratio effects. The most appropriate way in which to address these issues is through major modification to the structure of the model.

Chapter 7

Recommendations

Based on the conclusions drawn from the work carried out, the following recommendations have been made:

1. Whilst maintaining the current structure of the model, develop sets of kinetic coefficients, using the calibration process detailed in this research, for each individual EGR and equivalence ratio condition required. This should be thought of as a short-term solution for the FGAM.

2. Make fundamental changes to the structure of the model to ensure that it displays the correct sensitivity to the EGR and equivalence ratio effects. In addition, changes made should allow for the model to operate for mixtures with high levels of EGR at rich equivalence ratios, as discussed in section 4.3.1. Most importantly, these changes should maintain or improve upon the performance of the FGAM in all other regions. Recommended changes to be implemented have been included in section 4.3.3.

3. Once the revised model is functioning optimally, experimental validation of the FGAM should be performed.

References

[1] G Floweday. A New Functional Global Auto-ignition model for Hydrocarbon Fuels - Part 2 of 2: Model Formulation, Development and Performance Assessment. *SAE International*, 2010-01-2169, 2010.

[2] G Floweday. A New Functional Global Auto-ignition model for Hydrocarbon Fuels - Part 1 of 2: An Investigation of Fuel Auto-ignition Behaviour and Existing Global Models. *SAE International*, 2010-01-2161, 2010.

[3] M Mehl, H J Curran, W J Pitz, and C K Westbrook. Detailed Kinetic Model of Gasoline Surrogate Mixtures. *Lawrence Livermore National Laboratory*, pages 1–6, 2009.

[4] Marlan Perumal and Gareth Floweday. An Investigation of Cascading Autoignition and Octane Number using a Multi-zone Model of the CFR Engine. *SAE International*, 2011-01-0850, 2011.

[5] JB Heywood. *Internal Combustion Engines Fundamentals*, pages 462–470. McGraw-Hill, 1988.

[6] JB Heywood. *Internal Combustion Engine Fundamentals*, pages 470–474. McGraw-Hill, 1988.

[7] JB Heywood. *Internal Combustion Engine Fundamentals*, pages 456–457. McGraw-Hill, 1988.

[8] Bosch Automotive Handbook. Bosch, pp. 408, 1986.

[9] JB Heywood. *Internal Combustion Engines Fundamentals*, pages 539–549. McGraw-Hill, 1988.

[10] C Crua, DA Kennaird, SS Sazhin, and MR Heikal. Diesel autoignition at elevated in-cylinder pressures. *International Journal of Engine Research*, 5(3):1–11, 2004.

[11] YA Cengel and MA Boles. *Thermodynamics: An Engineering Approach, 6th Edition*, page 507. McGraw-Hill, 2007.

[12] Europa. Reduction of pollutant emissions from light vehicles. http://europa.eu/legislation_summaries/environment/air_pollution/l28186_en.htm, 2013. [Online; accessed 01-07-2013].

[13] United States Environmental Protection Agency. Light-Duty Vehicle and Light-Duty Truck – Clean Fuel Fleet Exhaust Emission Standards. http://www.epa.gov/otaq/standards/light-duty/ld-cff.htm, 2012. [Online; accessed 01-07-2013].

[14] T Johnson. Diesel Engine Emissions and Their Control. *Platinum Metals Review*, 52:23–37, 2010.

[15] Dae Sik Kim and Chang Sik Lee. Improved emission characteristics of HCCI engine by various premixed fuels and cooled EGR. *Fuel*, 85(5-6):695–704, 2006.

[16] Per Risberg. Describing the Auto-Ignition Quality of Fuels in HCCI Engines. *KTH Industrial Engineering and Management*, PhD Thesis, 2006.

[17] JB Heywood. *Internal Combustion Engine Fundamentals*, pages 539–549. McGraw-Hill, 1988.

[18] C. P. Halstead, M. P., Kirsch, L. J., Prothero, A., Quinn. A Mathematical Model for Hydrocarbon Autoignition at High Pressures. *Proceedings of the Royal Society of London. Series A, Mathematical and Physical Sciences*, 346(1647):515–538, 1975.

[19] G Floweday. Two Contrasting Approaches to Auto-Ignition Modelling for HCCI Engines by Gareth Floweday. *University of Cape Town, PhD Thesis*, 2010.

[20] Jincai Zheng, David L Miller, and Nicholas P Cernansky. A Global Reaction Model for the HCCI Combustion Process. *SAE International*, 2004-01-2950, 2004.

[21] A Schreiber, M, Sadat Sakak, A, Lingens and J F Griffiths. A Reduced Thermokinetic Model for the Autoignition of Fuels with Variable Octane Ratings. *Twenty Fifth Symposium on Combustion/The Combustion Institute*, pages 933–940, 1994.

[22] U C Müller and A Peters, N, Linan. Global Kinetics for n-Heptane Ignition at High Pressures. *Twenty Fourth Symposium on Combustion/The Combustion Institute*, 0:777–784, 1992.

[23] J.F. Griffiths. Reduced Kinetic Models and their Application to Practical Combustion Systems. *Progress in Energy and Combustion Science*, 21(1):25–107, January 1995.

[24] K Hughes, M Fairweather, J Griffiths, R Porter, and a Tomlin. The application of the QSSA via reaction lumping for the reduction of complex hydrocarbon oxidation mechanisms. *Proceedings of the Combustion Institute*, 32(1):543–551, 2009.

[25] A Winstanly. Computational Implementation of a Functional Global Auto-Ignition Model. *University of Cape Town, Undergraduate Thesis*, 2011.

[26] Rania Hassan, Babak Cohanim, Olivier De Weck, and Gerhard Venter. A Comparison of Particle Swarm Optimisation and the Genetic Algorithm. *Ameircan Institute of Aeronautics and Astronautics*, 2004.

[27] Kasemsit Teeyapan and Mike Stilman. Full Body Control Strategies for Dynamically Stable Humanoid Robots. http://jw.nebulis.org/research/, 2009. [Online; accessed 15-04-2012].

[28] Riccardo Poli, James Kennedy, and Tim Blackwell. Particle Swarm Optimization: an Overview. *Swarm Intelligence*, 1(1):33–57, August 2007.

[29] Gerhard Venter. Particle Swarm Optimization. *American Institute of Aeronautics and Astronautics*, AIAA 2002-1235, 2002.

[30] Sang-kyu Kim, Kazuma Ito, Daisuke Yoshihara, and Tomoyuki Wakisaka. Application of a Genetic Algorithm to the Optimization of Rate Constants in Chemical Kinetic Models for Combustion Simulation of HCCI Engines. *JSME International Journal*, 48(4):717–724, 2005.

[31] Adam Marczyk. Genetic Algorithms and Evolutionary Computation. http://www.talkorigins.org/faqs/genalg/genalg.html/, 2004. [Online; accessed 01-10-2012].

[32] J Monschke. Genetic Algorithms. http://janmonschke.com/Genetic-Algorithms/presentation/#/. [Online; accessed 13-11-2012].

[33] V. Hamosfakidis and R.D. Reitz. Optimization of a hydrocarbon fuel ignition model for two single component surrogates of diesel fuel. *Combustion and Flame*, 132(3):433–450, February 2003.

[34] H.J. Curran, P. Gaffuri, W.J. Pitz, and C.K. Westbrook. A Comprehensive Modeling Study of n-Heptane Oxidation. *Combustion and Flame*, 114(1-2):149–177, July 1998.

[35] Elisa Toulson, Casey M. Allen, Dennis J. Miller, Harold J. Schock, and Tonghun Lee. Optimization of a Multi-step Model for the Auto-ignition of Dimethyl Ether in a Rapid Compression Machine. *Energy & Fuels*, 24(6):3510–3516, June 2010.

[36] Unitrans Motors. Specifications of a Toyota Hilux 2.5 D-4D. http://www.um.co.za/specifications/toyota_hilux_2_5_d-4d_(2011).aspx/, 2012. [Online; accessed 13-11-2012].

[37] H Schapertons and W Lee. Multidimensional modelling of knocking combustion in SI engines. *SAE Technical Paper*, 94(850502):715–727, 1985.

[38] Darrell Whitley. An overview of evolutionary algorithms : practical issues and common pitfalls. *Information and Software Technology*, 43:817–831, 2001.

[39] JB Heywood. *Internal Combustion Engine Fundamentals*, page 43. McGraw-Hill, 1988.

[40] JB Heywood. *Internal Combustion Engine Fundamentals*, pages 836–840. McGraw-Hill, 1988.

[41] Robert M Wagner, Johney B Green, John M Storey, and C Stuart Daw. Extending Exhaust Gas Recirculation Limits in Diesel Engines. *Oak Ridge National Laboratory*, pages 1–10, 2009.

[42] M Vidal, W Wong, W J Rogers, and M S Mannan. Evaluation of lower flammability limits of fuel-air-diluent mixtures using calculated adiabatic flame temperatures. *Journal of Hazardous Materials*, 130(1-2):21–7, March 2006.

[43] The Engineering Toolbox. Gases - Explosive and Flammability Concentration Limits. http://www.engineeringtoolbox.com/explosive-concentration-limits-d_423.htmle/, 2008. [Online; accessed 27-11-2012].

[44] Gavin Evezard. An Innovative Rapid Compression Machine in Theory and Practice. *University of Cape Town*, PhD Thesis, 2011.

[45] S Samuels. Benchmarking the Performance of the Sasol Advanced Fuels Laboratory Rapid Compression Machine against International Standards. *University of Cape Town, Undergraduate Thesis*, 2011.

[46] L.R. Cancino, M. Fikri, a.a.M. Oliveira, and C. Schulz. Ignition delay times of ethanol-containing multi-component gasoline surrogates: Shock-tube experiments and detailed modeling. *Fuel*, 90(3):1238–1244, March 2011.

[47] Michael Downey. Design, Build and Commisioning of a Shock Tube Apparatus for Autoignition Research. *University of Cape Town*, MS Thesis, 2010.

[48] B.M. Gauthier, D.F. Davidson, and R.K. Hanson. Shock tube determination of ignition delay times in full-blend and surrogate fuel mixtures. *Combustion and Flame*, 139(4):300–311, December 2004.

[49] H J Curran, P Gaffuri, W J Pitz, and C K Westbrook. A Comprehensive Modeling Study of iso-Octane Oxidation. *Combustion and Flame*, 2180(01), 2002.

[50] CHEMKIN / CHEMKIN-PRO Theory Manual CHEMKIN Software. Reaction Design, 2010.

[51] Shengtai Li and Linda Petzold. Software and algorithms for sensitivity analysis of large-scale di erential algebraic systems. *Journal of Computational and Applied Mathematics*, 125:131–145, 2000.

[52] GT-Suite, General and Advanced Simulation Applications Manual v7.3. Gamma Technologies, 2013.

[53] GT-Suite, Engine Performance Application Manual v7.3. Gamma Technologies, 2013.

[54] Marlan Perumal. A Multi-Zone Model of the CFR Engine : Investigating Cascading Autoignition and Octane Rating. *University of Cape Town, MS Thesis*, 2011.

[55] Amar Patel, Song-Charng Kong, and Rolf D Reitz. Developement and Validation of a Reduced Reaction Mechanism for HCCI Engine Simulations. *SAE Technical Paper Series*, 2004-01-05, 2004.

Appendix A

Calibrated Coefficients of the FGAM

Table A.1: *Calibrated Kinetic Constants for n-heptane, iso-octane and PRF50*

	n-Heptane	iso-Octane	PRF 50
ln(A1a)	23.48	26.08	25.20
B1a	-12366.90	-14835.30	-13838.00
a1	-0.13	-0.15	-0.14
b1	0.88	0.70	0.86
ln(A1b)	19.59	20.29	21.13
n1b	-2.57	-2.71	-2.77
B1b	-19921.70	-15409.20	-19664.90
a2	0.92	1.21	1.22
c2	0.65	0.60	0.59
ln(A2)	25.19	22.55	22.51
n2	-1.17	-1.19	-1.17
B2	-8602.14	-8080.85	-7928.67
d3	2.70	2.86	2.90
ln(A3)	43.62	42.35	43.66
B3	-27914.70	-28048.60	-31010.50
c4	0.05	0.02	0.03
ln(A4)	52.54	37.78	44.85
B4	-40467.70	-24313.10	-33598.80
a5	1.02	0.94	1.02
b5	0.85	0.86	0.89
ln(A5)	22.07	21.44	21.75
n5	-0.60	-0.58	-0.54
B5	-18294.80	-16628.20	-17542.80
d6	6.25	5.64	5.60
b6	0.15	0.16	0.14
ln(A6)	25.71	25.44	27.37
n6	-0.04	-0.03	-0.03
B6	-15852.80	-16029.10	-15606.10
e7	5.54	3.24	4.83
b7	0.14	0.15	0.14
ln(A7)	12.37	11.57	12.89
n7	1.82	1.77	1.69
B7	-13203.80	-14894.70	-14702.10
f8	3.50	2.72	3.33
b8	0.17	0.23	0.20
ln(A8)	17.62	16.67	15.52
B8	-13232.80	-13833.10	-12614.10
g9	0.94	0.99	0.98
ln(A9)	23.44	21.11	20.52
B9	-47927.80	-45464.70	-41264.90

Appendix B

Backward Euler Derivation

The backward Euler method is an example of an implicit numerical integration scheme. The method uses the rate of change at the future position to predict the future position, as per the formula:

$$w_{i+1} = w_i + h \times f(w_{i+1}, t_{i+1}) \tag{B.1}$$

where,

h is the time step,
w_{i+1} is the new position,
w_i is the current position,
$f(w_i + t_i)$ is the rate of change of w_i.

The rate of change at the future position is derived as follows:

Consider the characteristic equation:

$$g(w) = w_{i+1} - w_i - h \times f(w_{i+1}, t_{i+1}) \tag{B.2}$$

Taking the derivative with respect to w:

$$\frac{d}{dw}g(w) = \frac{d}{dw}(w_{i+1} - w_i - h \times f(w_{i+1}, t_{i+1})) \tag{B.3}$$

Since w_i is known, this reduces to:

$$\frac{d}{dw}g(w) = \vec{I} - h\vec{J} \times f(w_{i+1}, t_{i+1}) \tag{B.4}$$

where,

h is the time step,
$\vec{I}$ is the identity matrix,
$\vec{J}$ is the Jacobian matrix formed by taking the derivative of each element of f with respect to each element of w.,
$f(w_i + t_i)$ is the rate of change of w_i,

Solving the characteristic equation using Newton's iterative scheme results in the equation for the backward Euler method:

$$(w_{i+1})_{n+1} = (w_{i+1})_n + ((w_{i+1})_n - w_i - h \times f((w_{i+1})_n, (t_{i+1})_n)(\vec{I} - h\vec{J}((w_{i+1})_n, (t_{i+1})_n) \tag{B.5}$$

Appendix C

FGAM iso-Octane & PRF50 Data

In this section, the ignition delay curves derived from the calibration of the FGAM (section 4) for iso-Octane and PRF50 are presented. The graphs consist of overall ignition delay, cool flame ignition delay and cool flame ceiling temperature curves. Note that left vertical axis is plotted on a log scale, with the cool flame ignition delay and overall ignition delay plotted against the vertical ignition delay axis, and the cool flame ceiling temperature plotted against the vertical temperature axis.

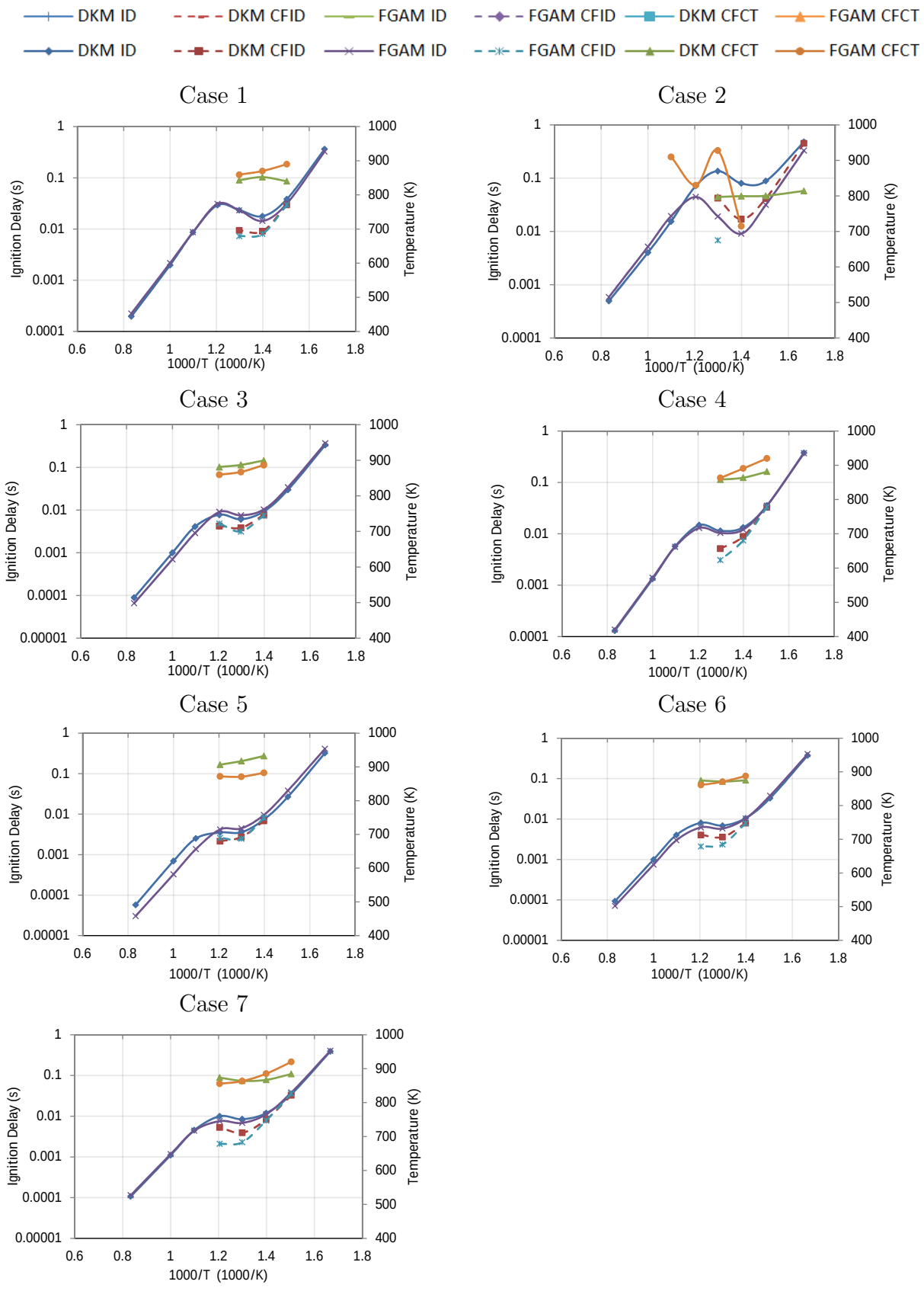

Figure C.1: *Calibration iso-Octane according to the cases described in Table 4.3.*

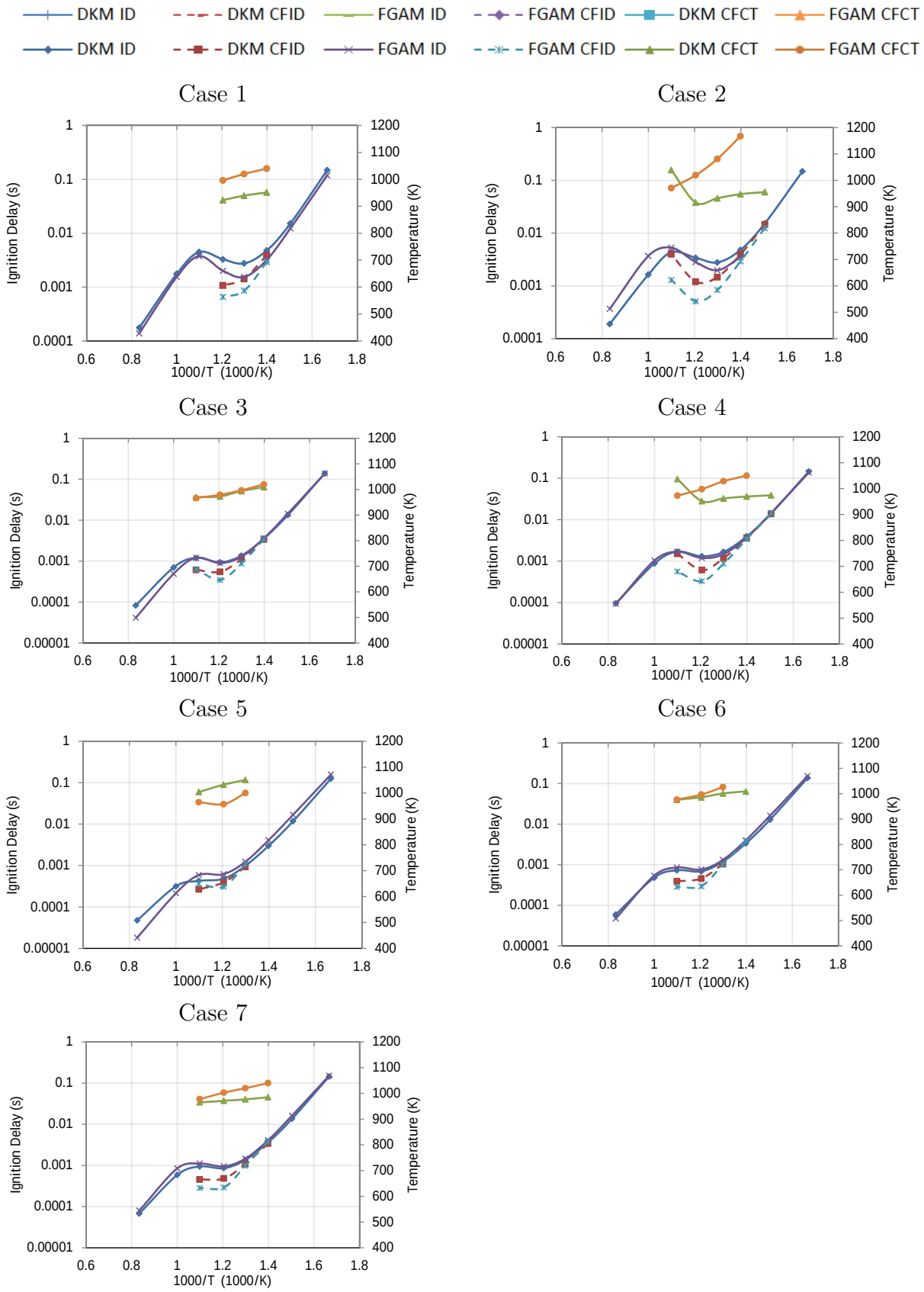

Figure C.2: *Calibration of PRF50 according to the cases described in Table 4.3.*

Appendix D

Calibration Code Manual

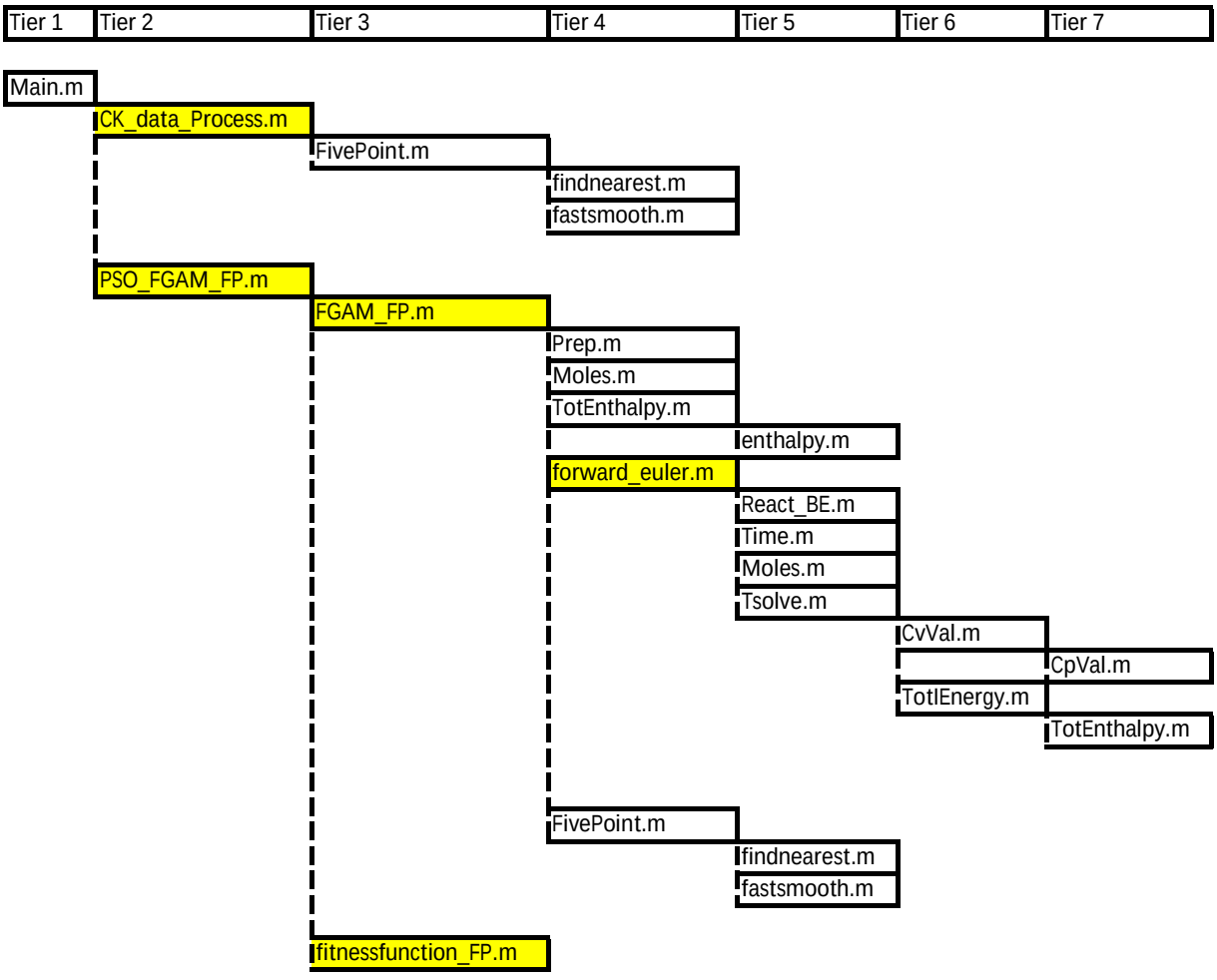

Figure D.1: *A diagram of the function calling hierarchy in the calibration routine. The function which initiates the calibration process,* `Main.m`*, is located in the top left corner. Functions with a yellow background contain loops which have to be completed before the next function of the same tier can be called.*

The files used for the calibration were written in MATLAB®. When using the calibration routine, only the reading sequences in the `Main` file need to be edited to point to the correct reference data and calibration conditions. Running the `Main` file will then initiate the calibration process.

The operations performed by each file used in the calibration process will be presented in this section according to the order in which they appear in Figure D.1 from top to bottom.

`Main`

- Main file for execution of calibration procedure.
- Reads calibration conditions, reference data and seed coefficient values from file
- Calls `CK_data_Process` and `PSO_FGAM_ID` functions.
- Writes calibrated coefficients to file.

`CK_data_Process`

- Extracts the required data from the DKM temperature-time traces for use with the Five Point fitness function.
- Calls the `FivePoint` function.
- Stores relevant data in a struct.

`FivePoint`

- Takes in a temperature-time data.
- Extracts ignition delay, cool flame ignition delay, cool flame temperature rise, second inflection point and initial temperature rise from the input data.
- Calls the `fastsmooth` and `findnearest` functions.
- Stores relevant data in a struct which it returns to the calling function.

`fastsmooth`

Available at:
http://www.mathworks.com/matlabcentral/fileexchange/19998-fast-smoothing-function
[Accessed: 14/08/2013]

- Smooths the input traces according to options selected.
- Options include choices between a rectangular, triangular or pseudo-Gaussian smooth types, width size of the smooth and how the ends of the smoothed data are treated.
- Returns smoothed data as a vector.

`findnearest`

Written by Thomas Benson, 2002

Available at:
http://www.mathworks.com/matlabcentral/fileexchange/2838-findnearest-m
[Accessed: 14/08/2013]

- Takes in target value, array to be searched and the option to bias the output toward values higher or lower than the target value.
- Returns subscript of closest match to target value in array.

`PSO_FGAM_FP`

- PSO optimisation routine which calls the `FGAM_FP` and the `fitnessfunction_FP` functions.
- Stores data in a struct.
- Returns calibrated coefficients.

`FGAM_FP`

- Main file of the FGAM.
- Calls `Prep`, `Moles`, `TotEnthalpy`, `forward_euler` and `FivePoint` functions.
- Returns a struct of five point auto-ignition data for the given set of kinetic coefficients.

`Prep`

- Calculates initial species concentration based on equivalence ratio, fuel mixture and EGR rate.
- Hydrocarbon fuel only.
- Returns species concentration vector.

`Moles`

- Calculates and returns the mole and mole fractions from the species concentration values.

`TotEnthalpy`

- Returns the total enthalpy of the mixture based on the mixture of individual species and total moles present.

`enthalpy`

- Calculates the total enthalpy of the species per mole based on their constant specific heat values.
- Returns enthalpy per mole and state enthalpy of the mixture.

`forward_euler`

- Main file for forward Euler integration method
- Calls `ReactBE`, `Time`, `Moles` and `Tsolve`.
- Writes temperature-time trace data to "FGAM_data.txt".
- Returns ignition delay value

`React_BE`

- Rate of change of species calculations according to the balanced reaction rate equations
- Returns rate of change of species with respect to time vector

`Time`

- Takes in species concentration and rate of change of species concentration.
- Implements adaptive time-stepping procedure.
- Returns the largest time step size for which the minimum species concentration in the mixture is zero.

`Tsolve`

- Solves for temperature based on species concentrations.
- Bases calculation on conservation of internal energy.
- Calls `CvVal` and `TotIEnergy` functions
- Returns temperature of the mixture.

`CvVal`

- Calculates and returns the C_v value of the mixture
- Calls `CpVal` and `TotIenergy` functions

`CpVal`

- Calculates and returns the C_p value of the mixture

`TotIEnergy`

- Calculates and returns the total internal energy of the mixture.
- Calls `TotEnthalpy`

`fitnessfunction_FP`

- Uses the data provided by the FivePoint function to compare the reference data to the FGAM data
- Calculates the relative error value for each condition
- Returns the sum of the relative error values

Appendix E

Manual of Implementation of FGAM into GT-Suite

This manual describes the method used to implement the FGAM into GT-Suite using the `EngCylChemGlobal` template for engine simulations. An engine model in GT-Suite requires a cylinder object. The FGAM will be used as the combustion kinetics descriptor of the cylinder object. The same process can be used when implementing the FGAM into the `GlobalReactions` template for constant volume adiabatic reactor simulations.

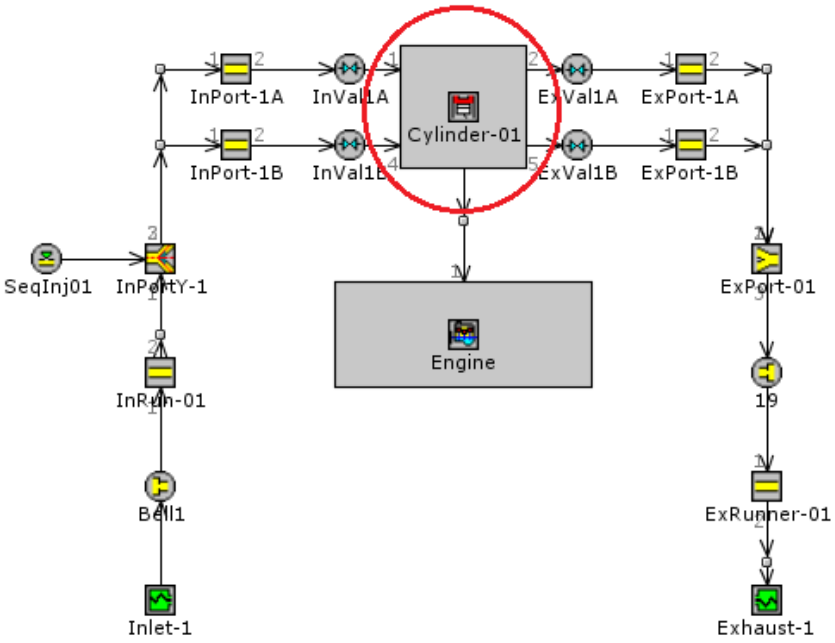

Figure E.1: *The cylinder object of the engine simulation, circled in red, which "houses" the FGAM.*

1. To begin with, edit the option in the cylinder object of the engine model. The cylinder object has been circled in red in Figure E.1. Point the combustion properties to a `EngCylCombHCCI`, `EngCylCombSI` or `EngCylComCI` template for simulations of either HCCI, SI or CI engines respectively. In this case, the "HCCI-Gaseous" object is referring to an `EngCylCombHCCI` template, as shown in Figure E.2.

2. Edit the combustion object settings, pointing the field named "Chemistry Object Reference Name" to the desired chemical kinetic descriptor, as shown in Figure E.3. In this case, it is pointed to the FGAM, an `EngCylChemGlobal` object.

3. In the main tab of the `EngCylChemGlobal` template, shown in Figure E.4, point to the correct species translation object. In this case *FGAM_species*, the contents of which are displayed in Figure E.5. Notice that in the Figure E.5, the fluid reference object of the species Q and Y is distinct from the fuel's fluid reference object. This was achieved by duplicating the fluid reference object of the fuel and renaming it. It is important that these fluid reference objects are distinct due to the way in which the built-in solvers solve the FGAM.

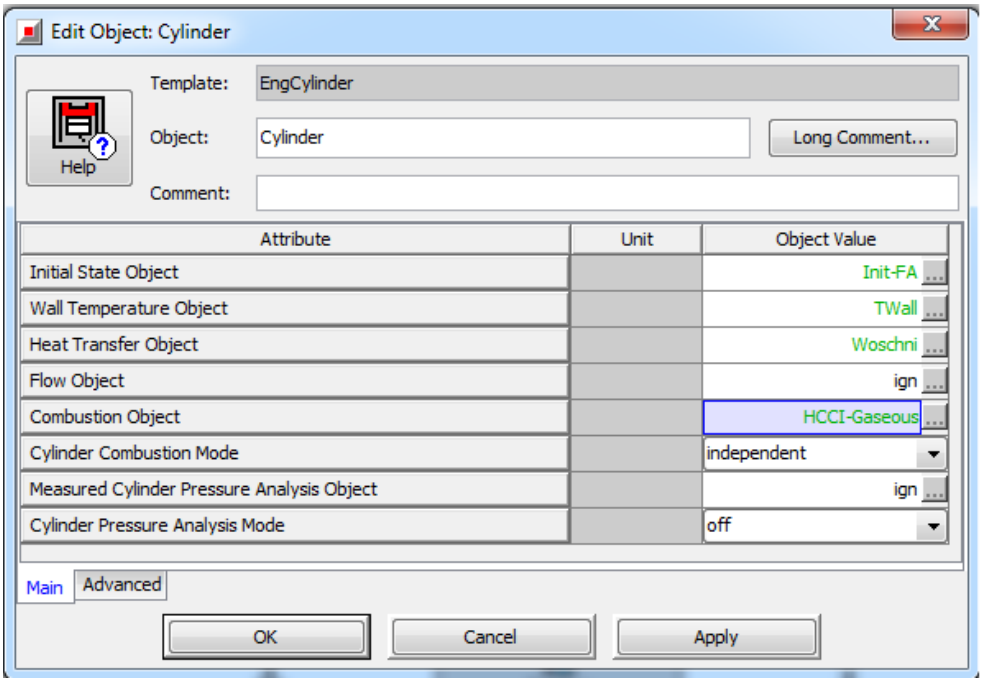

Figure E.2: *Cylinder object properties. The FGAM is invoked as part of the combustion object "HCCI-Gaseous".*

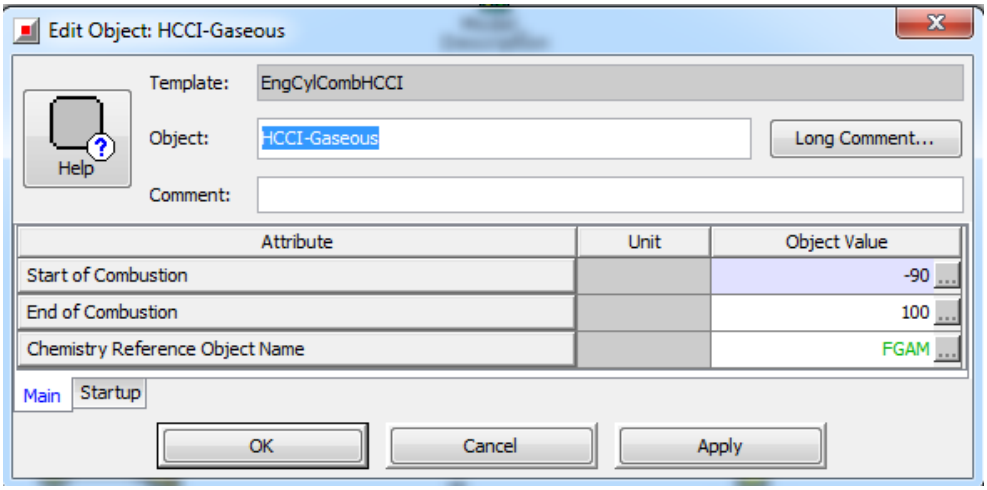

Figure E.3: *Combustion object properties. The FGAM is listed under the Chemistry Reference Object Name.*

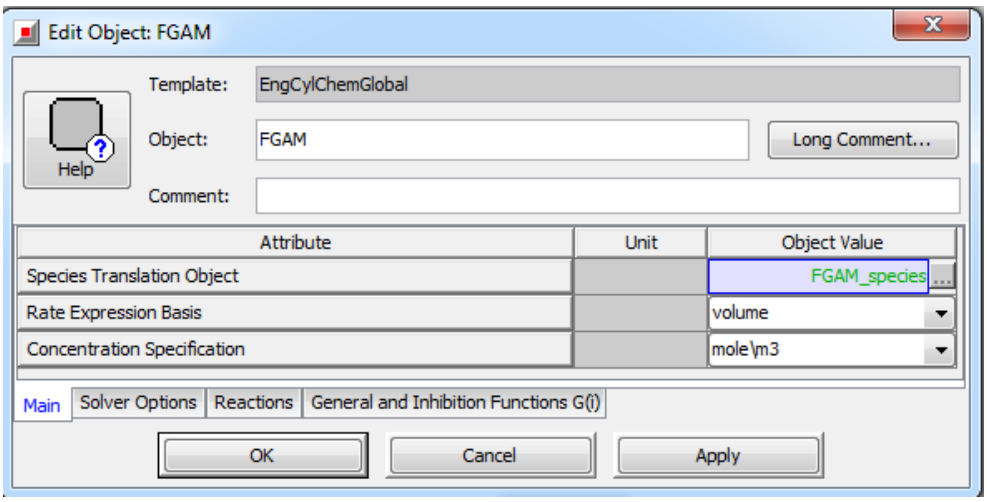

Figure E.4: *The main tab of the* `EngCylChemGlobal` *template.*

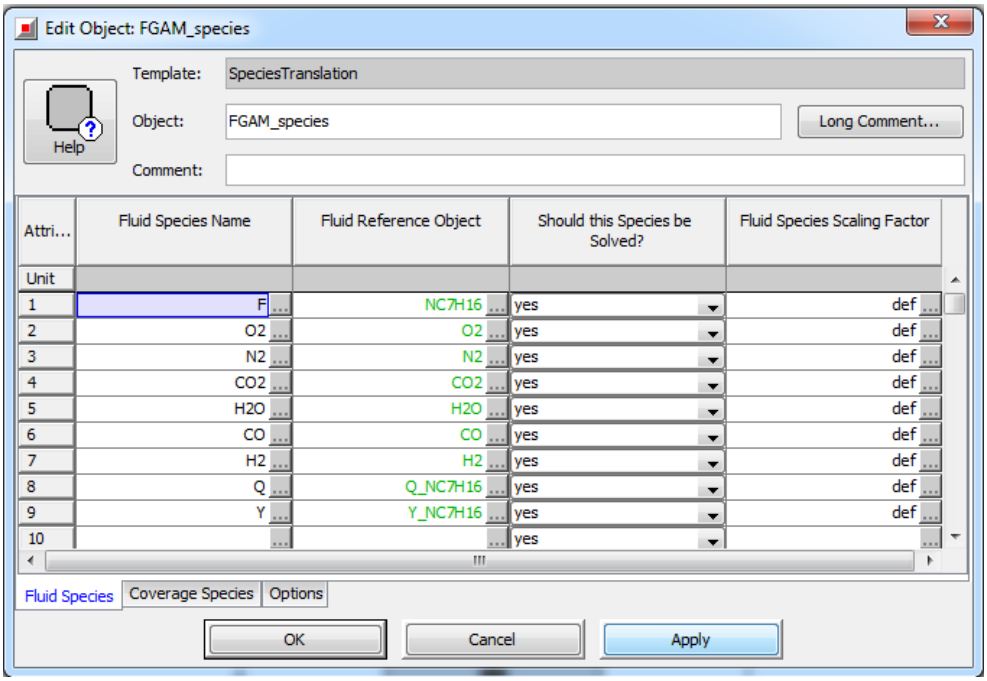

Figure E.5: *The species translation object of the FGAM. Note that species Q and Y have different Fluid reference objects compared to the fuel species F.*

4. In the solver tab of the `EngCylChemGlobal` template (Figure E.6) the solver selection and other related setting can be changed. In this case, the RADAU solver was chosen as it is the most robust, and the absolute tolerance of the solver was lowered to $1e-6$. This is the minimum value that can safely be used for the absolute tolerance according to the Gamma Technologies support team.

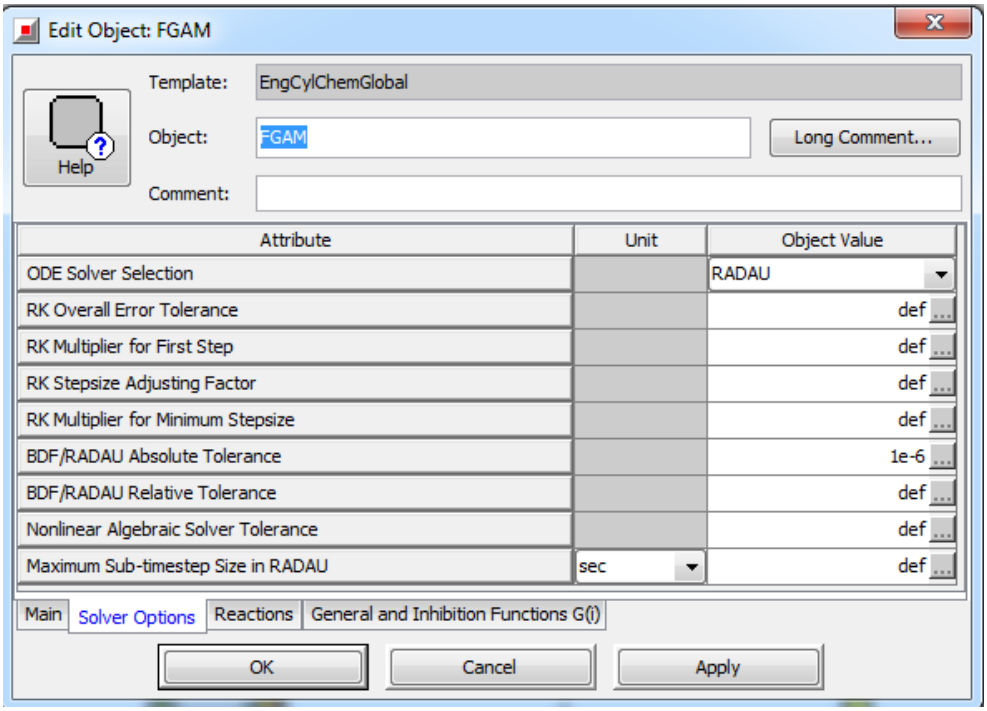

Figure E.6: *The solver options available in the* `EngCylChemGlobal` *template.*

5. Figure E.7 shows the FGAM entered into the Reactions tab of the `EngCylChemGlobal` template. The G function used under the concentration expressions are referring to function listed under the General and Inhibitions Functions tab, shown in Figure E.8. The concentration values for the species must be entered inside the curly brackets. The constant terms $(lnA1, B1)$ for the FGAM are imported from an Excel spreadsheet under "Case Setup". To access case setup from the menu bar at the top of the screen: Run-Case Setup-ExcelData.

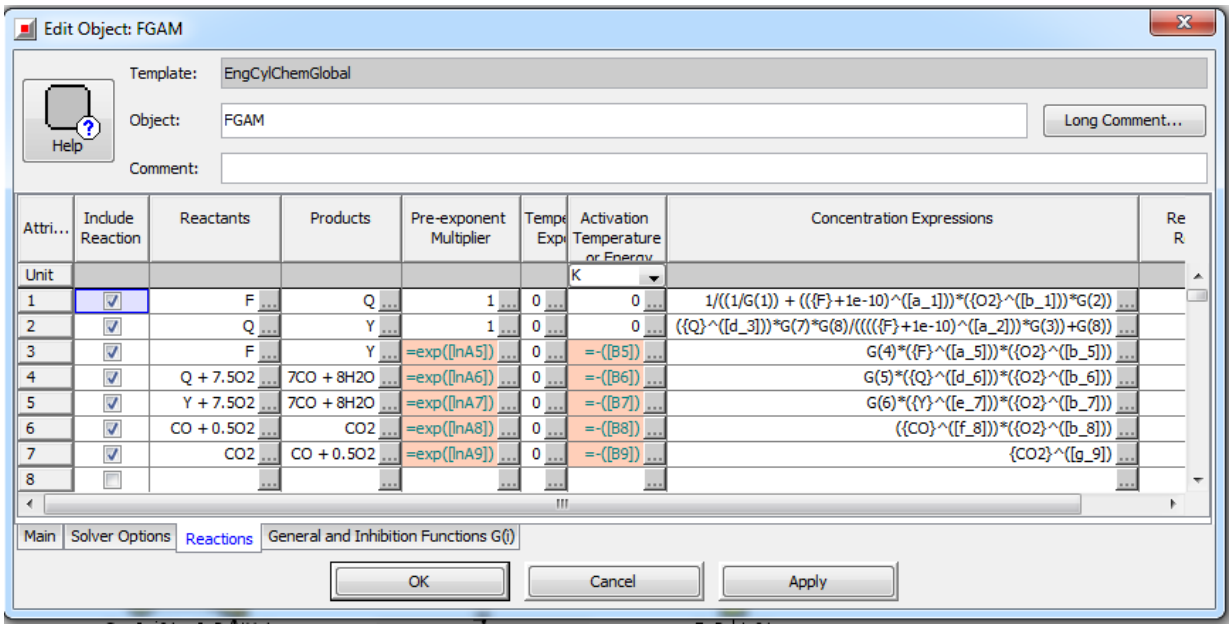

Figure E.7: *The Reactions tab of the* `EngCylChemGlobal` *template. The G terms under concentration expression are referring to functions in the General and Inhibition Functions tab.*

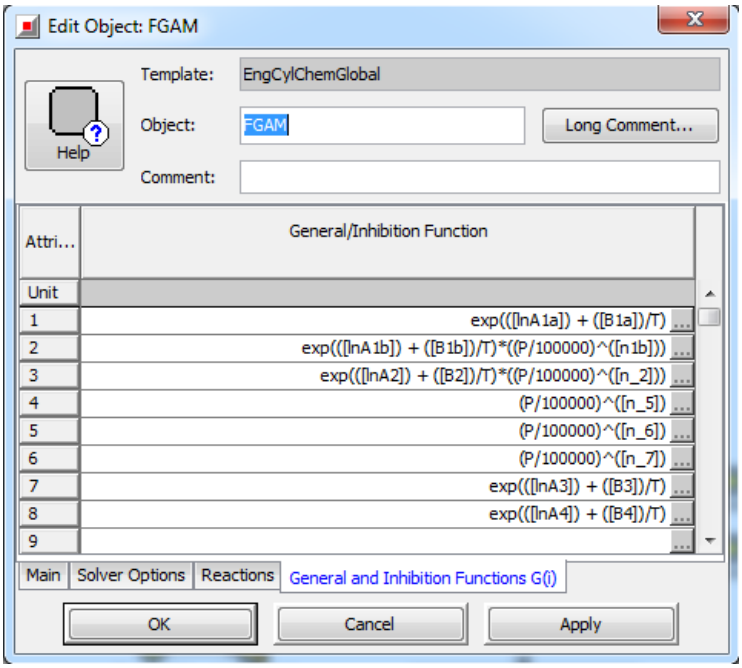

Figure E.8: *The General and Inhibition Functions tab of the* `EngCylChemGlobal` *template. This facility is used for entering the non-standard reaction rates, and is called from the Reactions tab.*